Molecular-Strain Engineering of Chiral Redox-Active Macrocycles

Lily Harriet Jane Collins

Master of Science by Research

University of York

Chemistry

December 2025

Abstract

Redox-active macrocycles featuring cyclical through-space conjugation represent an increasingly important class of molecular materials for both fundamental and application-oriented investigations — especially for their abilities to stabilise charge and assemble into porous electroactive nanostructures. In particular, chiral molecular triangles, consisting of three aromatic diimide (ADI) linkers bound together by enantiopure trans-1,2-diaminocyclohexane bridges, have proven to be a popular platform for accessing a wide range of attractive electronic and energy storage properties, thanks to their globally distributed LUMOs. However, although the effects of different ADI linkers (such as benzene, naphthalene and perylene diimides) on the physical, optical, electronic and self-assembly characteristics of molecular triangles have been explored in depth, diversification of the chiral vertex unit has yet to be investigated. This Thesis explores the consequences of manipulating the vertex chemistry of chiral pyromellitic diimide (PMDI) molecular triangles by systematically introducing modifications to the cyclohexane bridging unit. The first section of this Thesis discusses methods applied to introduce a homologous series of electron-rich trans-1,2-diamines groups, which allows for fundamental investigation of structural and electronic effects on account of aromatic groups. For the first time, the successful synthesis of a molecular triangle with an acyclic trans-1,2-diamine, suggesting that contrary to widely promoted design paradigms, the preorganisation offered by more rigid trans-1,2-diaminocyclohexanes is, in fact, unnecessary. The second section explores the extent at which even subtle changes in the degree of through-space orbital overlap and strain engineering via the aforementioned synthetic modifications can stabilise molecular triangle electron acceptors by lowering the energies required to access their multi-reduced states. This work ultimately serves to promote the advancement of this class of organic molecular materials as prime candidates for future rechargeable energy storage and related organic electronic applications.

Table of contents

Author’s declaration

I declare that this thesis is a presentation of original work, and I am the sole author. Unless otherwise stated, the work presented in this thesis is the work of the author. This work has not previously been presented for a degree or other qualification at this University or elsewhere. All sources are acknowledged as references.

Signed: L. H. J. Collins

Date: 12/12/2025

Acknowledgements

To Alyssa, thank you for everything you have done for me since I joined the group as a BSc student, I could not have asked for a better supervisor to support and guide me through my MRes. Thank you for being my biggest cheerleader and believing in my abilities even when I couldn't see it myself, from helping me during my application process for my MRes scholarship to encouraging me during presentations to show off everything I have achieved! Thank you for allowing me to be myself and share my feelings on my sleeve from the serious imposter syndrome to my overexcitement when I made a new compound, I have so much appreciation for you!

To Will, thank you for being the best mentor I could ask for, I am very grateful that you handed this project off to me and showed me the ropes of the triangle world. All the tip and tricks you taught me in the lab will stick with me for life and have helped me become the researcher I am today!

This thesis and who I am as a researcher today would not have been possible without the Avestro group, from the lab to the office the overwhelming support has been unforgettable. Maddy, thank you for all the coffee runs and lunch trips and helping me when I am having brain fog in the lab and forget how to do anything and everything and having a laugh along the way. It has been hard to be writing up away from everyone, but your daily check ins have helped more than you know! Caitlin, we both started our postgrad journey together and I could not think of a better person to do it with, thank you for being the best desk neighbour and for all the help with DFT calculations! To Shana and Biman, thank you for always being there in the lab and office, whether it was a silly question or advice on an experiment both of you were always there to lend a hand and thank you to all the past Avestro group members who have left a lasting imprint on my journey!

Thank you to the McGonigal group members for being great lab mates and for all the advice given after my research presentations and to all the technicians and the grad office in the department who helped keep all the show running. A massive thank you to Jenny, without you I would not have made it through my degree, you are amazing and a true credit to the department with your advice and support!

Generation Research, thank you for funding my MRes, there are not enough words to express how grateful I am for the opportunity you have given to me and others, it is truly amazing what you do and I cannot thank you enough.

To my family and friends, thank you for believing in me all the way and for listening to me talk about triangles and pretending I am not going mad! To Cy, I love you to the moon and back and am so grateful to have you in my life and thank you for trying to understand what I do, I will always look at the 'moth' crystal structure and think of you!

Finally, a huge thank you to me, you are stronger than you know and have grown so much as not only a chemist but as a person this year, remember to always give yourself grace and kindness and that you are amazing!

1. Introduction

1.1 Through-bond vs through-space conjugation in organic macrocycles

Macrocycles have become an increasingly important species in chemistry over the past 60 years from the discovery of crown ethers, by Pederson,[1] in 1967 to more recent compounds such as pillararenes and calixarenes that are being investigated due to their unique structures, functionalisation and host–guest abilities.[2–5] The ability to diversify macrocycles by functionalising the structure allows for use across a range of disciplines such as drug discovery,[6,7] catalysis,[8,9] material science,[10,11] and fundamental supramolecular chemistry. One of the challenges of functionalisied macrocycles is the synthesis required due to how difficult it is to form large rings with many functional groups.[12]

Through-space conjugation is an important non-covalent interaction that works alongside through-bond conjugation between π–units that can delocalise electrons through overlapping p-orbitals while influencing the electronic properties of a compound.[13] Although through-bond conjugation allows for π–electron transfer across bonds in a system, through-space conjugation enhances π–electron delocalisation through π-units that are interacting by intermolecular or intramolecular contacts.[14] One class of macrocycle that utilise through-space conjugation are cyclophanes, a cyclic system containing at least two atoms in an aromatic ring linked *via* aliphatic chains.[15] There have been many designs of cyclophanes, with one being synthesised by Stoddart and co-workers[16], known as the little blue box consisting of two 4,4′-bipyridinium units linked by *p*-xylene rings, to even bigger macrocycles such as a terylene diimide (TDI) cyclophane that also contain *p*-xylene linkers by Würthner *et. al* (Figure 1.1).[17]

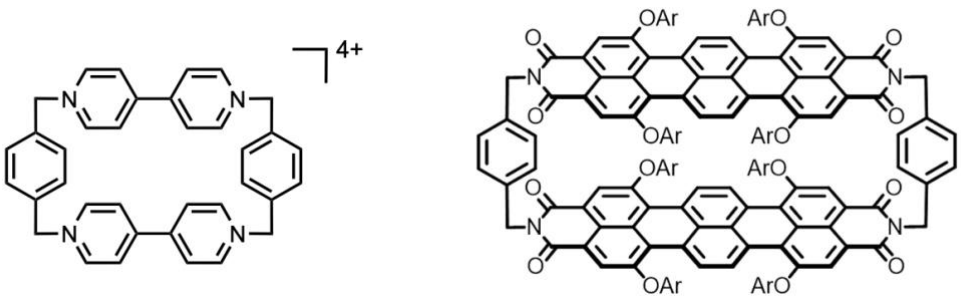

Figure 1.1 Structures of the little blue box (left)[16] and terylene diimide cyclophane (right)[17].

Through-space interactions can be measured by the distances between two π–units within the compounds (intramolecular) and the distances between two molecules (intermolecular) in the single crystal structures. Wang *et. al.*[18] synthesised a series of cyclophanes that include donor-acceptor π-units connected by *ortho*-xylene units that exhibit both intra- and intermolecular interactions. One of the compounds, named **C8BDT-NDI**, was synthesised by a Stille coupling reaction of a naphthalene diimide (NDI) moiety and a benzo-dithiophene (BDT) tin compound and single crystals of the cyclophane were grown by slow evaporation of toluene. X-ray diffraction analysis of **C8BDT-NDI**

demonstrates a closely packed structure with a distance of 3.4 Å between the BDT and NDI units, ideal for through-space charge transfer. Packing arrangement of the cyclophanes show interactions between *o*-xylene linkers and the BDT donor unit of one molecule to the acceptor unit (NDI) of another with a π–π distance of 3.7 Å further reinforcing the through-space conjugation (Figure 1.2)

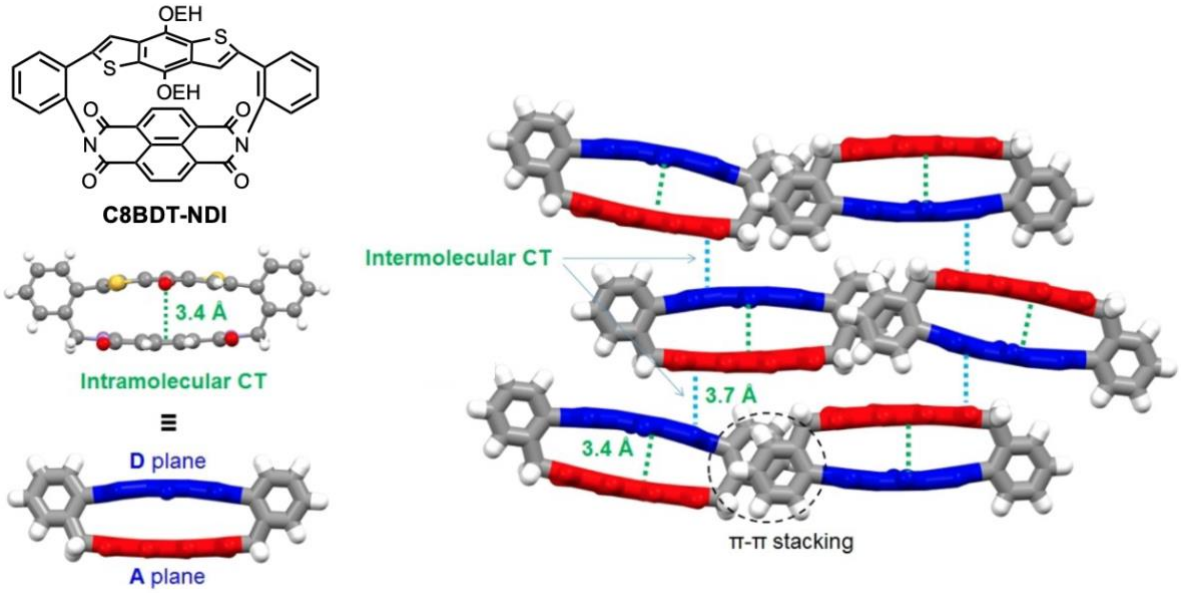

Figure 1.2 Single crystal X-ray structure of **C8BDT-NDI** (alkyl chains omitted for clarity) showing the intra- and intermolecular interactions.[18]

Theoretical calculations using density functional theory (DFT) at the B3LYP-D3BJ/6-31G(d) level in the gas phase were run to further establish the donor–acceptor interactions of **C8BDT-NDI** and the other synthesised cyclophanes. All four compounds show the HOMO localised on the donor units and the LUMO on the acceptor units, as expected, while the *o*-xylene linkers have minimal contribution in either energy level (Figure 1.3). Cyclophane **C8KZ-NDI** has the largest bandgap of this series (2.38 eV) because of the least destabilised HOMO energy level due to the carbazole unit having the weakest electron-donating strength of the three donor units. **C8DN-PDI**, a cyclophane made of a dihydroindolo-indole unit coupled with a perylene diimide (PDI) unit, has the most stabilised LUMO energy (−3.34 eV) and destabilised HOMO energy (−4.82 eV) compared to **C8BDT-NDI**, **C8KZ-NDI** and **C8DN-NDI** likely due to the strong electron deficient nature of the PDI unit and electron-donating capabilities of C8DN. The cyclophanes have a band gap energy ranging between 1.48–2.38 eV, the small band gap can be attributed to the intramolecular through-space conjugation between the donor and acceptor units within the macrocycle. This demonstrates how through-space conjugation has a positive influence on compounds and employs properties that enable the use as functional electronic materials.

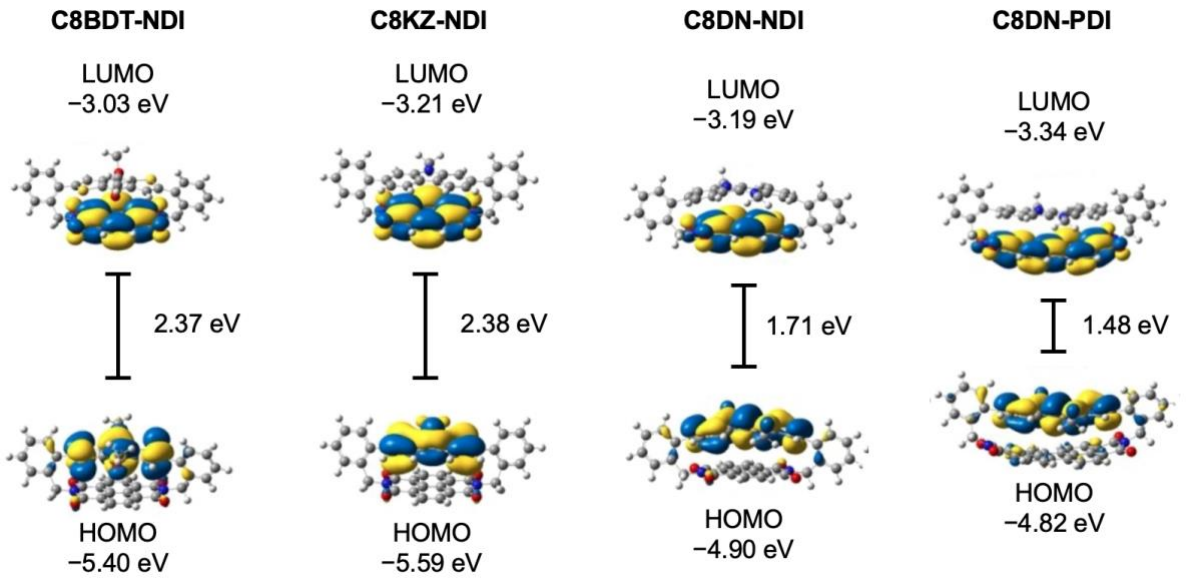

Figure 1.3 Geometry optimised MOs of **C8BDT-NDI**, **C8KZ-NDI**, **C8DN-NDI** and **C8DN-PDI** at the B3LYP/6-31G(d) DFT level.[18]

1.2 Aromatic diimide macrocycles

Rigid macrocycles that consist of aromatic diimide (ADI) linkers connected *via* an organic bridge have become vital redox–active compounds due to their ability to transfer electrons through the linkers by through-space conjugation.[19–21] The most common ADI linkers are naphthalene diimide (NDI),[19,22,23] pyromellitic diimide (PMDI),[20,24–26] and perylene diimide (PDI)[27–29] that engage in redox reactions to form multiple reduced states involving two electrons for each ADI. Barendt and coworkers have synthesised a cyclophane called the pink box containing two PDI units linked by *p*-xylene units at the bay position of the ADI (Figure 1.4.a).[30] The PDI macrocycle was formed by a multi-step synthesis that utilises a copper (I) catalysed "click" cycloaddition of an azide and alkyne in high-dilution conditions to obtain the compound in a 22% yield. Single crystals of the pink box were grown by slow vapour diffusion of methanol into a chloroform solution of the sample to provide further product confirmation and to establish any intramolecular interaction between the PDI units. X-ray analysis of the macrocycle shows axial chirality by each ADI unit because of the twisted (21º) aromatic framework which is complementary to the homochiral π–π stacking between the PDI units of the pink box (Figure 1.4.b). The intramolecular π–π distance between the PDI units is 3.7 Å demonstrating the through-space conjugation that allows for communication between the ADI units that stabilises the macrocycle for use as functional chiroptical materials.

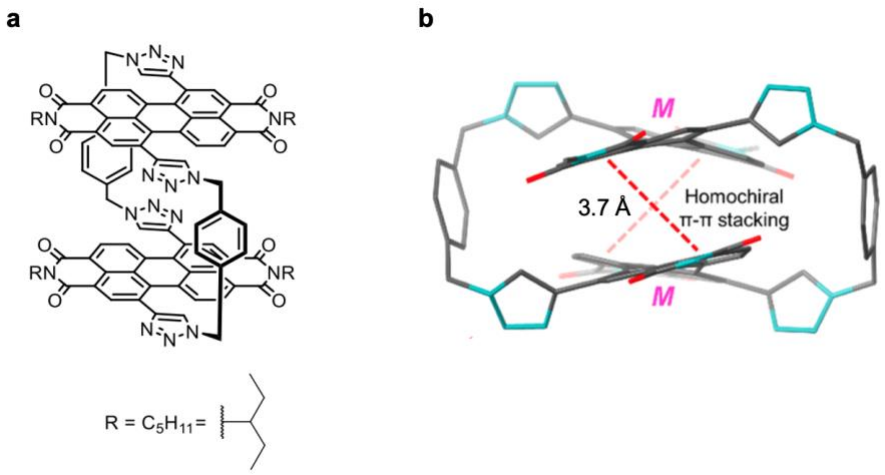

Figure 1.4 (a) Structure and (b) single crystal structure of the pink box.[30]

Due to the unique structural, optical and electronic properties, the ADI units have been employed in a series of cyclic dimers, trimers and tetramers linked by *trans*-1,2-diaminocyclohexane bridges. (Figure 1.5).[21,31] Each type of macrocycle offers different properties from the structural features to supramolecular chemistries to the electronic behaviour across each type of ADI. The synthesis of cyclohexane ADI macrocycles requires equal equivalents of aromatic dianhydride and either (*R,R*)- or (*S,S*)-*trans*-1,2-diaminocyclohexane reacted in *N,N*-dimethylformamide (DMF) or acetic acid at reflux for 24 h before purification by column chromatography to obtain the desired products.

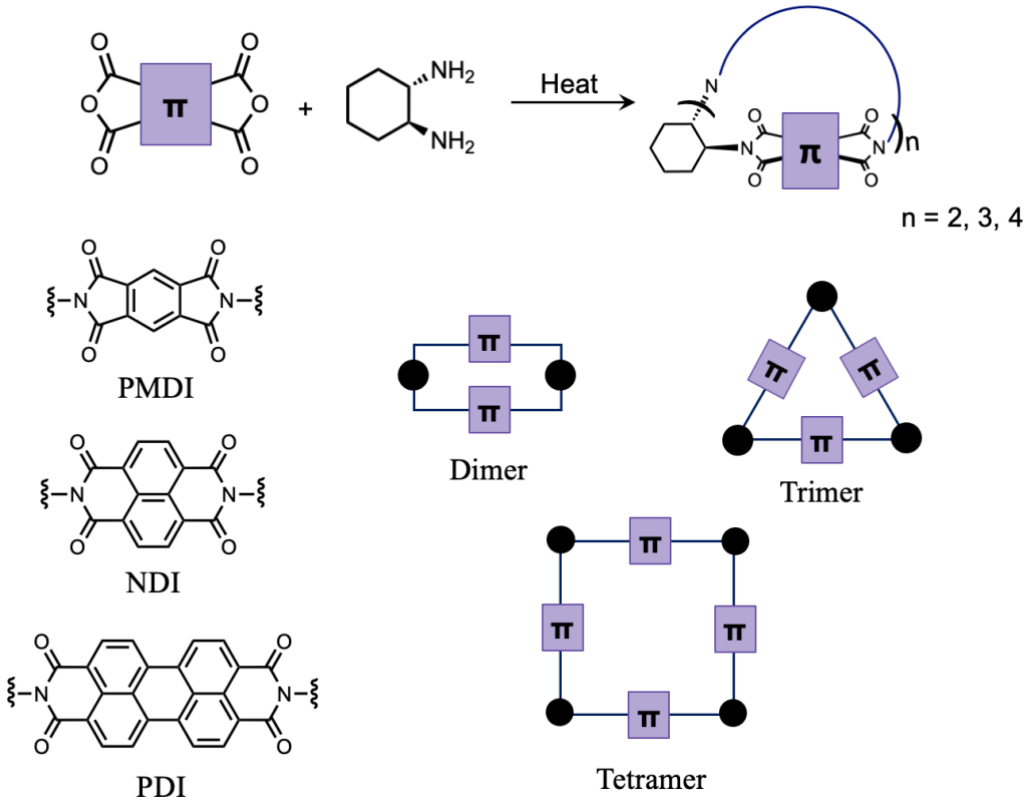

Figure 1.5 ADIs PMDI, NDI and PDI alongside schematic dimer, trimer and tetramer structures.

The smallest ADI, PMDI, has been used in procedures by Gawroński *et. al.*[26] to synthesise a dimer, (−)-**2PMDI**, consisting of two PMDI units that are connected by two cyclohexane bridges enabling the ADI units to stack over each other and a trimer, (−)-**3PMDIΔ** that has three PMDI units and cyclohexane bridges that take the form of a molecular triangle. To investigate how the organisation of the PMDI units influences the electronic properties, alongside (−)-**2PMDI** and (−)-**3PMDIΔ**, a reference molecule, **PMDI-ref**, containing one PMDI unit capped by a cyclohexane group was synthesised for comparison with the cyclic dimer and trimer. The redox properties were examined by Stoddart and coworkers by cyclic voltammetry (CV) and differential pulse voltammetry (DPV) analysis in a DMF electrolyte solution and recorded in a sweep covering 0 to -2.0 V (Figure 1.6).[20] DPV analysis gives greater insight into the redox processes than CV analysis because of the poor resolution of the CV reduction peaks. **PMDI-ref** shows two reduction peaks at −0.69 and −1.38 V (V vs Ag/AgCl) and (−)-**2PMDI**, whilst showing an almost identical CV profile to the reference molecule, has two additional peaks adding up to four reduction peaks at −0.41, −0.70, −1.73 and −1.92 V (V vs Ag/AgCl). (−)-**3PMDIΔ** has a profile with six single electron reductions peaks in two groups of three transitions at −0.61, −0.70, −0.77 and −1.33, −1.55, −1.72 V.

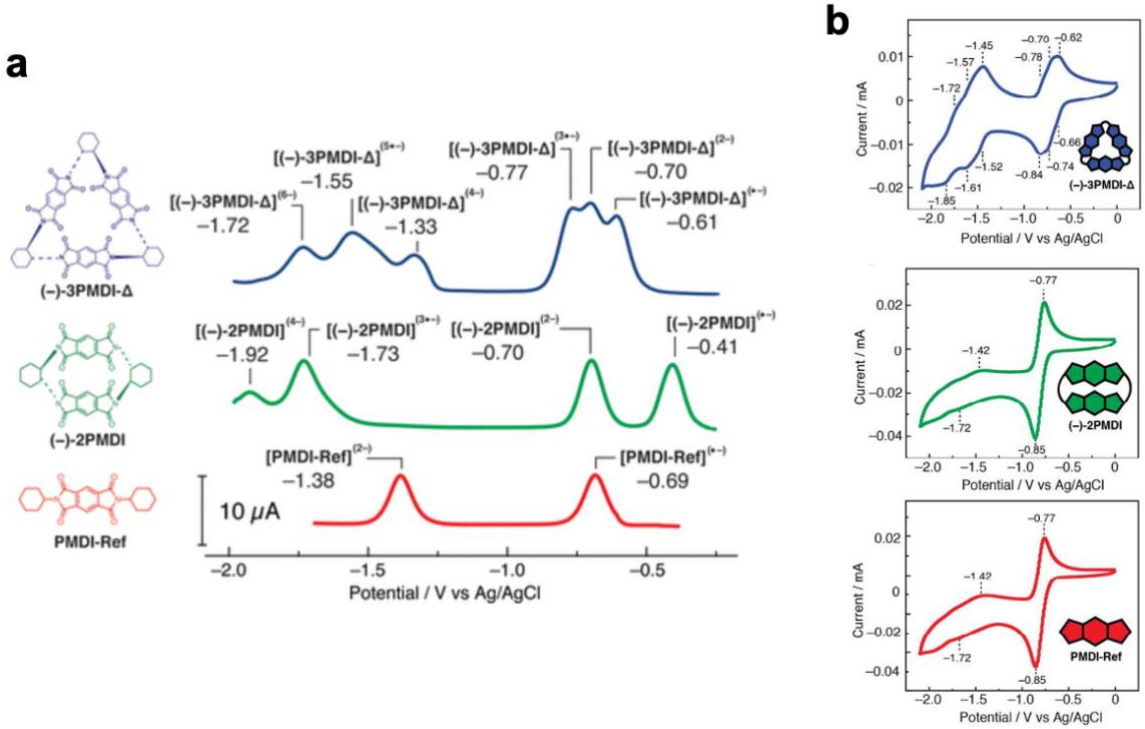

Figure 1.6 (a) DPV and (b) CV analysis of 1.0 mM solutions of **PMDI-ref**, (−)-**2PMDI** and (−)-**3PMDIΔ** in 0.1 M $TBAPF_6$ in DMF. Scan rate: 10 mV s^{-1}.[20]

To illustrate how increasing the π–surface area of the ADI within a macrocycle will influence the electronic properties, the smaller ADI molecular triangle (−)-**3PMDIΔ**, was compared with the larger molecular triangle, (−)-**3NDIΔ**, synthesised by Stoddart and co-workers.[19] CV analysis of the two

molecular triangles and their reference compounds (one ADI unit capped with cyclohexane) were carried out in a CH_2Cl_2 electrolyte solution to give the CV waves in Figure 1.7.[32] Compared to the reference compounds, both (−)-**3PMDIΔ** and (−)-**3NDIΔ** exhibit three times the amount of electron processes as expected due to the increased number of ADI units in the molecular triangles. While (−)-**3NDIΔ** has a wave with six single electron processes, (−)-**3PMDIΔ** only shows three single electron processes due to the other three processes occurring after the cut off for the voltage range in CH_2Cl_2. The half potential of the first reduction peak for (−)-**3NDIΔ** is more easily accessible than (−)-**3PMDIΔ** because the NDI units are more electron-deficient compared to the PMDI units. This experiment indicates that by increasing the π–surface area of the ADI unit within a molecular triangle, the electronics are improved by more easily accessible reduction peaks which is optimal for use in energy applications.

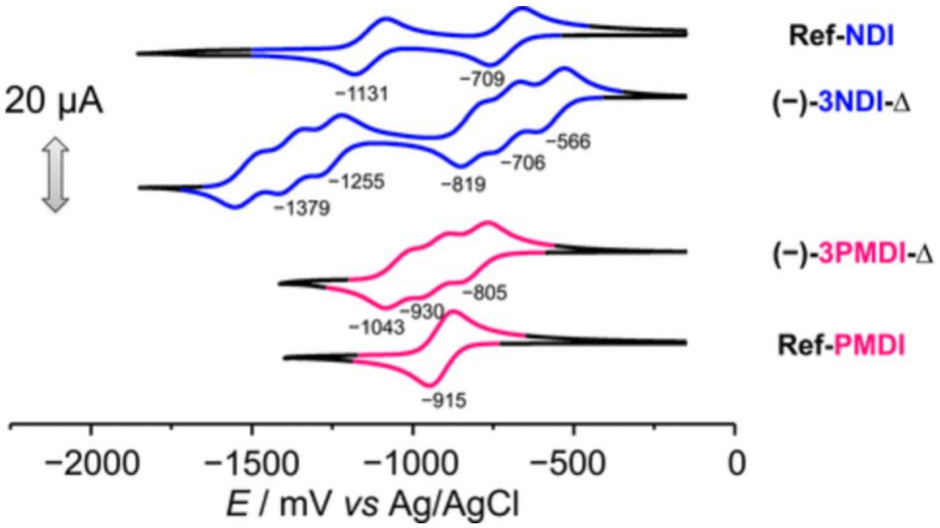

Figure 1.7 CV analysis of 1 mM solutions of **Ref-NDI**, (−)-**3NDIΔ**, (−)-**3PMDIΔ** and **Ref-PMDI** in 0.1 M $TBAPF_6$ in CH_2Cl_2.[32]

Alongside the molecular triangles containing three identical ADI units and three cyclohexane bridges, there have also been a series of isosceles molecular triangles that contain differing ADI units.[27,32] By employing alternate ADIs, characterisation of the through-space electron transfer pathways between the differing sizes of π–conjugated units can be established. Four isosceles triangles have been synthesised using PMDI and NDI as well as the largest ADI PDI in varying mixes of the three, (−)-**2NDI-1PMDIΔ**, (−)-**2PMDI-1NDIΔ**, (−)-**2NDI-1PDIΔ**, and (−)-**2PMDI-1PDIΔ** (Figure 1.8 and Figure 1.9). One of the main differences of the isosceles molecular triangles to the equilateral compounds is their single crystal packing arrangements. Molecular triangles (−)-**3NDIΔ** and (−)-**3PMDIΔ** form into one-dimensional (1D) columnar arrangements to form a prism like structure with interactions between the NDI and PMDI units, respectively.[19,20] However, the isosceles molecular triangles adopt a different formation highlighting the effects of the alternate ADI units, (−)-**2NDI-1PMDIΔ** does not display π–π stacking of the NDIs between two molecules or any interactions between a NDI and PMDI units. The switch of an

NDI for a PMDI unit means that there are no longer hydrogen bond interactions of the carbonyl oxygen on the ADI to a hydrogen atom on another molecule which is necessary for the columnar stacking (Figure X.X). In the case of (−)-**2PMDI-1NDIΔ**, the molecule triangles employ two types of helical supramolecular structures to form a (*P*)-dimer and an (*M*)-dimer due to two different interactions of the ADI units. The (*P*)-dimer forms because of π–π stacking between the PMDI and NDI unit of two molecules with a distance of 3.4 Å between the two, while the (*M*)-dimer is formed due to interactions between the NDI units of two different molecules with the same π–π stacking distance (3.4 Å) (Figure 1.8).

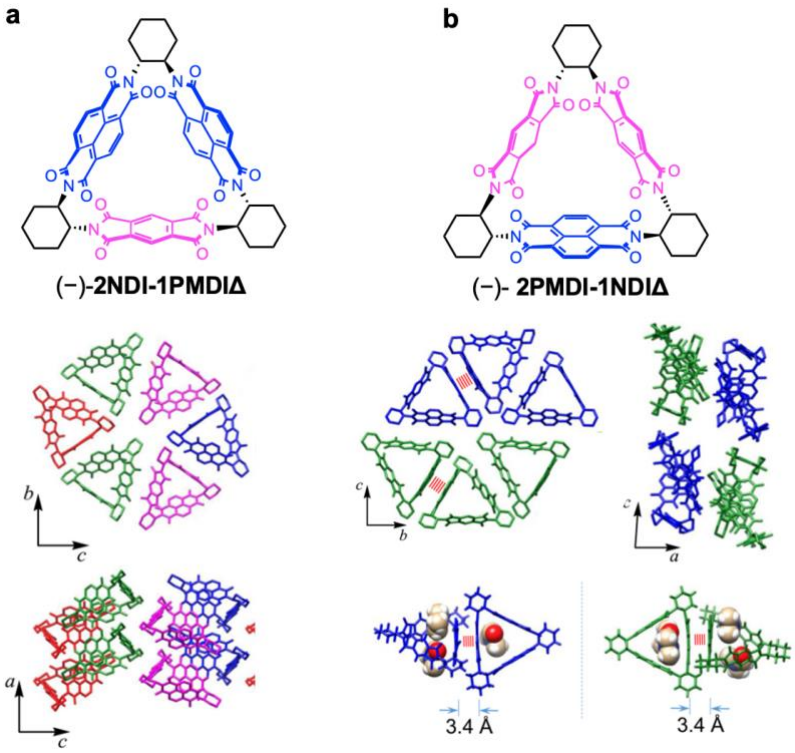

Figure 1.8 Single-crystal structures of a) (−)-**2NDI-1PMDIΔ** and b) (−)-**2PMDI-1NDIΔ** alongside their packing arrangements.[32]

The PDI isosceles molecular triangles form similar packing arrangements to each other of close to face-to-face π–π stacking (3.4 Å) between two PDI units of two molecules the compound. Although the PDI units are almost parallel, there is a slight offset in (−)-**2PMDI-1PDIΔ** of 0.6 Å vertically and 1.3 Å horizontally and (−)-**2NDI-1PDIΔ** shows a greater offset of 4.0 Å vertically and 2.0 Å horizontally. This is likely attributed to the fact that in (−)-**2PMDI-1PDIΔ** the PDI units are more bent because of the smaller size of the PMDI units compared to NDI allowing a larger π–surface area for π–π stacking. Also, the steric constraints of the cyclohexane bridges are lessened which support the overlap of the PDI units across the two molecules compared to (−)-**2NDI-1PDIΔ** (Figure 1.9). There was also a lack of hydrogen bonding seen between the carbonyl oxygen on any of the ADI units with a hydrogen atom

on another molecules ADI for both (−)-**2NDI-1PDIΔ** and (−)-**2PMDI-1PDIΔ** as well as an absence of interactions between NDI and PMDI units respectively.

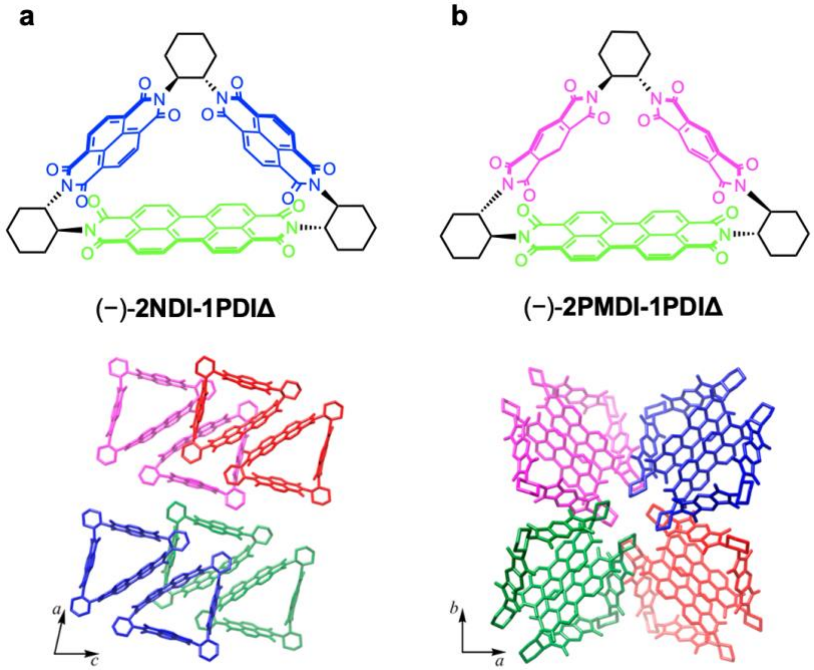

Figure 1.9 Single-crystal structures of a) (−)-**2NDI-1PDIΔ** and b) (−)-**2PMDI-1PDIΔ** alongside their packing arrangements.[27]

Geometry-optimised DFT structures of (−)-**2NDI-1PMDIΔ** and (−)-**2PMDI-1NDIΔ** were calculated at the B3LYP/6-31G* level of theory while (−)-**2NDI-1PDIΔ** and (−)-**2PMDI-1PDIΔ** were calculated at the M06-2X-D3BJ/6311G(d,p) level of theory in CH_2Cl_2. Although direct comparison of the energy levels for the four compounds cannot be made due to the different functionals used, insight can still be made from the positions of the molecular orbitals (MOs) of the HOMOs and LUMOs (Figure 1.10). For (−)-**2NDI-1PMDIΔ** and (−)-**2PMDI-1NDIΔ** the HOMOs are localised on the NDI units in both compounds while for (−)-**2NDI-1PMDIΔ** the LUMO and LUMO+1 are also localised on the two NDI units indicating the through-space conjugation between the NDI units for the first reductions. (−)-**2PMDI-1NDIΔ** also sees a similar pattern with the LUMO located on the single NDI unit in the compound however, the LUMO+1 is seen on the two PMDI units meaning the di- and tri-reduced states occur between the two conjugated ADI units. The PDI isosceles molecular triangles exhibit different patterns of where the MOs are localised, (−)-**2NDI-1PDIΔ** shows that although the HOMO is located on the PDI unit, the HOMO−1 is located on the two NDI units. The LUMO of (−)-**2NDI-1PDIΔ** is located on the PDI unit with partial conjugation to the NDI units meaning that the mono-reduced state occurs on the PDI unit with the di-reduced state on the NDI units. For (−)-**2PMDI-1PDIΔ** the HOMO−1 is delocalised across the cyclohexane bridging units and the PDI unit connecting the two bridges while the HOMO and LUMO are located on the PDI unit.

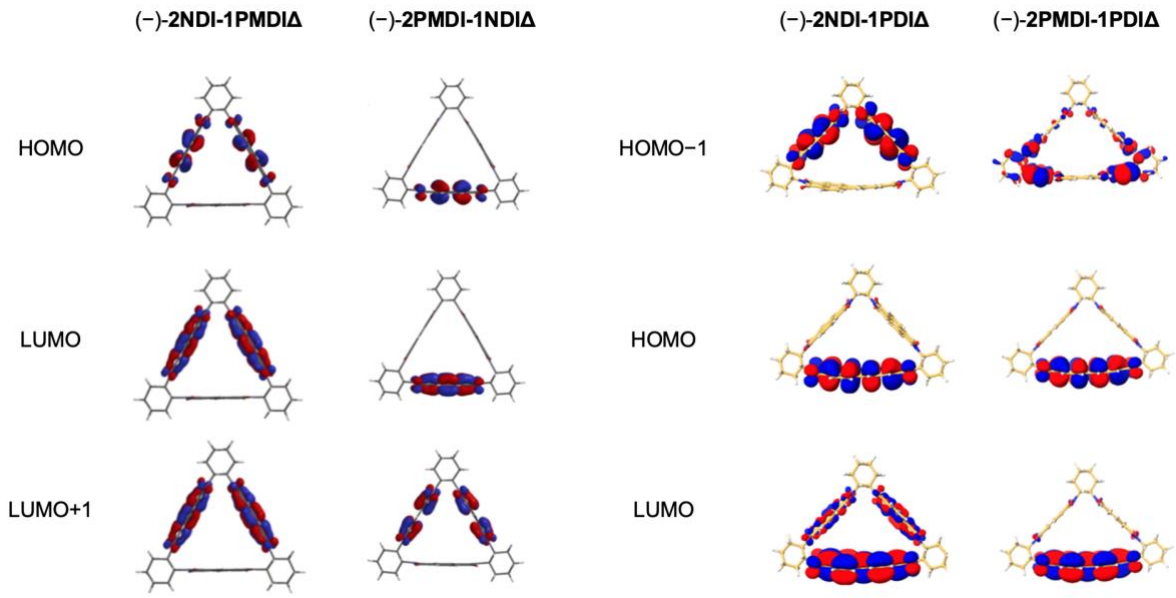

Figure 1.10 Visual representation of the HOMO, LUMO, and LUMO+1 of (−)-**2NDI-1PMDIΔ** and (−)-**2PMDI-1NDIΔ** calculated at the B3LYP/6-31G* level of theory,[32] and the HOMO−1, HOMO, and LUMO of (−)-**2NDI-1PDIΔ** and (−)-**2PMDI-1PDIΔ** calculated at the M06-2X-D3BJ/6311G(d,p) level of theory in CH_2Cl_2.[27]

A shape-persistent chiral molecular square, (+)-**4NDI□** and (−)-**4NDI□**, has been synthesised containing four NDI units and four cyclohexane bridges to investigate how the electronic communication differs from that of that smaller NDI macrocycles.[31] A stepwise synthetic approach isolated **4NDI□** in an overall yield of 8 % which is an improved yield from the one-pot condensation route (~1 %) (Figure 1.11). The first product formed from the stepwise reaction is (−)-**2NIA**, two NDI units connected by one cyclohexane unit, then (−)-**2NIA** is reacted with two equivalents of a Boc protected cyclohexane to make (−)-**2NIA-Boc**. The Boc protected compound is then deprotected with TFA to form (−)-**2NIA-NH_2** which is then reacted with (−)-**2NIA** in DMF at reflux to isolate (−)-**4NDI□** in a 20 % reaction yield and an 8 % overall yield.

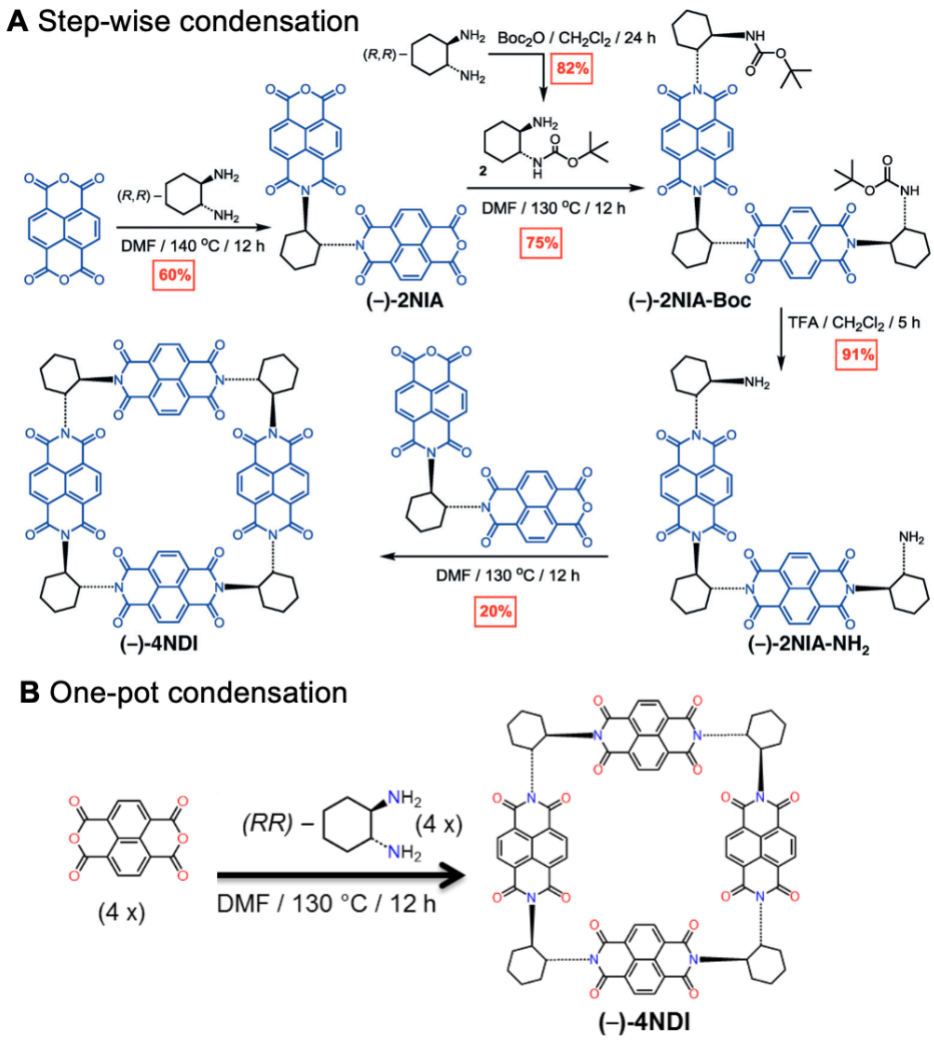

Figure 1.11 A Stepwise procedure to synthesis (−)-**4NDI**☐ and **B** One-pot condensation reaction to form (−)-**4NDI**☐.[31]

X-ray diffraction analysis of single crystals of (+)-**4NDI**☐ grown by slow vapour diffusion of *n*-hexanes into a chloroform solution of (+)-**4NDI**☐, shows a rigid macrocycle structure with an internal face-to-face cavity height of 11 Å (Figure 1.12). The superstructure of (+)-**4NDI**☐, displays two distinct molecules of the tetracycle that are held together by intermolecular hydrogen bonding (3.2 Å) of the carbonyl oxygen on one ADI interacting with the hydrogen atoms on the NDI unit on another molecule of (+)-**4NDI**☐. The top (+)-**4NDI**☐ is twisted by 45° compared to the teracycle underneath and the two (+)-**4NDI**☐ molecules stack to form infinite channels and the nanotubes of (+)-**4NDI**☐ stack closely together to form an ordered packing arrangement.

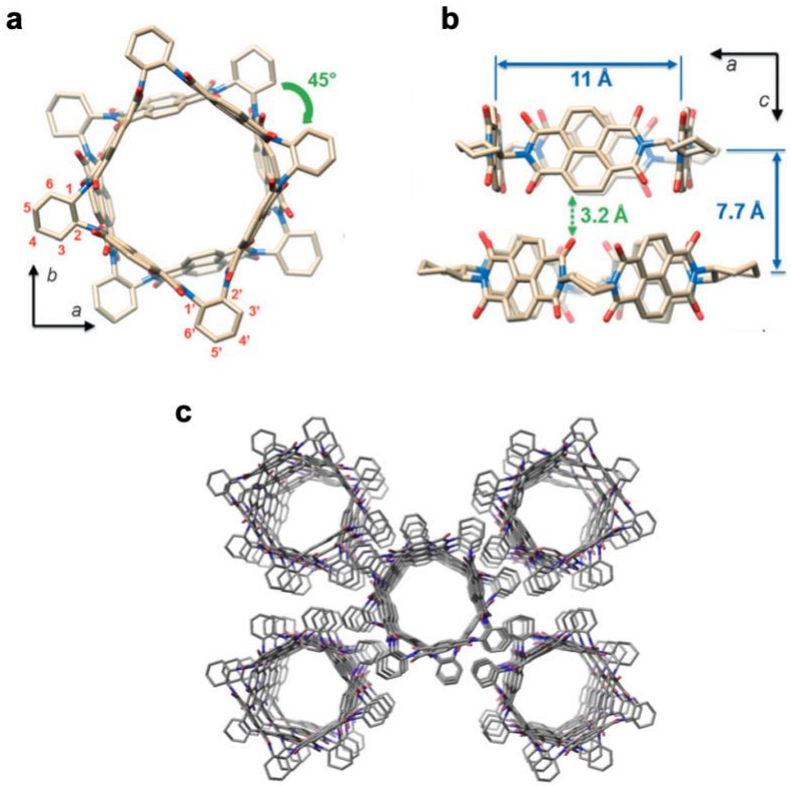

Figure 1.12 Single-crystal structures of a) Two (+)-**4NDI□** molecules down the *c* axis, b) Two (+)-**4NDI□** molecules down the *b* axis and c) Overall packing arrangement of (+)-**4NDI□** down the *c* axis.[31]

To compare the electronics of (−)-**3NDIΔ** and (−)-**4NDI□**, CV analysis was conducted in an electrolyte solution in CH_2Cl_2 to establish the reduction potentials of the electron processes in the macrocycles (Figure 1.13). The CV wave of (−)-**3NDIΔ** shows six distinct reversible one electron processes because of the strong global conjugation seen between the NDI units of the molecular triangle however, the tetracycle wave is less resolved. DPV analysis of (−)-**4NDI□** presents the first reduction peak at −0.71 V forms the mono-radical anion followed by a three-electron process at −0.85 V to form the tetra-reduced (−)-**4NDI□**. Then at −1.32 V a broad four-electron process occurs, which is surprising that the complete multi-electron reduction of (−)-**4NDI□** requires a small Columbic energy penalty meaning the tetracycle is an appealing compound for use in electronic materials because of the ability to accept up to eight electrons.

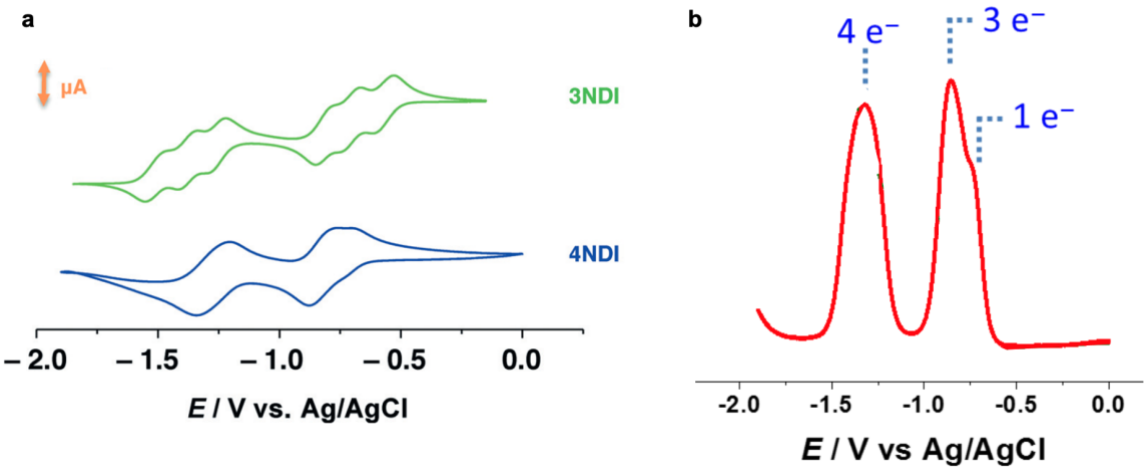

Figure 1.13 a) CV analysis of (−)-**3NDIΔ** and (−)-**4NDI□** and b) DPV of (−)-**4NDI□** (0.5 mM in CH_2Cl_2, 0.1 M $TBAPF_6$, 50 mV s^{-1}, 298 K).[31]

1.3 Overview

Up until now, the investigation of redox-active molecular triangles based on ADIs and 1,2-*trans*-diamines has been limited to the use of rigid cyclohexane vertices, which serve to pre-organise and ultimately guide the kinetically controlled macrocyclisation. No other *trans*-1,2-diamine bridges have been utilised to date, despite the fact that even slight shifts in the dihedral angle and macrocycle geometry could have profound influences on macrocycle assembly and packing (i.e. in the single-crystalline in the solid state) and through-space conjugation between ADI linkers, as shown by prior examples where the size of the ADI unit was varied to achieve these effects. This Master's by Research project has set out to expand the synthetic chemistry of ADI molecular triangles to include both acyclic and polycyclic aromatic *trans*-1,2-diamine bridges for the first time. Contrary to the fundamental belief that a rigid precursor offers the preorganisation necessary to encourage the macrocyclisation reaction,[12] acyclic derivatives have been employed to challenge the requirement for preorganisation. In this work, PMDI is used as a convenient and symmetric ADI building block, and both pre- and post-synthetic strategies have been explored to manipulate the bridge geometry. The influence of bridge geometry on the structural, electronic and electrochemical properties of novel PMDI molecular triangles is established using a combination of X-ray crystallography, absorption spectroscopy, electrochemistry, spectroelectrochemistry, and computational chemistry. The introduction of new functionality to molecular triangles at the vertex opens new opportunities for additional post-synthetic structure modification and novel supramolecular assembly or energy transfer phenomena that are currently not accessible with former ADI molecular triangle designs.

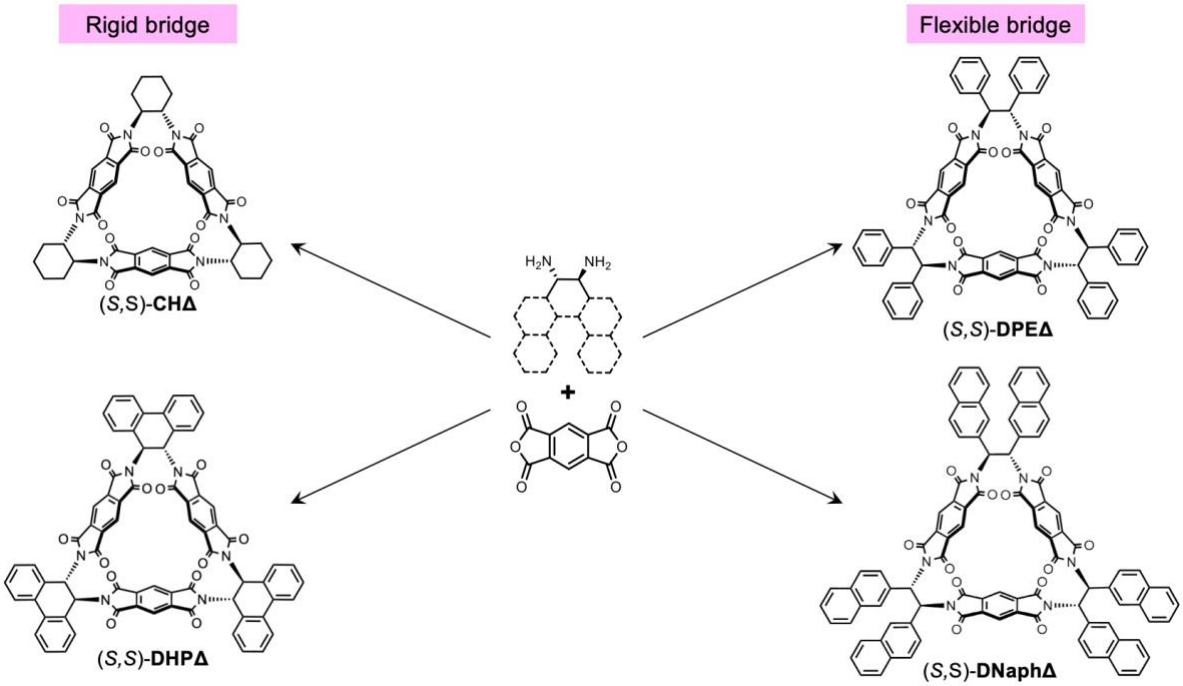

Figure 1.14 Structures of PMDI vertex modified molecular triangles.

2. Results and discussion

2.1 Macrocycle synthesis with chiral *trans*-1,2-ethanes

The first chiral acyclic molecular triangle synthesised utilised a commercially available diamine with two phenyl groups connected by an ethane bridge, (*S,S*)-1,2-diphenyl-1,2-ethylenediamine. The diamine was reacted with pyromellitic dianhydride (PMDA) in a similar procedure to **3PMDIΔ** (referred to as **CHΔ** in this thesis). Although DMF is a common solvent in ADI macrocyclisation reactions, the solvent molecules decompose into dimethylamine at the high temperatures needed to facilitate the reactions which can complicate the purification therefore acetic acid is a viable alternative as long as the diamine is soluble. After the diamine and PMDA were reacted in acetic acid for 16 h, the reaction mixture was purified by automated flash column chromatography on a silica column using a 5% gradient of acetone in CH_2Cl_2 before a trituration with acetone is used to remove any of the polymeric byproducts formed during the reaction. The molecular triangle, (*S,S*)-**DPEΔ**, was isolated as an off-white solid in a 21% yield, which is typical for this class of compound. [19,20,31–33] After the success of synthesising the first ADI molecular triangle with chiral acyclic aromatic vertices that was previously thought to be unattainable due to the less preorganised precursor, another acyclic derivative was applied with an extended π–system to test whether the design can be applied to other systems. A naphthyl diamine, (*S,S*)-1,2-di(naphalen-2-yl)ethane-1,2-diamine was reacted with PMDA under the same conditions used to isolate (*S,S*)-**DPEΔ** before purification by automated flash column chromatography on a silica column with a 5% gradient of acetone in CH_2Cl_2 followed by an acetone trituration to remove

the reaction by products. (*S,S*)-**DNaphΔ** was isolated as an off-white solid in a 39%, a nearly two-fold increase compared to (*S,S*)-**DPEΔ** demonstrating how less preorganised acyclic precursors can be applied in macrocyclisation reactions and that the steric hinderance of the dinaphthyl diamine may assist in the reaction.

Product characterisation was carried out using atmospheric pressure chemical ionisation high-resolution mass spectrometry (APCI-HRMS) which confirmed the protonated (*S,S*)-**DPEΔ** species, $[M+H]^+$, at m/z = 1183.2968. ^{1}H NMR analysis of (*S,S*)-**DPEΔ** shows the characteristic PMDI aromatic proton signal as a singlet at δ = 8.06 ppm alongside the aromatic protons of the phenyl vertices between 7.00 and 7.80 ppm (Figure 2.1). The PMDI proton signal was observed to be further downfield than those of the parent (*S,S*)-**CHΔ** macrocycle (δ = 8.03 ppm) and although there is only a 0.03 ppm difference, this suggests that the introduction of aromatic rings to the diamine bridge has a deshielding effect around the macrocycle structure because of the additional electrons altering the overall electronics of (*S,S*)-**DPEΔ**. There is also a notable downfield shift of 1.84 ppm of the protons on the ethane bridge next to the imide group in the modified molecular triangle due to the aromatic system adjacent to the environment, another indication of the change in electronics of the macrocycle.

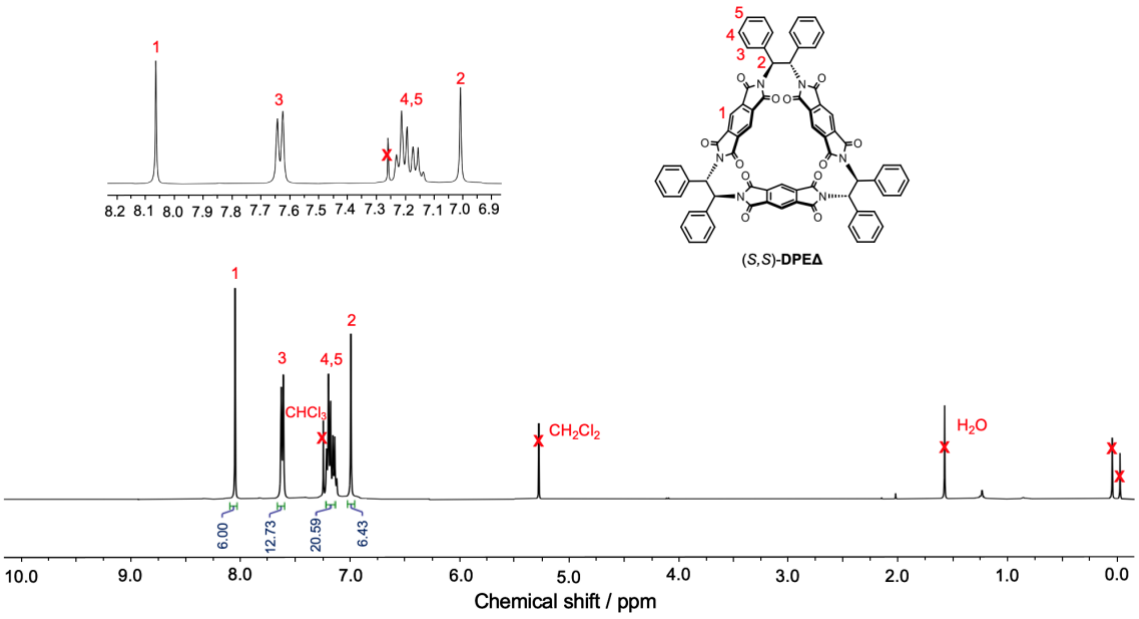

Figure 2.1 ^{1}H NMR spectra (400 MHz, $CDCl_3$, 298 K) of (*S,S*)-**DPEΔ**.

(*S,S*)-**DNaphΔ** was characterised by APCI-HRMS confirming the species $[M+H]^+$ at m/z = 1483.3938. ^{1}H NMR spectroscopic analysis conducted on (*S,S*)-**DNaphΔ** shows the characteristic PMDI aromatic proton signal as a singlet at δ_H 8.10 ppm and analogous signals for the dinaphthyl rings appearing between 7.20 and 8.00 ppm (Figure 2.2). The PMDI proton signal was observed to be even further downfield than those of (*S,S*)-**DPEΔ** (8.06 ppm) and **CHΔ** macrocycle (8.03 ppm), with an overall

downfield shift of 0.07 ppm from the parent macrocycle suggesting that increasing the size of the aromatic vertices further influences the deshielding around the macrocycle structure to a much greater degree. There is also a downfield shift 0.21 ppm of the alpha protons next to the nitrogen atoms compared to (*S,S*)-**DPEΔ**, due to the additional electrons from the naphthyl rings adding to the electronics of the entire compound.

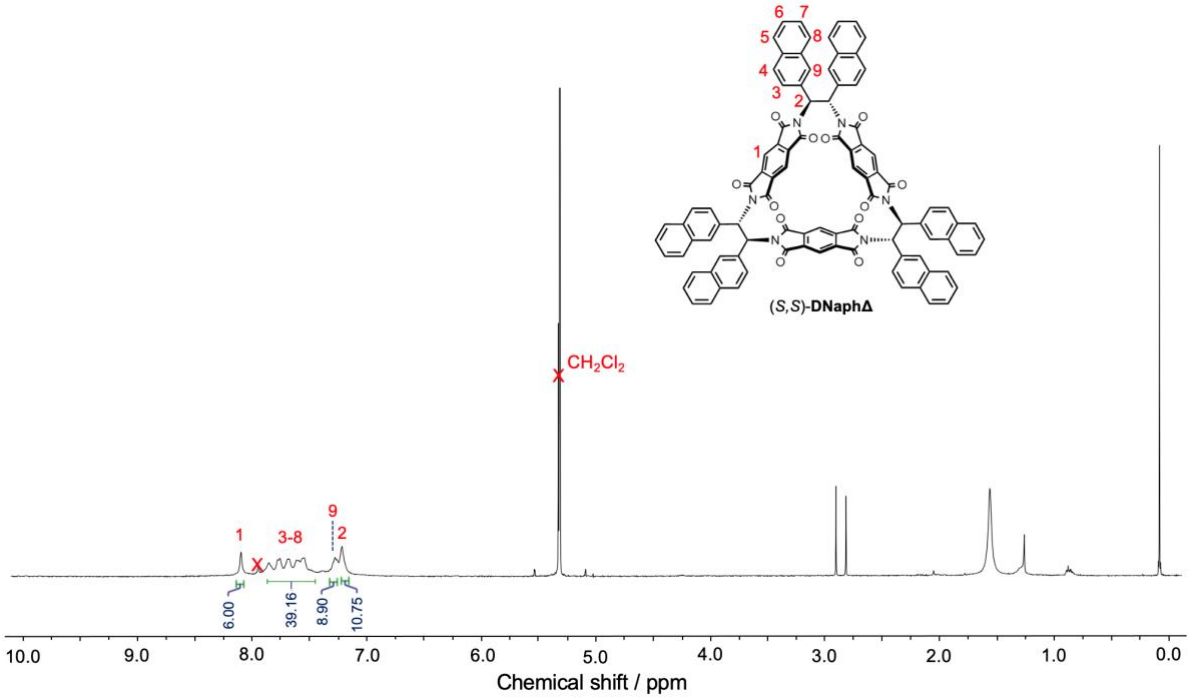

Figure 2.2 ^{1}H NMR spectra (400 MHz, CD_2Cl_2, 298 K) of (*S,S*)-**DNaphΔ**.

Unfortunately, due to solubility issues good quality single crystals of (*S,S*)-**DNaphΔ** were unable to be grown but, single crystals of (*S,S*)-**DPEΔ** were grown and analysed by X-ray diffraction to provide not only product confirmation but also provide detailed insights into what impact, if any, the lack of rigidity of the vertex has on macrocycle geometry and solid-state assembly behaviour. After several attempts to screen appropriate conditions, high quality crystals of (*S,S*)-**DPEΔ** were grown *via* slow vapour diffusion of acetone into a chloroform solution of the sample. Interestingly, the two triangles, (*S,S*)-**DPEΔ** and (*S,S*)-**CHΔ**, show similar cavity size of 9.6 Å measured as the distance between one of the vertices to the PMDI unit opposite to it, implying the rigidity of the pore formed by the PMDI is still maintained independent of the flexibility of the vertices. By modifying the vertices to remove the strain ((*S,S*)-**DPEΔ**), the average N-C-C-N dihedral angle decrease from 51.01º for the parent macrocycle, (*S,S*)-**CHΔ**, to 46.26º because the flexibility of the vertices allows the most favourable conformation that aligns the PMDI units (Figure 2.3). Inspection of the X-ray superstructure can also inform their supramolecular behaviour in solution (to an extent) as well as the properties in the solid state as porous materials. For instance, the superstructure of (*S,S*)-**CHΔ** shows a tubular arrangement of these triangular nanoprisms to form continuous one-dimensional (1D) channels that are stabilised by intermolecular π–

π stacking (3.18 Å) of adjacent PMDI units (Figure 2.3.a). On the other hand, (*S,S*)-**DPEΔ** reveals edge-to-face π-stacking (4.93 Å) of the phenyl vertices with no apparent interaction of the PMDI units or a uniform tubular arrangement that is seen in the superstructure of parent macrocycle, (*S,S*)-**CHΔ** (Figure 2.3.b). This is likely due to the positioning of the phenyl rings causing steric hinderance between adjacent molecules of (*S,S*)-**DPEΔ**. Therefore, the vertex engineering of molecular triangles not only influences the electronic properties of the molecule but also modulate the self-assembly of these molecules. Further insights into the impact of the strain induced by the vertices on the properties of the molecular triangles can be achieved by the development of rigid analogues of these systems, which will be explored in the following section

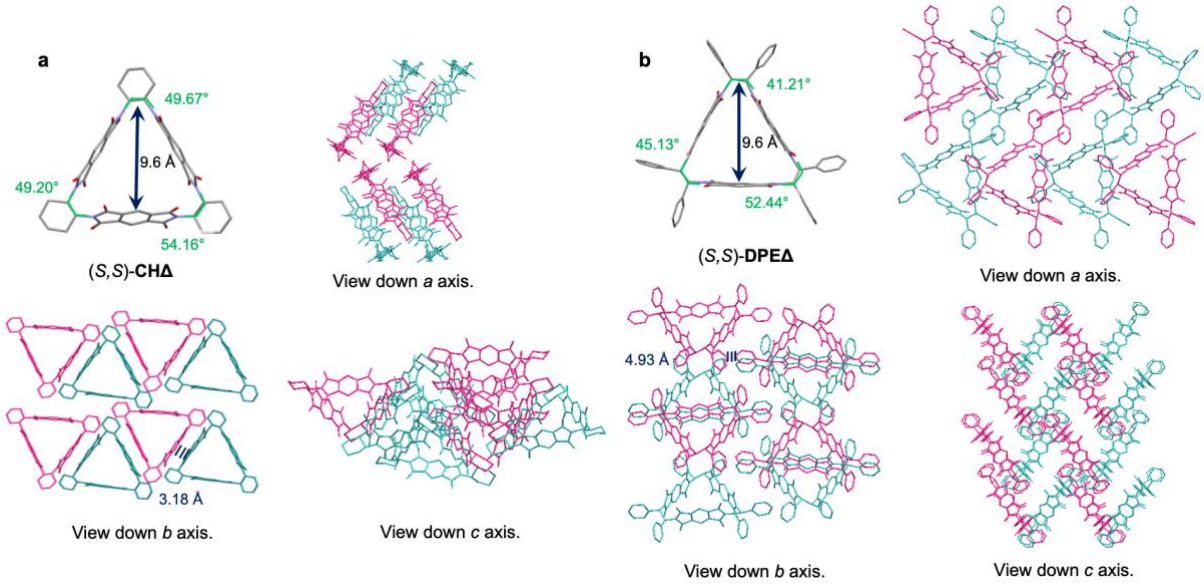

Figure 2.3 Single crystal structure and packing arrangements of (a) (*S,S*)-**CHΔ** and (b) (*S,S*)-**DPEΔ**.

2.2 Macrocycle synthesis with chiral *trans*-1,2-cyclohexanes

Investigations into how a more rigid system on the vertices of PMDI molecular triangles will influence the structural and electronic properties by inducing more strain into the macrocycle compared to the acyclic counterparts can be made by employing an oxidative cyclodehydrogenation reaction on (*S,S*)-**DPEΔ** and (*S,S*)-**DNaphΔ**. Given the established chemistry for Scholl oxidation to occur between 1,2-diphenyl compounds (Figure 2.4), this chemistry was explored in the context of (*S,S*)-**DPEΔ** and (*S,S*)-**DNaphΔ** to see if it would be possible to post-synthetically prepare cyclohexane bridged molecular triangles in a single atom-efficient step. Although the exact mechanistic pathway of the Scholl oxidation is unknown, two pathways have been proposed that form an arenium cation or a radical cation.[34] Both of the pathways eliminate H_2 with assistance of a Lewis acid and a catalyst to form a new C-C bond as shown in Figure 2.4 by the reaction of *o*-terphenyl.[35,36] A variety of oxidants can be used in a Scholl oxidation such as 2,3-dichloro-5,6-dicyano benzoquinone (DDQ) alongside a sulfonic acid, iron (III)

chloride ($FeCl_3$), aluminium (III) chloride ($AlCl_3$), molybdenum pentachloride ($MoCl_5$) and copper (II) chloride ($CuCl_2$).[37–39]

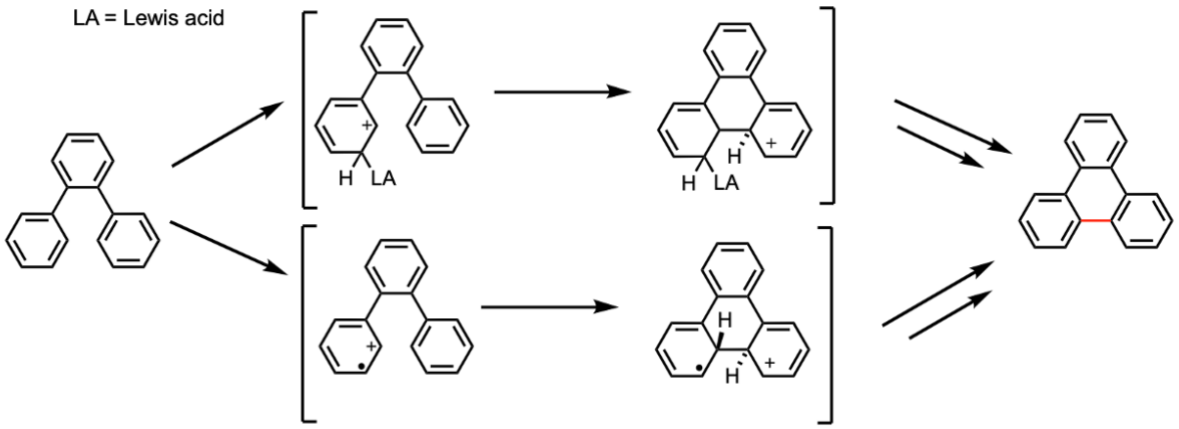

Figure 2.4 Mechanistic pathways of the Scholl oxidation of *o*-terphenyl by an arenium cation (top) and radical cation (bottom) intermediate.

Here, (*S,S*)-**DPEΔ** was subjected to a series of oxidation reactions using DDQ and $FeCl_3$ to establish which conditions facilitate the reaction and if so, optimise the synthesis of (*S,S*)-**DHPΔ**. Firstly the diphenyl molecular triangle was reacted with DDQ and methane sulfonic acid in CH_2Cl_2 at 0 ºC under inert conditions, to prevent any side reactions with air or moisture, (Table 2.5, entry 1) for two hours while being monitored by ^{1}H NMR analysis. Then (*S,S*)-**DPEΔ** was reacted with DDQ again but with trifluoromethane sulfonic acid, a higher strength acid, under the same conditions as the first reaction and was also monitored by ^{1}H NMR analysis (Table 2.5, entry 2). Finally, (*S,S*)-**DPEΔ** was reacted with $FeCl_3$ in CH_2Cl_2 and CH_3NO_2 (to help with the solubility of $FeCl_3$) at room temperature under an inert atmosphere (Table 2.5, entry 3). Unfortunately, none of the reactions allowed for conversion of (*S,S*)-**DPEΔ** to (*S,S*)-**DHPΔ** and only the starting material was seen in the reaction mixture by ^{1}H NMR analysis.

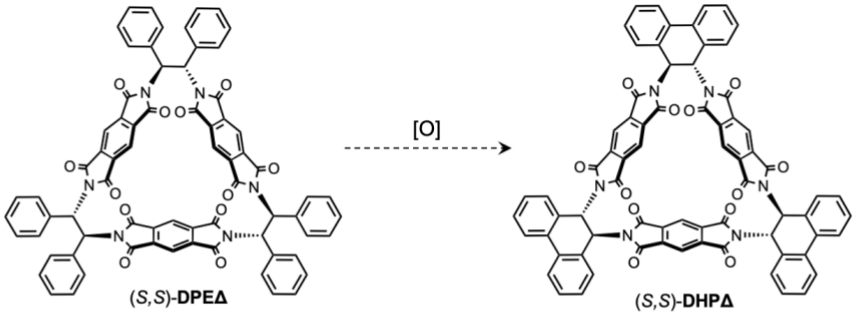

Condition	Oxidant	Acid	Solvent	Temperature	Time / h	Conversion? (by ^{1}H NMR)
1	DDQ	CH_3SO_3H	CH_2Cl_2	0 °C	2	SM
2	DDQ	CF_3SO_3H	CH_2Cl_2	0 °C	2	SM
3	$FeCl_3$	-	CH_2Cl_2/CH_3NO_2	rt	2	SM

Figure 2.5 Oxidation conditions for conversion of (*S,S*)-**DPEΔ** to (*S,S*)-**DHPΔ**.

Although the oxidative cyclodehydrogenation reaction of (*S,S*)-**DPEΔ** was unsuccessful, because (*S,S*)-**DNaphΔ** has additional electron density on the vertices compared to the other acyclic molecular triangle, there is a likely chance that the naphthyl groups will serve as directing groups for the C-C bond formation. (*S,S*)-**DNaphΔ** was subject to an array of NMR scale reactions in deuterated solvents so direct monitoring of the reaction could be conducted, firstly (*S,S*)-**DNaphΔ** was reacted with $FeCl_3$ in CD_2Cl_2 and CD_3NO_2 at room temperature under inert conditions for 72 h with ^{1}H NMR monitoring at frequent intervals until 72 hours (Table 2.6, entry 1). The molecular triangle was also reacted with $AlCl_3$, $MoCl_5$ and DDQ with trifluoromethane sulfonic acid at room temperature under inert conditions for 72 h as well (Table 2.6, entries 2, 3 and 4). Even with the variety of oxidants used, there was no conversion of (*S,S*)-**DNaphΔ** to (*S,S*)-**DHNaphΔ** in any of the reactions seen by ^{1}H NMR analysis.

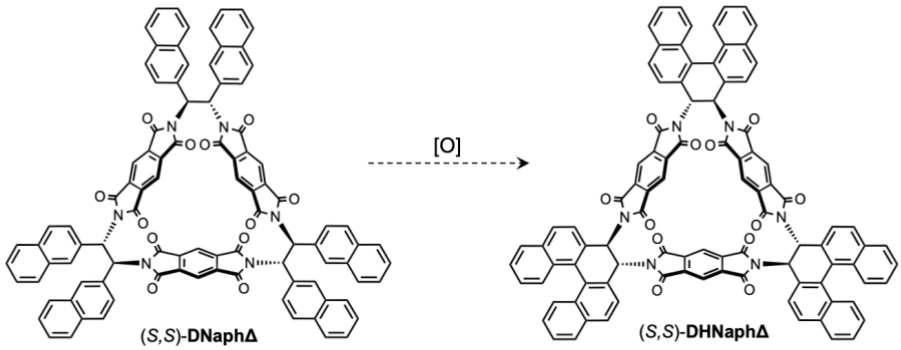

Condition	Oxidant	Additive	Solvent	Temperature	Time / h	Conversion (by ^{1}H NMR)
1	$FeCl_3$	-	CD_2Cl_2/CD_3NO_2	rt	72	SM
2	$AlCl_3$	-	CD_2Cl_2	rt	72	SM
3	$MoCl_5$	-	CD_2Cl_2	rt	72	SM
4	DDQ	CF_3SO_3H	CD_2Cl_2	rt	72	SM

Figure 2.6 Oxidation conditions for conversion of (*S,S*)-**DNaphΔ** to (*S,S*)-**DHNaphΔ**.

Even though these initial attempts at oxidative cyclodehydrogenation reactions have not afforded the desired products (*S,S*)-**DHPΔ** and (*S,S*)-**DHNaphΔ**, there are still options to induce harsher conditions such as increasing the temperature and adding stronger acids to aid the reaction. If the reaction conditions can be established for the oxidation reaction, the possibilities open to synthesise the completely aromatised form of (*S,S*)-**DHPΔ** and (*S,S*)-**DHNaphΔ**, (*S,S*)-**PhenΔ** and (*S,S*)-**HeliΔ** respectively (Figure 2.7), to investigate how an even more strained system influences the global conjugation of the macrocycles.

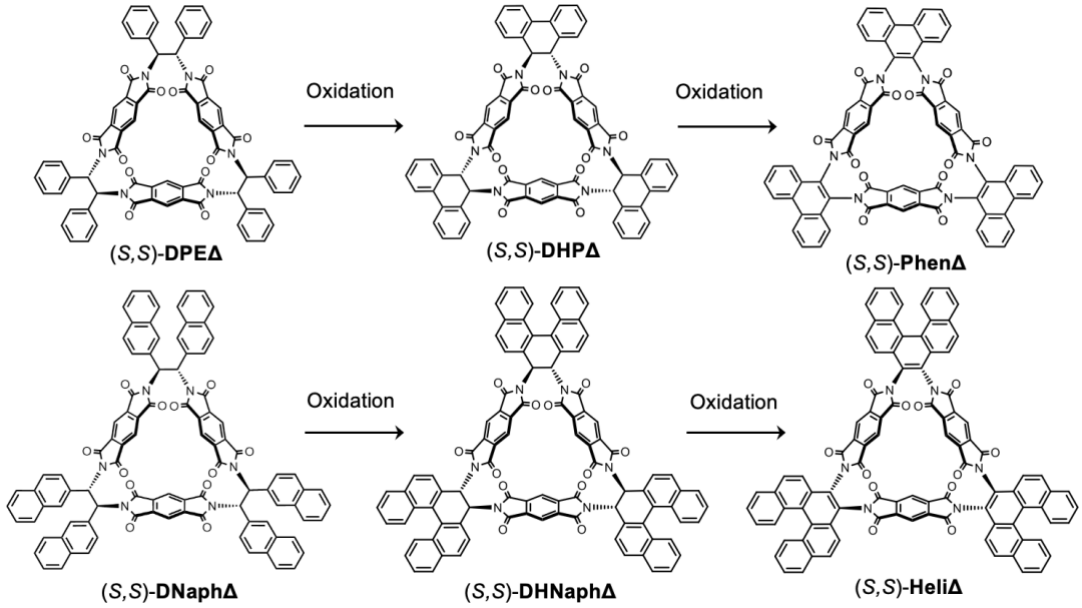

Figure 2.7 Structures of vertex engineered PMDI molecular triangles.

Another way to form (*S,S*)-**DHPΔ** is by synthesising the dihydrophenanthrene diamine precursor and then reacting with PMDA in a macrocyclisation. Originally the synthesis of diamine **6** was attempted according to procedures reported by Liu *et. al.*[40] because the dihydrophenanthrene diamine is not commercially available, which took advantage of orthogonal protecting group and diastereomeric resolution strategies to isolate pure 1,2-*trans*-diamine enantiomers. In our hands, while it was possible to reproduce the synthesis of (*R,R*)- and (*S,S*)-**6** faithful to the original report, the yields of the diastereomeric resolution steps were always low owing to the difficult separation by column chromatography. To eliminate the complicated diastereomeric resolution step, a robust enantiomeric resolution procedure was employed that utilises enantiopure tartaric acid to isolate the enantiomers of diamines as salts.[41,42] A racemic mixture of *trans*-1,2-diaminocyclohexane is reacted with either *D*-(-) or *L*-(+)-tartaric acid, depending on whether the (*S,S*)- or (*R,R*)- enantiomer is required to be isolated, in water and acetic acid at room temperature before being placed in the fridge overnight. Then the tartrate salt of the diamine precipitates out of the solution and is washed and filtered for isolation. Before the enantiomeric resolution steps, compounds **2**-**4** were synthesised using a Suzuki homo-coupling of 2-bromobenzaldehyde to form dicarbaldehyde **2**, then aldehyde-imine **3** is synthesised by a nucleophilic

attack of *S-tert*-butylsulfinimide on **2**. Finally, the fully protected diamine **4** is made by an aminative cyclisation reaction as a mixture of the (*S,S*)- and (*R,R*)- isomers (Figure 2.8).[40]

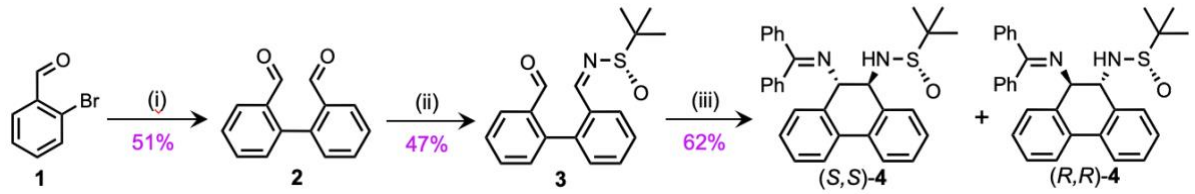

Figure 2.8 (i) B_2pin_2, $Pd(OAc)_2$, PPh_3, K_2CO_3, 1,4-dioxane, N_2, 80 °C, 24 h (ii) (*S*)-*tert*-butylsulfinimide, Cs_2CO_3, CH_2Cl_2, N_2, 40 °C, 12 h (iii) 2,2'-diphenyl glycine, K_2CO_3, THF-H_2O (7:3 v/v), 40 °C, 48 h.

The first stage before the enantiomeric resolution step is to obtain the racemic mixture of diamine **6**, by a global deprotection on (*S,S*)-**4** and (*R,R*)-**4** using a strong acid and reacting for one hour before isolating the dichloride ammonium salt from the reaction mixture. The salt is then neutralised to obtain *rac*-**6**, with product confirmation by ^{1}H NMR analysis (Figure S1.22). Then the racemic mixture is reacted with either *D*-(-) or *L*-(+)-tartaric acid in water and acetic acid at room temperature before being placed in the fridge (4 ºC) overnight. Unfortunately, unlike the cyclohexane counterpart, the dihydrophenanthrene salt does not precipitate out of the reaction mixture so an aqueous work-up is then performed instead to isolate either the (*S,S*)- or (*R,R*)-tartrate salt **7** in a 66% or 71% yield (with respect to the corresponding starting enantiomer in the racemic mixture of **6**), respectively, before being neutralised with a base to isolate the free diamine, (*S,S*)-**6** or (*R,R*)-**6** (Figure 2.9). The difference of the yields between (*S,S*)-**6** and (*R,R*)-**6** is likely due to the difficulty of isolating the diamine due to the compound favouring both the aqueous and organic layers.

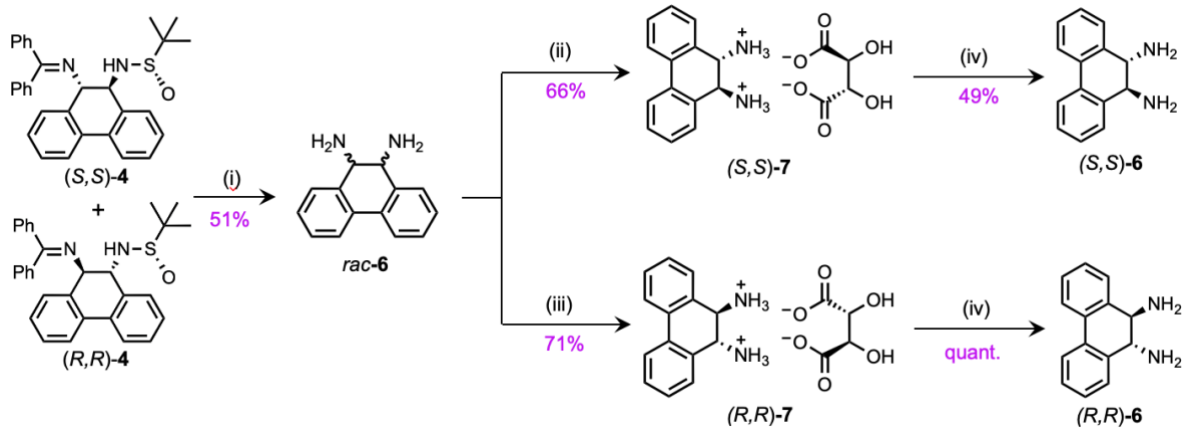

Figure 2.9 (i) 6 M HCl, THF, rt, 1 h (ii) (*D*)-(-)-tartaric acid, H_2O, AcOH, rt to 4 °C
(iii) (*L*)-(+)-tartaric acid, H_2O, AcOH, rt to 4 °C (iv) K_2CO_3, H_2O, CH_2Cl_2-MeOH (2:1 v/v), rt.

Diamine (*R,R*)-**6** is reacted in a one-pot condensation with PMDA in DMF at reflux overnight to obtain a crude mixture of (*R,R*)-**DHPΔ**, polymeric and higher order macrocyclic counterparts. DMF is used as

the solvent in this reaction rather than acetic acid due to there being increased reactivity of diamine **6** with acetic acid that elicit side reactions that complicate the purification. The reaction mixture was then purified by automated column chromatography and an acetone trituration, removing most of the reaction impurities. However, ^{1}H NMR analysis (Figure 2.10) shows the presence of a higher order macrocycle that could not be removed. From previous work within our research group, the unknown macrocycle has been confirmed as the tetrameric counterpart to (*R,R*)-**DHPΔ** known as (*R,R*)-**DHP□**, due to the similarities seen by ^{1}H NMR analysis of the unmodified derivative. [The same procedures were carried out for the (*S,S*) enantiomer and similar observations to the (*R,R*) were seen.] As the two macrocycles have similar polarity, purification by a recrystallisation using acetone and hexane after automated flash column chromatography was necessary (and only achieved successfully once) to obtain a small sample of (*S,S*)-**DHPΔ** from a mixture of (*S,S*)-**DHPΔ** and (*S,S*)-**DHP□** that was analytically pure enough for ^{1}H NMR analysis. Although attempts of separation by recrystallisation and trituration were made, isolation of a significant amount of pure **DHPΔ** and **DHP□** for complete structural, electronic and optical characterisation was not successful for either enantiomer.

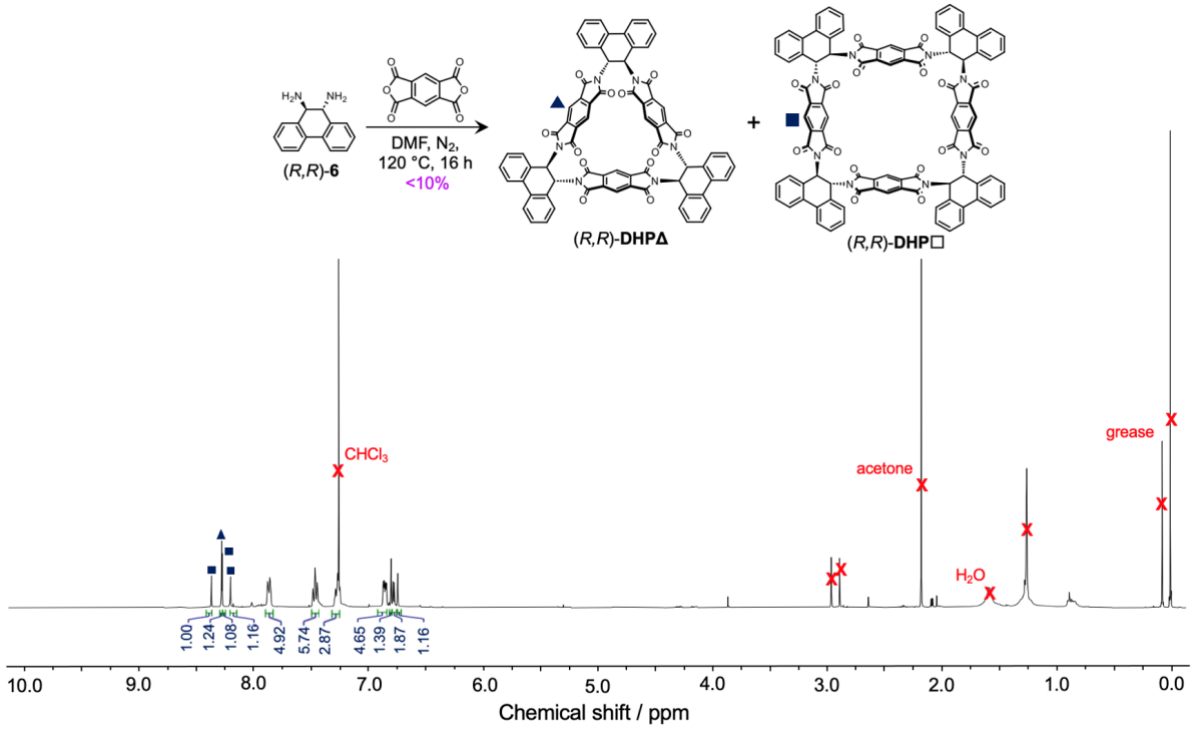

Figure 2.10 ^{1}H NMR spectra (400 MHz, 298 K, $CDCl_3$) of (*R,R*)-**DHPΔ** and (*R,R*)-**DHP□**.

The mixture of macrocycles was characterised by APCI-HRMS, confirming the species $[M+H]^+$ at *m/z* = 1177.2488 and 1569.3209 respectively. ^{1}H NMR spectroscopic analysis carried out on (*S,S*)-**DHPΔ** and (*S,S*)-**DHP□** shows a singlet at 8.28 ppm corresponding to the molecular triangle PMDI proton environment alongside three other singlets from 8.20 to 8.40 ppm that represent the molecular square (by comparison to a pure sample of (*S,S*)-**DHPΔ**, Figure 2.11). There is a significant shift in the PMDI proton signal compared to **CHΔ** likely due to the improvement of electronic communication around the

compound thanks to the bond linking the aromatic rings. In the aromatic region from 6.70 to 7.95 ppm there are signals corresponding to the dihydrophenanthrene vertex protons of both (*S,S*)-**DHPΔ** and (*S,S*)-**DHP□** that show broadening due to there being overlapping peaks.

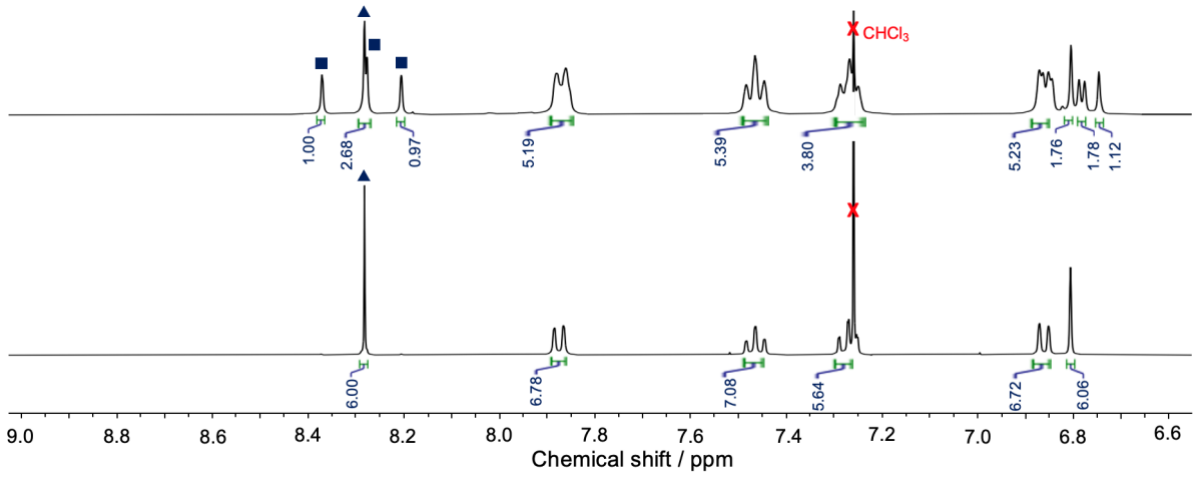

Figure 2.11 ^{1}H NMR spectra (400 MHz, 298 K, $CDCl_3$) of a mixture of (*S,S*)-**DHPΔ** and (*S,S*)-**DHP□** (top) and pure (*S,S*)-**DHPΔ** (bottom).

Comparison of the molecular triangles synthesised so far show an increasing downfield shift of the PMDI proton signal, from 8.03 to 8.28 ppm, indicating a positive change in the global conjugation due to the electronic influence of vertex groups on the overall electronic structure. There is also a change in the chemical shift of the alpha protons next to the imide group with the biggest difference between (*S,S*)-**CHΔ** and (*S,S*)-**DNaphΔ** (2.05 ppm) demonstrating how the extended π–system is contributing to the electronics of the molecular triangles (Figure 2.12). In particular, the Δδ effect of the PMDI aromatic proton signals appears to correlate to the increasing rigidity of the diamine linker — a promising indication that macrocycle electronics could potentially be tuned *via* vertex engineering.

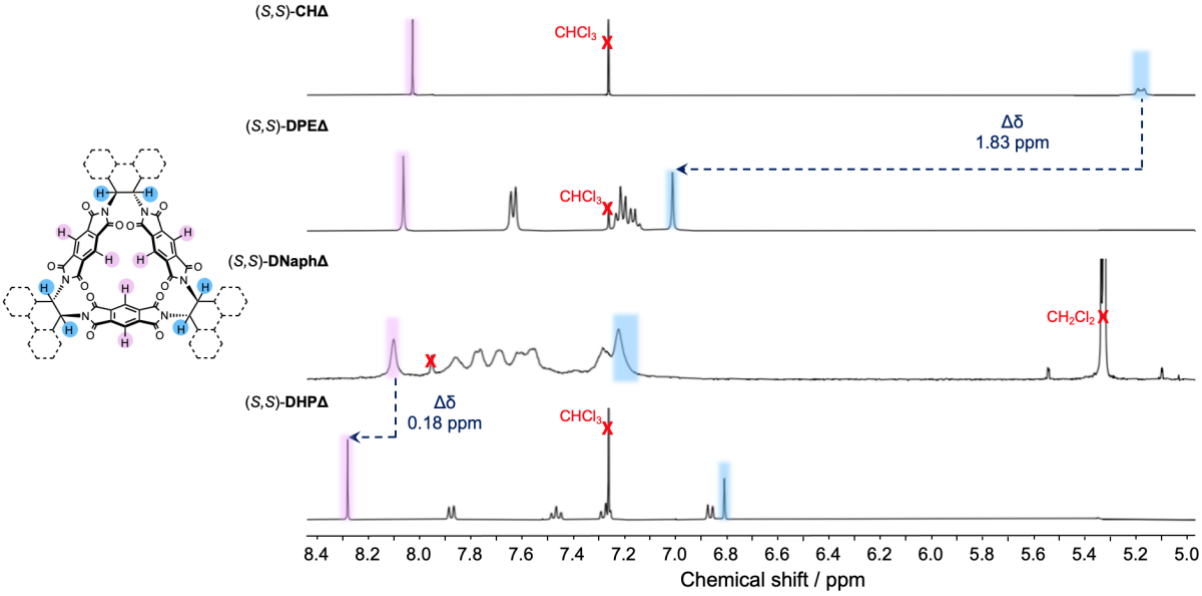

Figure 2.12 ^{1}H NMR spectra (5.0–8.4 ppm) of (*S,S*)-**CHΔ**, (*S,S*)-**DPEΔ**, (*S,S*)-**DNaphΔ** and (*S,S*)-**DHPΔ** highlighting the PMDI (pink) and the cyclohexane proton environments (blue).

The molecular triangles presented in this thesis have shown symmetrical structures which is confirmed by a singlet for the PMDI proton environments in ^{1}H NMR analysis and further confirmation through X-ray crystal analysis. However, ^{1}H NMR analysis in $CDCl_3$ of (*S,S*)-**DHPΔ** shows a singlet for the PMDI aromatic proton signal at 8.28 ppm but also an additional three singlets at 8.37, 8.27 and 8.21 ppm accounting for a tetracycle, confirmed by APCI-HRMS. Previous work in our research group has shown that in different solvents the parent tetracycle, (*S,S*)-**CH□**, can adopt either a D_4, C_2 or a mixture of the two conformations, confirmed by single crystal structures and ^{1}H NMR analysis (Figure 2.13).

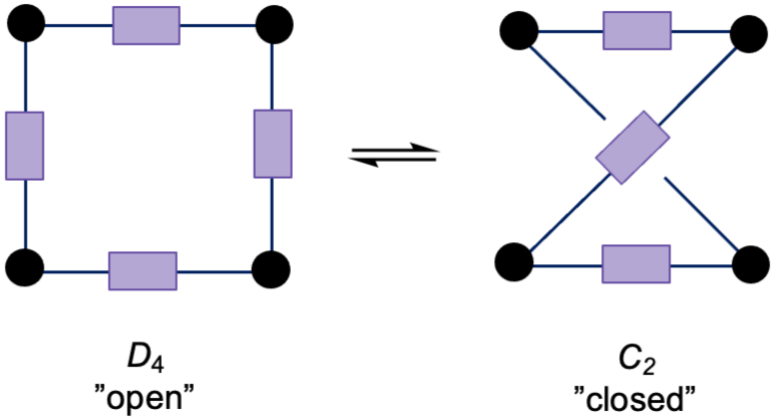

Figure 2.13 Schematic representation of tetracycle D_4 and C_4 conformations.

The ^{1}H NMR spectra of (*S,S*)-**CH□** in different solvents show the evidence of the two conformations by the PMDI aromatic proton signals, the D_4 conformation is displayed by a singlet with an integration of 8 at 7.95 ppm in DMF-d_7 and the C_2 conformation as three singlets with an integration ratio of 2:4:2 at 8.20, 7.76 and 7.58 ppm in THF-d_8 (Figure 2.14). Further confirmation of the two conformations is shown in the single crystal structure of (*S,S*)-**CH□**, in DMF and water the D_4 "open" conformation is seen while the single crystals of the tetracycle grown in THF and hexane adopts the C_2 "folded" conformation. ^{1}H NMR analysis of (*S,S*)-**CH□** in CD_2Cl_2 shows four singlets between 7.5 and 8.3 ppm with integration ratio of 1:6:2:1 for the PMDI aromatic protons meaning that in dichloromethane the tetracycle is in a mixture of the D_4 and C_2 conformations while (*S,S*)-**CH□** in $CDCl_3$ displays the PMDI proton signals as three singlets 8.25, 7.87 and 7.57 ppm similar to THF-d_8.

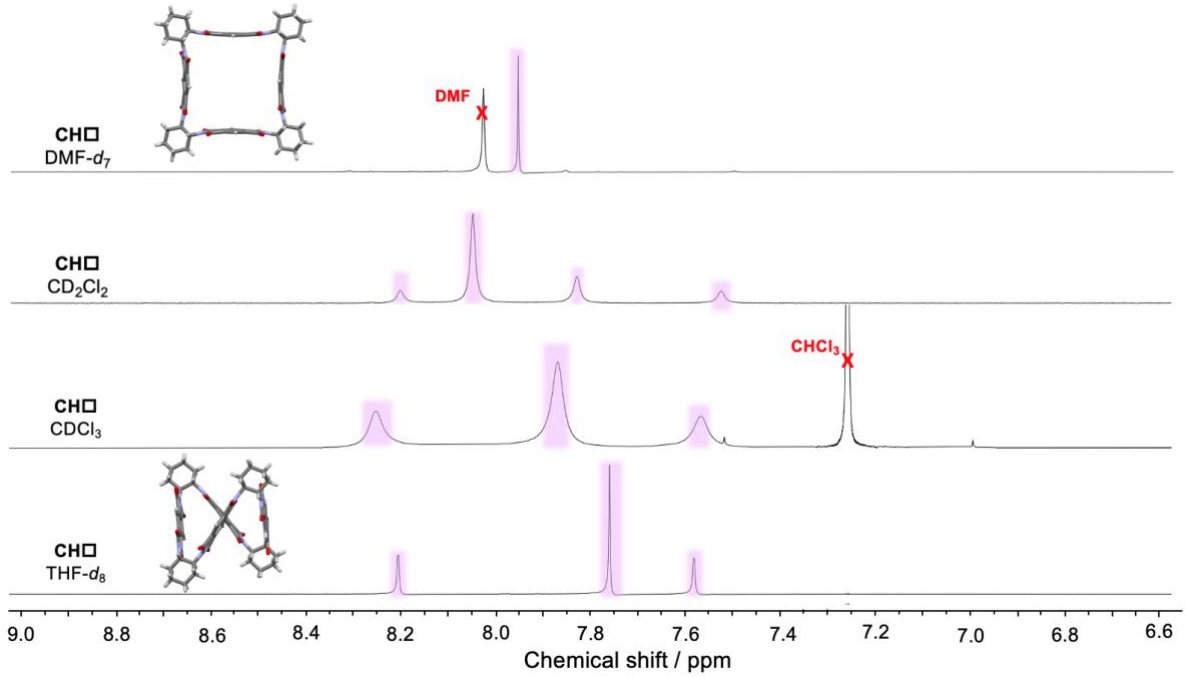

Figure 2.14 Solvent-dependent ^{1}H NMR spectra (6.6–9.0 ppm) of **CHO** in DMF-d_7, CD_2Cl_2, $CDCl_3$, and THF-d_8, highlighting the PMDI proton environment (pink) as well as the single crystal structures.

When conducting the solvent-dependent ^{1}H NMR studies of the mixture of (*S,S*)-**DHPΔ** and (*S,S*)-**DHPO**, a similar pattern to the parent tetracycle (*S,S*)-**CHO** in DMF-d_7, CD_2Cl_2, $CDCl_3$ and THF-d_8. Unfortunately, due to the overlap of the aromatic proton signals, direct quantitative analysis is unable to be conducted but comparison to the parent tetracycle (*S,S*)-**CHO** can be made. The ^{1}H NMR spectra of (*S,S*)-**DHPΔ** and (*S,S*)-**DHPO** in DMF-d_7 display two singlets at 8.26 and 8.14 ppm meaning the tetracycle (*S,S*)-**DHPO** is adopting the D_4 conformation while the compound in CD_2Cl_2 shows three singlets between 8.10 and 8.40 ppm which means that the sample contains a mixture of the tetracycle in both the D_4 and C_2 conformation (Figure 2.15). ^{1}H NMR analysis of the molecular triangle and tetracycle mixture in $CDCl_3$ and THF-d_8 shows three singlets for the PMDI aromatic protons of (*S,S*)-**DHPO** alongside the singlet for the PMDI proton environments of (*S,S*)-**DHPΔ** with an integration ratio of 1:2:1 likely meaning the tetracycle is adopting the C_2 "folded" conformation.

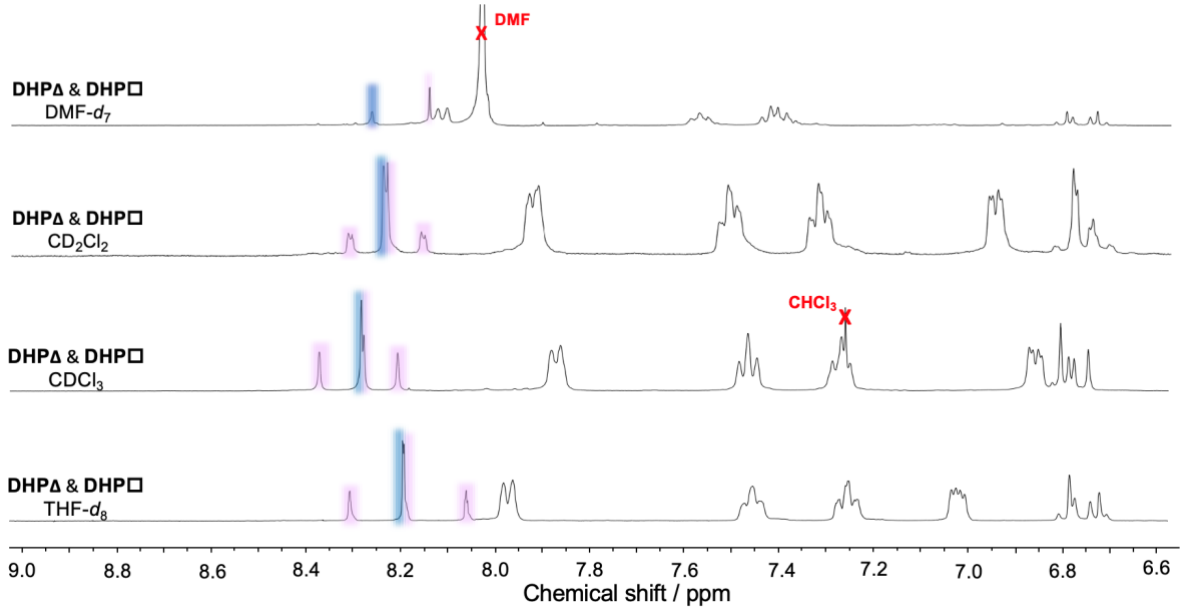

Figure 2.15 Solvent-dependent ^{1}H NMR spectra (6.6–9.0 ppm) of **DHPΔ** & **DHP□** in DMF-d_7, CD_2Cl_2, THF-d_8 and $CDCl_3$, highlighting the PMDI proton environment of **DHP□** (pink) and **DHPΔ** (blue).

Fortunately, and despite challenges in reproducibly separating (*S,S*)-**DHPΔ** and (*S,S*)-**DHP□**, it was possible to grow high quality single crystals of (*S,S*)-**DHPΔ** from a small amount of pure product. The single crystals were grown by slow vapour diffusion of methanol into a chloroform solution of the sample. By modifying the vertices of the molecular triangle to increase the strain ((*S,S*)-**DHPΔ**) compared to (*S,S*)-**CHΔ**, there was a decrease in the average N-C-C-N dihedral angle from 51.01º to 50.33º due to the rigidity of the dihydrophenanthrene vertices limiting the degrees of freedom available for the macrocycle (Figure 2.16). The X-ray superstructure of (*S,S*)-**DHPΔ** exhibits a similar continuous tubular packing arrangement with the channels formed also supported by intermolecular π-π stacking (3.27 Å). There is an additional twist of 58º of one of the layers of molecular triangles due to the steric constraints of the dihydrophenanthrene units stacking over each other.

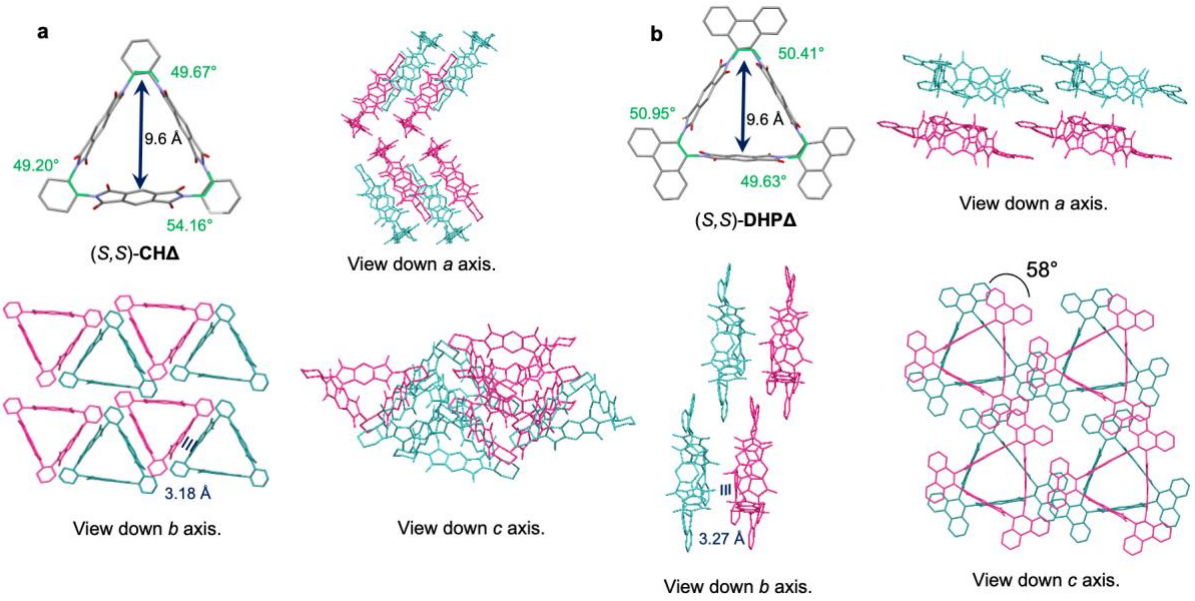

Figure 2.16 Single crystal structure and packing arrangements of (a) (*S,S*)-**CHΔ** and (b) (*S,S*)-**DHPΔ**.

2.3 Electronic properties analysis

Computational analysis was carried out at the B3LYP-D3BJ/6-31G++ level of theory in CH_2Cl_2 (IEFPCM) for all seven (*S,S*)-molecular triangles to obtain the geometry-optimised structures (Figure 2.17). Although there are slight differences of values between the DFT and single crystal structures, this can be attributed to the different solvent systems and the general pattern can still be confirmed for the compounds that have not been synthesised yet. In comparison to **CHΔ** (48.21º), **DPEΔ** has a similar average dihedral angle (ϖ) of 48.49º while the π-extended acyclic molecular triangle **DNaphΔ** shows a decrease of 1.76º compared to the parent macrocycle, due to the less rigid nature of the vertices allowing for a closer alignment of the PMDI units. For the more rigid macrocycles, **DHPΔ** and **DHNaphΔ**, there is a decrease of 0.51º and 1.49º respectively compared to **CHΔ** because the increased rigidity from the phenanthrene and dihydronaphthyl vertices limiting the degrees of freedom of the entire macrocycles. The completely aromatised molecular triangles **PhenΔ** and **HeliΔ** have ϖ close to zero (1.00º and 2.66º respectively) meaning the PMDI units of the compounds are completely parallel to each allowing for better electronic communication between the units.

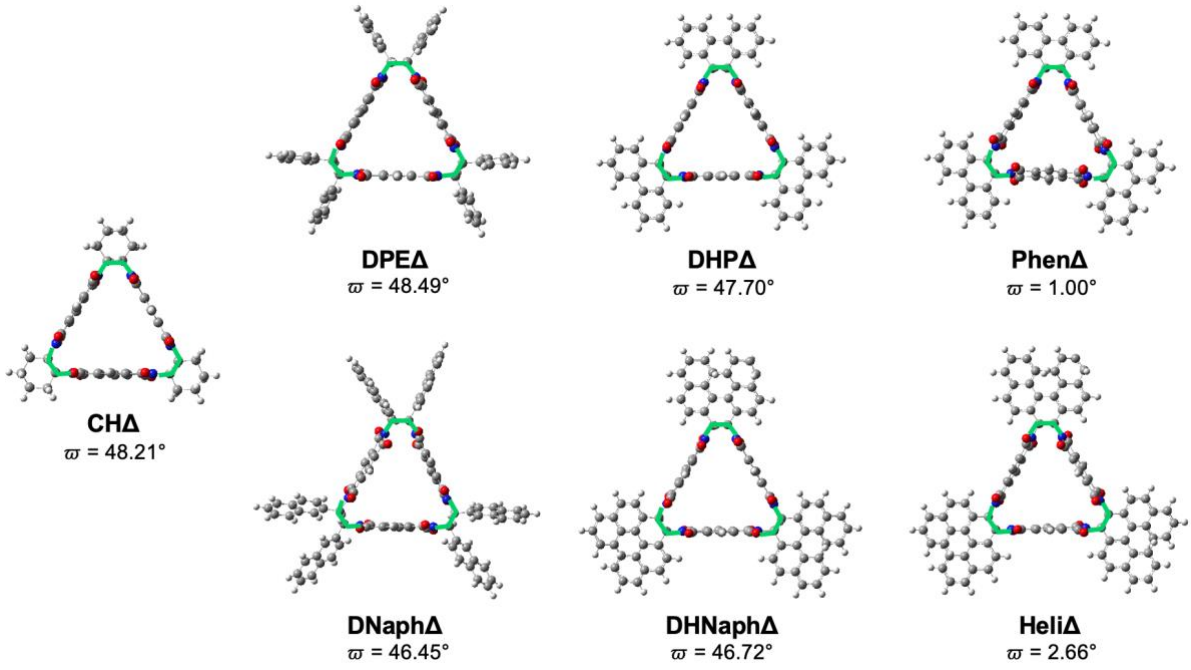

Figure 2.17 Geometry-optimised DFT structures of **CHΔ**, **DPEΔ**, **DNaphΔ**, **DHPΔ**, **DHNaphΔ**, **PhenΔ** and **HeliΔ** calculated at the B3LYP-D3BJ/6-31G ++ level of theory in CH_2Cl_2 (IEFPCM).

Before proceeding to collect experimental data on the electronic and electrochemical properties of the novel triangles, computational analysis to visualise and predict the arrangement of their molecular orbitals, which are shown in Figure 2.18 at an isovalue of 0.004. This analysis shows a small stabilisation of 0.14 eV across the LUMO levels of the compounds and a destabilisation of the HOMO levels by 1.92 eV, it can also be noted that while on **CHΔ** the HOMO is located on the whole molecule, further modification from the acyclic to the cyclic vertices shows the HOMO localised on the vertices. Alongside the current electrochemical data (Figure X.X), there is a good indication that as the LUMO energy decreases, the molecular triangles will be more readily reduced, which is ideal for the use in energy materials. The fully aromatised **PhenΔ** and **HeliΔ** have an increased bandgap of 0.14 and 0.25 eV respectively, compared to their counterparts **DHPΔ** and **DHNaphΔ** with the LUMO energy levels being of similar values (~ −3.94 eV) while the HOMO energy levels have the greatest difference of 0.15 and 0.25 eV for the diphenyl and dinaphthyl derivatives respectively. All the molecular triangles in Figure 2.18 demonstrate degenerate HOMO and HOMO-1 energy levels as well as degenerate LUMO and LUMO+1 levels, apart from **DNaphΔ** which shows the quasi-degenerate MOs (Figure SX.X).[43] Therefore, the DFT models suggest that the vertex engineering by introducing strain as well as electron density to the molecular triangles influence the optical and electronic properties— (i) decrease in E_g going from **CHΔ** to **DPEΔ** to **DNaphΔ** — due to electron density of the vertices (ii) further E_g reduction going from **DPEΔ** and **DNaphΔ** to **DHPΔ** and **DHNaphΔ**, attributed to the strain induced at the vertices. The computational structural models obtained are in good agreement with the experimental

structures collected from X-ray diffraction analysis, therefore the theoretical models can be used to predict the optical and electrochemical properties of the compounds and used as a comparison.

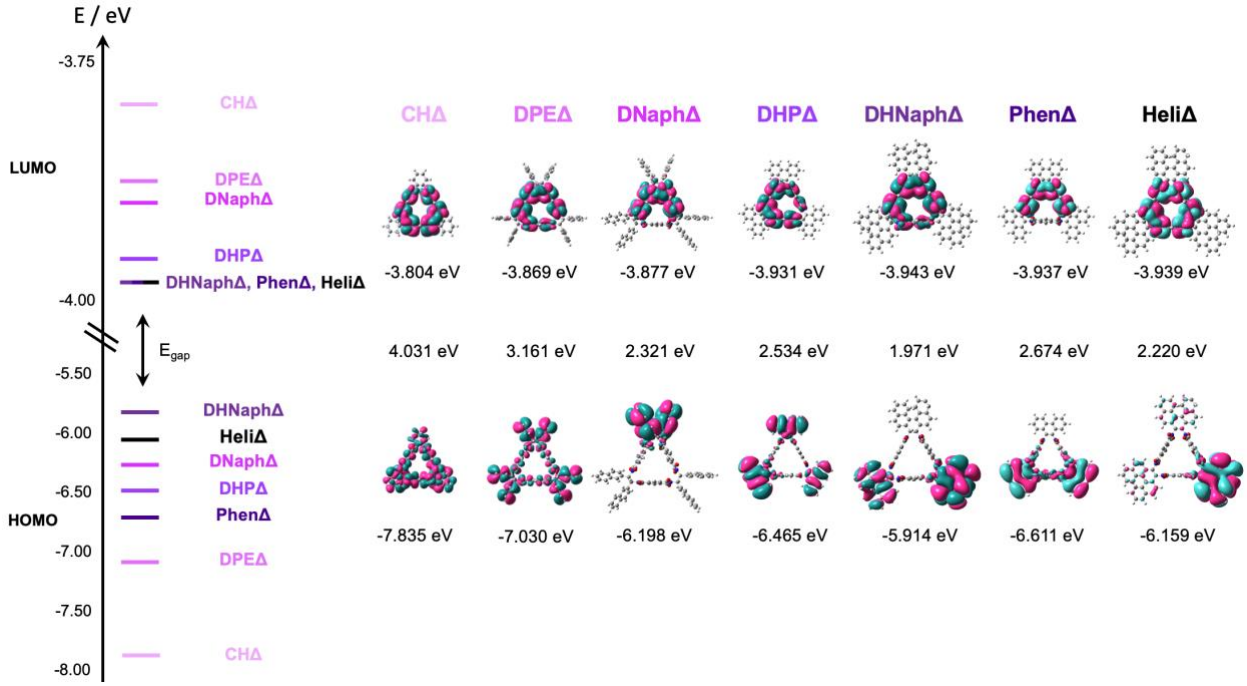

Figure 2.18 Computational molecular orbital energy diagram of **CHΔ**, **DPEΔ**, **DNaphΔ**, **DHPΔ**, **DHNaphΔ**, **PhenΔ** and **HeliΔ** (B3LYP-D3BJ/6-31G ++ in CH_2Cl_2, isovalue = 0.004).

Therefore, in order to understand the influence of the vertices engineering on the optical properties, absorption spectra of **CHΔ**, **DPEΔ** and **DNaphΔ** were recorded in CH_2Cl_2, displaying π–π* transitions at ~310 nm and ~320 nm while **DNaphΔ** has an additional blue-shifted transition at 306 nm (Figure 2.19). Although there is overlap of the transitions at ~310 nm and ~320 nm for all the compounds, **DNaphΔ** shows a much greater overlap of these transitions as well as the one at 306 nm. The similarities of the spectra imply that the vertices of the molecular triangles are not the main influence in the absorption profile, but the PMDI units are the most influential. At ~320 nm the molar absorption coefficient increases from **CHΔ** to **DPEΔ** to **DNaphΔ** with values of 5830, 7930 and 8680 M^{-1} cm^{-1}, respectively. The increase of the molar absorption coefficients is due to the enhanced conjugation attributed to the aromatic vertices on the molecular triangles influencing the optical properties. The increase in the molar absorption coefficients further reflects the ease of the HOMO to LUMO transition. This result matches with the trend in E_g obtained from the DFT models of the frontier molecular orbitals of the compounds. While the frontier molecular orbitals of **DNaphΔ** showed potential for charge transfer due to their spatial separation, there was no obvious charge transfer band in the absorption spectrum. More insights into this potential charge transfer property of **DNaphΔ** can be gained by additional optical analyses, such as emission and excitation studies, which is anticipated to be performed in the future. However, this result may be implying that **DNaphΔ** may not be the best donor compound which is why the oxidation product **DHNaphΔ** may allow for better donor qualities.

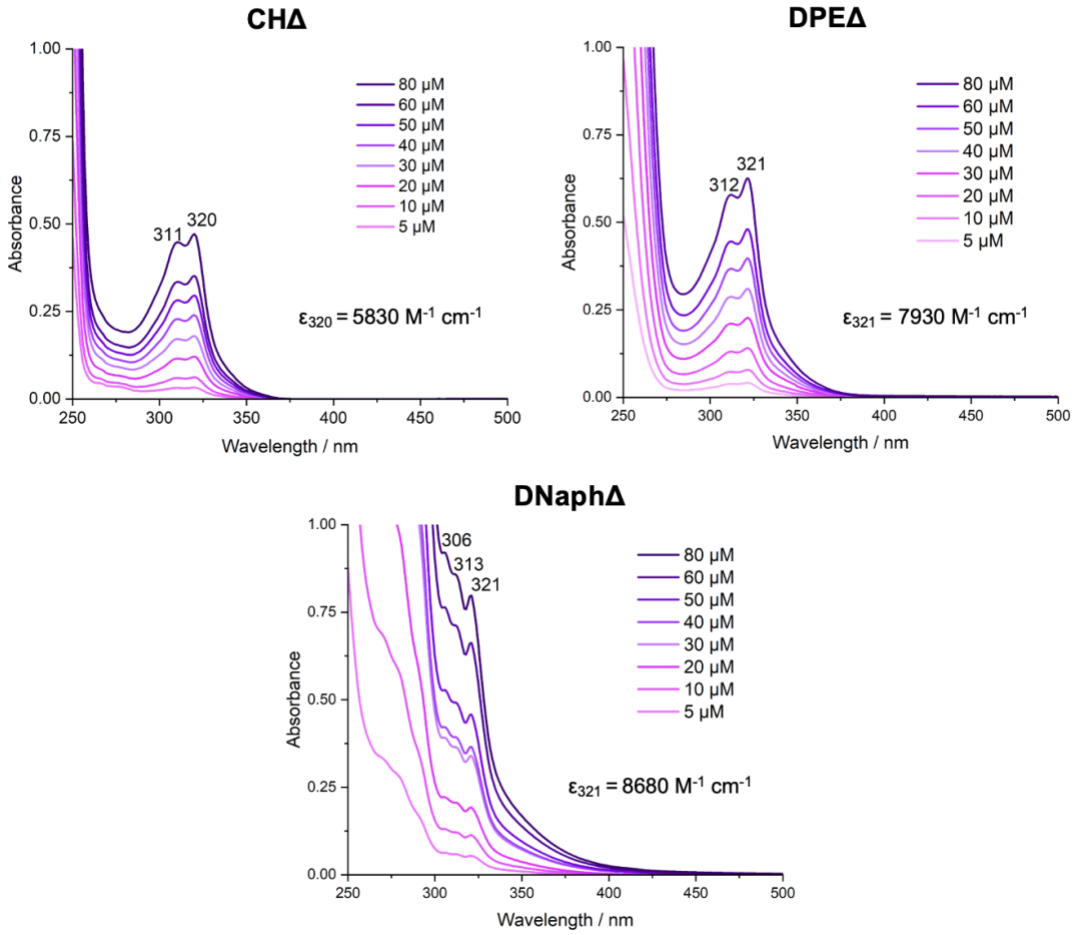

Figure 2.19 Concentration-dependent UV-Vis absorption spectrum of **CHΔ**, **DPEΔ** and **DNaphΔ** in CH_2Cl_2 (5 μM–80 μM).

Table 2.20 Experimental and theoretical data for **CHΔ**, **DPEΔ**, **DNaphΔ**, **DHPΔ**, **DHNaphΔ**, **PhenΔ** and **HeliΔ** from absorption, electrochemical and DFT analysis in CH_2Cl_2.

	E_{LUMO} / eV		E_{HOMO} / eV		E_{gap} / eV	
	Exp.	DFT	Exp.	DFT	Exp.	DFT
CHΔ	-3.56	-3.80	-6.92	-7.84	3.36	4.03
DPEΔ	-3.61	-3.87	-6.71	-7.03	3.10	3.16
DNaphΔ	-3.61	-3.88	-6.22	-6.20	2.61	2.32
DHPΔ	-	-3.93	-	-6.47	-	2.53
DHNaphΔ	-	-3.94	-	-5.91	-	1.97
PhenΔ	-	-3.94	-	-6.61	-	2.67
HeliΔ	-	-3.94	-	-6.16	-	2.22

Cyclic voltammetry (CV) analysis is a key experiment to probe electron transfer processes in a variety of compounds by relating electron transfer to chemical differences.[44] In the case of ADI macrocycles the electron transfer processes are reduction and oxidation reactions that occur on the ADI unit. For

CHΔ, **DPEΔ**, and **DNaphΔ**, the electrochemical processes occur on the PMDI unit which is a two-electron acceptor. Due to there being three PMDI units it is expected to see six single electron reduction peaks in the CV profile with each peak relating to a reduced state of the molecular triangle. The CV traces of **CHΔ**, **DPEΔ**, and **DNaphΔ** (Figure 2.21) show that the latter two macrocycles have a more easily accessible onset reduction potential of −0.65 V compared to **CHΔ** (−0.73 V), meaning **DPEΔ** and **DNaphΔ** require less energy to be reduced (Table 2.20). For the second group of reductions to obtain the quad-, quin- and hexa-reduced states, a similar pattern is observed where the fourth reduction peak is more easily accessible at −1.46 and −1.45 V for **DPEΔ** and **DNaphΔ** respectively while the fourth reduction for **CHΔ** is accessed at −1.53 V. This demonstrates that the acyclic molecular triangles have more accessible reduced states even at the hexa-reduced states compared to that of the parent molecular triangle **CHΔ**, showing that the increase in the global conjugation rendered by the vertices have a positive influence on the electronics. DFT analysis shows the same trend in the LUMO energy levels of **CHΔ**, **DPEΔ**, and **DNaphΔ** with a 0.24–0.27 eV difference between the theoretical and experimental values (Table 2.20). Additionally, the experiment E_g values were found to decrease with respect to the increase in global conjugation attributed by the vertices (Table 2.20), similar to the trend observed from the computational models. The modified molecular triangles also have better resolution of the peaks corresponding to the higher order reduced states, such as the tetra-, quin- and hexa-reduced between −1.40 and −1.80 V, due to the flexibility of the macrocycles allowing better reorganisation, overlap and communication between the PMDI units. This result is supported by computational analysis of the molecular orbitals that show the LUMO, LUMO+1 and LUMO+2 MOs are quasi-degenerate and display global conjugation across the three PMDI units (Figure S5).

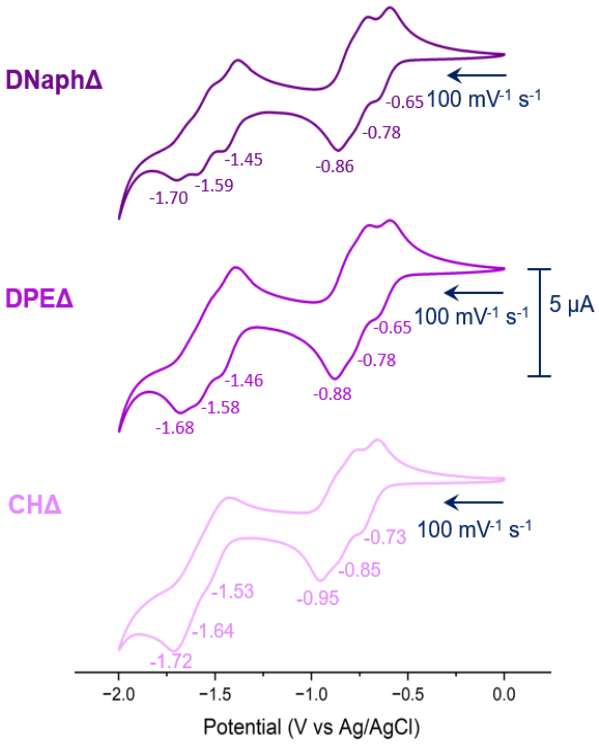

Figure 2.21 Solution-state CV analysis of **CHΔ**, **DPEΔ**, and **DNaphΔ** from -2.0 V to 0.0 V (V vs Ag/AgCl).

On comparing the experimental data obtained for the isolated compounds from CV and SEC analyses and the theoretical analysis from DFT, there is good agreement of the values and the same trend is seen across the LUMO, HOMO and band gap energies. The theoretical values for the frontier molecular orbitals of **DHPΔ** and **DHNaphΔ** are the most promising due to the decrease in band gap and LUMO energies compared to their less rigid counterparts **DPEΔ** and **DNaphΔ** respectively. Although we have hypothesised that by inducing even more strain into the vertices by fully aromatising **DHPΔ** and **DHNaphΔ** to form **PhenΔ** and **HeliΔ** would improve the electronics even further, DFT predictions show that the LUMO energy remains consistent for **DHPΔ**, **DHNaphΔ**, **PhenΔ** and **HeliΔ**, whilst the HOMO energies differ by <0.7 eV. The calculated band gap for **DHPΔ** and **DHNaphΔ** are greater than **PhenΔ** and **HeliΔ**, contradicting the initial hypothesis that completely aromatising the molecular triangles will improve the electronic properties for energy storage materials.

Spectroelectrochemical (SEC) analysis is a technique that combines both absorption and CV studies to investigate how the optical properties differ for the charged states of a compound. For the case of the synthesised molecular triangles so far, a voltage is applied to a sample (1.0 mM) of the compound in an electrolyte (0.1 M $TBAPF_6$) solution in CH_2Cl_2 to reach the tri- and hexa-reduced states, based on the previous CV analysis conducted, and an absorption spectrum is recorded to note any changes in the transitions. For **CHΔ**, **DPEΔ**, and **DNaphΔ**, the tri-reduced states exhibit a red-shifted λ_{max} from 320 nm to ~720 nm, which suggests that the tri-reduced state can delocalise the three electrons around the macrocyclic structure without any columbic repulsion (Figure 2.22). This is why the hexa-reduced states of **CHΔ**, **DPEΔ**, and **DNaphΔ** exhibit a smaller red-shifted λ_{max} compared to the neutral state from 320 nm to ~400 nm demonstrating that there is greater columbic repulsion of the paired electrons which leads to a higher energy compared to the tri-reduced states. To further investigate the influence of the vertices on the reduced states, theoretical calculations are on-going of the reduced states so further insights can be made. Overall, the current results imply that by careful vertex engineering of the molecular triangles, fine-tuning of their optical and more importantly, electronic properties can be achieved, which could potentially define their ability as functional materials towards energy storage application.

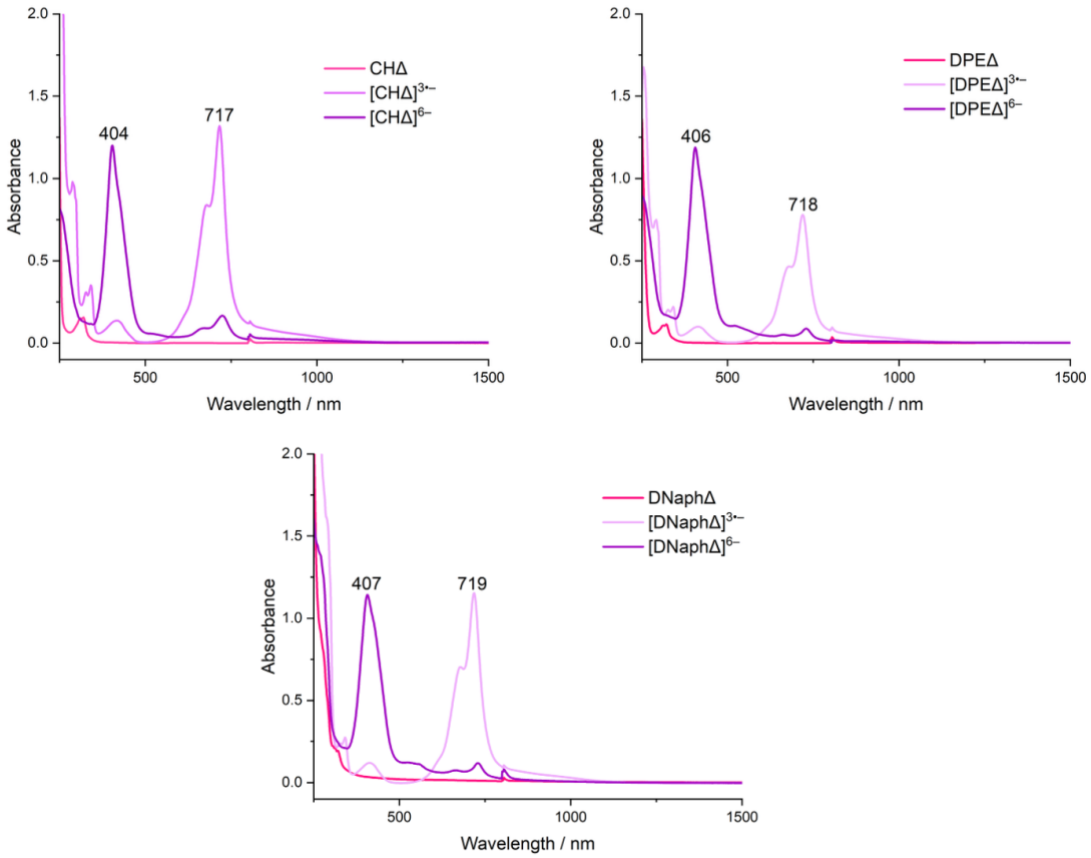

Figure 2.22 Solution-state SEC analysis of 1mM solutions of a) **CHΔ**, b) **DPEΔ**, and c) **DNaphΔ** in 0.1M $TBAPF_6$ in CH_2Cl_2 based on the CV analysis above in **Figure 2.21**.

3. Conclusions

Two molecular triangles with acyclic vertices, (*S,S*)-**DPEΔ** and (*S,S*)-**DNaphΔ** were synthesised with diphenyl and dinaphthyl groups and their properties analysed in the solid and solution state. Single crystals of (*S,S*)-**DPEΔ** revealed shallower dihedral angles (46.26º) compared to the parent macrocycle (*S,S*)-**CHΔ** (51.01º) because the flexibility of the diphenyl vertices allows for the most favourable conformation to align the PMDI units. The superstructure of (*S,S*)-**DPEΔ** shows edge-to-face π–π stacking (4.93 Å) of the diphenyl vertices with no apparent interactions between the PMDI units likely due to the steric hinderance of the aromatic bridges.

To begin investigating how strain influences the structural and electronic properties of the PMDI molecular triangles, a series of oxidative dehydrogenation reactions were employed on (*S,S*)-**DPEΔ** and (*S,S*)-**DNaphΔ** to form the cyclic analogues, (*S,S*)-**DHPΔ** and (*S,S*)-**DHNaphΔ** respectively. Although there was no success in the oxidative dehydrogenation reactions, synthesis of the dihydrophenanthrene diamine precursor allowed for the formation of (*S,S*)-**DHPΔ** and the tetracycle counterpart (*S,S*)-**DHP□**. Solvent dependent ^{1}H NMR analysis of (*S,S*)-**DHPΔ** and (*S,S*)-**DHP□** shows the dynamic

behaviour of the tetracycle that adopts either a D_4 "open" or C_2 "folded" conformation that is seen with the parent compound (*S,S*)-**CH□**. Single crystals of (*S,S*)-**DHPΔ** show a decrease in the dihedral angle (50.33º) because of the rigidity of the dihydrophenanthrene vertices limiting the degrees of freedom available for the macrocycle.

Electronic analysis of (*S,S*)-**DPEΔ** and (*S,S*)-**DNaphΔ** reveals a more easily accessible onset reduction potential in the CV analysis compared to (*S,S*)-**CHΔ** which is a pattern seen for the higher order reduced states including the hexa-reduced molecular triangles. Computational analysis of the molecular triangles synthesised and analogue compounds that have yet to be prepared have shown that even though there is a slight variation in the theoretical values compared to the experimental, the same pattern of improved LUMO energies with modification to the vertices is seen. (*S,S*)-**DHPΔ** and (*S,S*)-**DHNaphΔ** exhibit the best improvement in the computational band gap energies (2.53 and 1.97 eV) of the vertex modified PMDI molecular triangles due to the most stabilised and destabilised LUMO and HOMO energies respectively.

This thesis has outlined how modifications to the vertices of PMDI molecular triangles have a positive influence on the macrocyclic structure, supramolecular chemistries and the global conjugation between the ADI units. Therefore, if the predicted electronic properties of the cyclic derivatives of (*S,S*)-**DPEΔ** and (*S,S*)-**DNaphΔ** can be accessed, the macrocycles will be great contenders for use as energy storage materials.

4. References

(1) Pedersen, C. J. Cyclic Polyethers and Their Complexes with Metal Salts. *J. Am. Chem. Soc.* **1967**, *89*, 2495– 2496, DOI: 10.1021/ja00986a052.

(2) Wojaczyńska, E.; Ostrowska, M.; Lower, M.; Czyżyk, N.; Jakieła, A.; Marra, A. Recent Advances in Synthesis and Applications of Calixarene Derivatives Endowed with Anticancer Activity. *Molecules,* **2024**, *29* (17), 4240, https://doi.org/10.3390/molecules29174240.

(3) Farber, M.; Rawat, V.; Diskin-Posner, Y.; Dobrovetsky, R.; Vigalok, A. Polyaromatic Calixarene Hosts: Calix[4]Pyrenes. *Org. Lett.*, **2024**, *26* (27), 5731–5735. https://doi.org/10.1021/acs.orglett.4c01850.

(4) Tian, Y.; Guo, Y.; Dong, X.; Wan, X.; Cheng, K. H.; Chang, R.; Li, S.; Cao, X.; Chan, Y. T.; Sue, A. C. H. Synthesis of Covalent Organic Pillars as Molecular Nanotubes with Precise Length, Diameter and Chirality. *Nature Synth.*, **2023**, *2* (5), 395–402. https://doi.org/10.1038/s44160-022-00235-w.

(5) Wang, Z. Q.; Wang, X.; Yang, Y. W. Pillararene-Based Supramolecular Polymers for Adsorption and Separation. *Adv. Mater.*, **2024**, 36 (4), 2301721. https://doi.org/10.1002/adma.202301721.

(6) Garcia Jimenez, D.; Poongavanam, V.; Kihlberg, J. Macrocycles in Drug Discovery─Learning from the Past for the Future. *J. Med. Chem.*, **2023**, *66* (8), 5377–5396. https://doi.org/10.1021/acs.jmedchem.3c00134.

(7) Darlami, O.; Pun, R.; Ahn, S. H.; Kim, S. H.; Shin, D. Macrocyclization Strategy for Improving Candidate Profiles in Medicinal Chemistry. *Eur. J. Med. Chem.*. **2024**, 272, 116501. https://doi.org/10.1016/j.ejmech.2024.116501.

(8) Wang, Q. Q. Anion Recognition-Directed Supramolecular Catalysis with Functional Macrocycles and Molecular Cages. *Acc. Chem. Res.*, **2024**, *57* (21), 3227–3240. https://doi.org/10.1021/acs.accounts.4c00583.

(9) Ning, R.; Zhou, H.; Nie, S. X.; Ao, Y. F.; Wang, D. X.; Wang, Q. Q. Chiral Macrocycle-Enabled Counteranion Trapping for Boosting Highly Efficient and Enantioselective Catalysis. *Angew. Chem. Int. Ed.*, **2020**, *59* (27), 10894–10898. https://doi.org/10.1002/anie.202003673.

(10) Lou, X. Y.; Zhang, S.; Wang, Y.; Yang, Y. W. Smart Organic Materials Based on Macrocycle Hosts. *Chem. Soc. Rev*. **2023**, 52 (19), 6644–6663. https://doi.org/10.1039/d3cs00506b.

(11) Chen, B.; Jäkle, F. Boron-Nitrogen Lewis Pairs in the Assembly of Supramolecular Macrocycles, Molecular Cages, Polymers, and 3D Materials. *Angew. Chem Int. Ed*., **2024**. 62 (3), e 202313379. https://doi.org/10.1002/anie.202313379.

(12) Martí-Centelles, V.; Pandey, M. D.; Burguete, M. I.; Luis, S. V. Macrocyclization Reactions: The Importance of Conformational, Configurational, and Template-Induced Preorganization. *Chem. Rev*., **2015**, 115 (16), 8736–8834. https://doi.org/10.1021/acs.chemrev.5b00056.

(13) Han, Y. Q.; Xie, Y.; Zhang, J.; Tan, S.; Zhang, H.; Tang, B. Z.; Sessler, J. L.; Huang, F. Fjord-Type AIEgens Based on Inherent Through-Space Conjugation. *CCS Chem.*, **2024**, *6* (7), 1739–1747. https://doi.org/10.31635/ccschem.023.202303387.

(14) Xu, Q.; Zhang, J.; Sun, J. Z.; Zhang, H.; Tang, B. Z. Efficient Organic Emitters Enabled by Ultrastrong Through-Space Conjugation. *Nature Photon.* **2024**, *18* (11), 1185–1194. https://doi.org/10.1038/s41566-024-01527-7.

(15) Hassan, Z. Molecular Insights into [2.2]Paracyclophane-Based Functional Materials: Chemical Aspects Behind Functions. *Adv. Funct. Mater*., **2024**, 34 (47), 2311828. https://doi.org/10.1002/adfm.202311828.

(16) Odell, B.; Reddington, M. V.; Slawin, A. M. Z.; Spencer, N.; Stoddart, J. F.; Williams, D. J. Cyclobis(Paraquat-p-phenylene). A Tetracationic Multipurpose Receptor. *Angew. Chem. Int. Ed. Engl.*, **1988**, *27* (11), 1547–1550. https://doi.org/10.1002/anie.198815471.

(17) Rühe, J.; Rajeevan, M.; Shoyama, K.; Swathi, R. S.; Würthner, F. A Terrylene Bisimide Based Universal Host for Aromatic Guests to Derive Contact Surface-Dependent Dispersion Energies. *Angew. Chem. Int. Ed.* **2024**, *63* (17), e202318451. https://doi.org/10.1002/anie.202318451.

(18) Wang, Z.; Liu, Y.; Quan, X.; Zhang, W.; Tan, R.; Gu, H.; Sheng, C.; Duan, C.; Xing, P.; Wan, J. H. Planar Chiral Charge-Transfer Cyclophanes: Convenient Synthesis, Circularly Polarized Light-Responsive Photothermal Conversion and Supramolecular Chiral Assembly. *Angew. Chem. Int. Ed.* **2025**, *64* (1), e202413295.

(19) Schneebeli, S. T.; Frasconi, M.; Liu, Z.; Wu, Y.; Gardner, D. M.; Strutt, N. L.; Cheng, C.; Carmieli, R.; Wasielewski, M. R.; Fraser Stoddart, J.; Liu, Z.; Wu, Y.; Strutt, N. L.; Cheng, C.; Stoddart, J. F.; Gardner, D. M.; Carmieli, R.; Wasielewski, M. R. Electron Sharing and Anion–π Recognition in Molecular Triangular Prisms. *Angew. Chem. Int. Ed.* **2013**, *52* (49), 13100–13104. https://doi.org/10.1002/ANIE.201307984.

(20) Kim, D. J.; Hermann, K. R.; Prokofjevs, A.; Otley, M. T.; Pezzato, C.; Owczarek, M.; Stoddart, J. F. Redox-Active Macrocycles for Organic Rechargeable Batteries. *J. Am. Chem. Soc.* **2017**, *139* (19), 6635–6643. https://doi.org/10.1021/jacs.7b01209

(21) Wang, Y.; Wu, H.; Stoddart, J. F. Molecular Triangles: A New Class of Macrocycles. *Acc. Chem. Res.* **2021**, *54* (8), 2027–2039. https://doi.org/10.1021/acs.accounts.1c00108.

(22) Liu, Z.; Liu, G.; Wu, Y.; Cao, D.; Sun, J.; Schneebeli, S. T.; Nassar, M. S.; Mirkin, C. A.; Stoddart, J. F. Assembly of Supramolecular Nanotubes from Molecular Triangles and 1,2-Dihalohydrocarbons. *J. Am. Chem. Soc.* **2014**, *136* (47), 16651–16660. https://doi.org/10.1021/ja509480u.

(23) Diac, A.; Matache, M.; Grosu, I.; Hădade, N. D. Naphthalenediimide – A Unique Motif in Macrocyclic and Interlocked Supramolecular Structures. *Adv. Synth. Catal*., **2018**, 360 (5), 817–845. https://doi.org/10.1002/adsc.201701362.

(24) Spenst, P.; Würthner, F. Photo- and Redoxfunctional Cyclophanes, Macrocycles, and Catenanes Based on Aromatic Bisimides. *J. Photochem. Photobio. C: Photochem. Rev*., **2017**, 31, 114–138. https://doi.org/10.1016/j.jphotochemrev.2017.03.002.

(25) Wu, S.; Song, X.; Du, C.; Liu, M. Macroscopic Homochiral Helicoids Self-Assembled via Screw Dislocations. *Nat. Commun.* **2024**, *15* (1). https://doi.org/10.1038/s41467-024-50631-3.

(26) Gawroński, J.; Brzostowska, M.; Gawrońska, K.; Koput, J.; Rychlewska, U.; Skowronek, P.; Nordén, B. Novel Chiral Pyromellitdiimide (1,2,4,5-Benzenetetracarboxydiimide) Dimers and Trimers: Exploring Their Structure, Electronic Transitions, and Exciton Coupling. *Chem. Eur. J.* **2002**, *8* (11), 2484–2494. https://doi.org/10.1002/1521-3765(20020603)8:11<2484::AID-CHEM2484>3.0.CO;2-O.

(27) Mohan Nalluri, S. K.; Zhou, J.; Cheng, T.; Liu, Z.; Nguyen, M. T.; Chen, T.; Patel, H. A.; Krzyaniak, M. D.; Goddard, W. A.; Wasielewski, M. R.; Stoddart, J. F. Discrete Dimers of Redox-Active and Fluorescent Perylene Diimide-Based Rigid Isosceles Triangles in the Solid State. *J. Am. Chem. Soc.* **2019**, *141* (3), 1290–1303. https://doi.org/10.1021/jacs.8b11201.

(28) Wu, Y.; Young, R. M.; Frasconi, M.; Schneebeli, S. T.; Spenst, P.; Gardner, D. M.; Brown, K. E.; Würthner, F.; Stoddart, J. F.; Wasielewski, M. R. Ultrafast Photoinduced Symmetry-Breaking Charge Separation and Electron Sharing in Perylenediimide Molecular Triangles. *J. Am. Chem. Soc.* **2015**, *137* (41), 13236–13239. https://doi.org/10.1021/jacs.5b08386.

(29) Hartmann, D.; Penty, S. E.; Zwijnenburg, M. A.; Pal, R.; Barendt, T. A. A Bis-Perylene Diimide Macrocycle Chiroptical Switch. *Angew. Chem. Int. Ed.* **2025**, 64 (15), e202501122. https://doi.org/10.1002/anie.202501122.

(30) Penty, S. E.; Zwijnenburg, M. A.; Orton, G. R. F.; Stachelek, P.; Pal, R.; Xie, Y.; Griffin, S. L.; Barendt, T. A. The Pink Box: Exclusive Homochiral Aromatic Stacking in a Bis-Perylene Diimide Macrocycle. *J. Am. Chem. Soc.* **2022**, *144* (27), 12290–12298. https://doi.org/10.1021/jacs.2c03531.

(31) Wu, Y.; Nalluri, S. K. M.; Young, R. M.; Krzyaniak, M. D.; Margulies, E. A.; Stoddart, J. F.; Wasielewski, M. R. Charge and Spin Transport in an Organic Molecular Square. *Angew. Chem.* **2015**, *127* (41), 12139–12145. https://doi.org/10.1002/ange.201504576.

(32) Nalluri, S. K. M.; Liu, Z.; Wu, Y.; Hermann, K. R.; Samanta, A.; Kim, D. J.; Krzyaniak, M. D.; Wasielewski, M. R.; Stoddart, J. F. Chiral Redox-Active Isosceles Triangles. *J. Am. Chem. Soc.* **2016**, *138* (18), 5968–5977. https://doi.org/10.1021/jacs.6b02086.

(33) Fisher, S.; Malaspina, L. A.; Gozálvez Martínez, C.; Prescimone, A.; Balmohammadi, Y.; Grabowsky, S.; Šolomek, T. Leveraging Halogen Interactions for a Supramolecular Nanotube. *Chem. Eur. J.* **2024**, *30* (27). https://doi.org/10.1002/chem.202400295.

(34) Jassas, R. S.; Mughal, E. U.; Sadiq, A.; Alsantali, R. I.; Al-Rooqi, M. M.; Naeem, N.; Moussa, Z.; Ahmed, S. A. Scholl Reaction as a Powerful Tool for the Synthesis of Nanographenes: A Systematic Review. *RSC Adv*., **2021**, 51, 32158–32202. https://doi.org/10.1039/d1ra05910f.

(35) Grzybowski, M.; Sadowski, B.; Butenschön, H.; Gryko, D. T. Syntheseanwendungen Synthetic Applications of Oxidative Aromatic Coupling – From Biphenols to Nanographenes. *Angew. Chem. Int. Ed.* **2020**, *132* (8), 3020–3050. https://doi.org/10.1002/ange.201904934.

(36) Zhai, L.; Shukla, R.; Wadumethrige, S. H.; Rathore, R. Probing the Arenium-Ion (ProtonTransfer) versus the Cation-Radical (Electron Transfer) Mechanism of Scholl Reaction Using DDQ as Oxidant. *J. Org. Chem.* **2010**, *75* (14), 4748–4760. https://doi.org/10.1021/jo100611k.

(37) Míguez-Lago, S.; Mariz, I. F. A.; Medel, M. A.; Cuerva, J. M.; Maçôas, E.; Cruz, C. M.; Campaña, A. G. Highly Contorted Superhelicene Hits Near-Infrared Circularly Polarized Luminescence. *Chem. Sci.* **2022**, *13* (35), 10267–10272. https://doi.org/10.1039/d2sc03452b.

(38) Zhang, Z.; Zhu, H.; Gu, J.; Shi, H.; Hirose, T.; Jiang, L.; Zhu, Y.; Zhong, D.; Wang, J. Nonplanar Nanographene with a Large Conjugated π-Surface. *J. Am. Chem. Soc.* **2024**, *146* (35), 24681–24688. https://doi.org/10.1021/jacs.4c09167.

(39) Pun, S. H.; Wen, E. C. H.; Xia, Z.; Chen, H.; Fischer, F. R.; Miao, Q. Reactivity, Regioselectivity, and Synthetic Application of 2-Pyrenyl Units in Scholl Reactions. *CCS Chem.* **2023**, *5* (9), 2069–2077. https://doi.org/10.31635/ccschem.023.202302970.

(40) Liu, F.; Zhao, G.; Cai, W.; Xu, D.; Zhao, B. Aminative Umpolung Cyclization for Synthesis of Chiral Exocyclic Vicinal Diamines. *Org. Biomol. Chem.* **2018**, *16* (40), 7498–7502. https://doi.org/10.1039/C8OB02000K.

(41) Walsh, P. J.; Smith, D. K.; Castello, C. Resolution of Trans-Cyclohexane-1,2-Diamine and Determination of the Enantiopurity Using Chiral Solid-Phase HPLC Techniques and Polarimetry. *J. Chem. Educ.* **1998**, *75* (11), 1459

(42) Stead, D.; O'Brien, P.; Sanderson, A. A New Sparteine Surrogate for Asymmetric Deprotonation of N-Boc Pyrrolidine. *Org. Lett.* **2008**, *10* (7), 1409–1412. https://doi.org/10.1021/ol800109s.

(43) Sakamaki, D. Modular Construction of a Three-Layered π-System Using Cruciform Azaacene Dimers. *Org. Lett.* **2025**, *27* (32), 9014–9018. https://doi.org/10.1021/acs.orglett.5c02718.

(44) Elgrishi, N.; Rountree, K. J.; McCarthy, B. D.; Rountree, E. S.; Eisenhart, T. T.; Dempsey, J. L. A Practical Beginner's Guide to Cyclic Voltammetry. *J. Chem. Educ.* **2018**, *95* (2), 197–206. https://doi.org/10.1021/acs.jchemed.7b00361.

(45) Becke, A. D. Density-Functional Thermochemistry. III. The Role of Exact Exchange. *J Chem. Phys.* **1993**, *98* (7), 5648–5652. https://doi.org/10.1063/1.464913.

(46) Lee, C.; Yang, W; Parr, R. G. Development of the Colic-Salvetti Correlation-Energy Formula into a Functional of the Electron Density. *Phys. Rev.* **1988**, *37*(2), 785-789. https://doi.org/10.1103/PhysRevB.37.785.

(47) Grimme, S.; Ehrlich, S.; Goerigk, L. Effect of the Damping Function in Dispersion Corrected Density Functional Theory. *J. Comput. Chem.* **2011**, *32* (7), 1456–1465. https://doi.org/10.1002/jcc.21759.

5. Experimental details

5.1 General remarks

Materials. All reagents and solvents were purchased from commercial suppliers and used without further purification unless stated otherwise. Automated flash column chromatography was performed on a Teledyne Combiflash NextGen 300+ with pre-packed silica (SiO_2) columns from the same supplier. Analytical thin-layer chromatography was carried out on pre-coated aluminium-backed silica gel sheets impregnated with F254 indicator (Merck) and were typically visualised under UV light (254 nm and 365 nm) and/or with the use of dip stains (i.e. $KMnO_4$) as a general oxidising stain and ninhydrin for amine-containing compounds.

NMR spectroscopy. Nuclear magnetic resonance (NMR) spectra were recorded using a 400 MHz JEOL ECS400D instrument (^1H and ^{13}C NMR data acquired at 400 and 101 MHz, respectively). Chemical shifts (δ) are reported in parts per million (ppm) and referenced to the residual non-deuterated solvent peaks ($CDCl_3$: $\delta_H = 7.26$, $\delta_C = 77.16$; D_2O: $\delta_H = 4.79$; CD_2Cl_2: $\delta_H = 5.32$, $\delta_C = 53.84$). Coupling constants (J) are reported in hertz (Hz) and ^1H multiplicities are described using the following convention: s = singlet, d = doublet, t = triplet, q = quartet and m = multiplet. ^1H and ^{13}C signals were assigned with the help of 2D NMR (COSY, HSQC, HMBC) experiments.

Mass spectrometry. High-resolution mass spectrometry (HR-MS) was recorded at 298 K on a Bruker Daltronics microTOF spectrometer using electrospray ionisation (ESI) or atmospheric pressure chemical ionisation (APCI) as the ionisation technique.

Single-crystal X-ray analysis. X-ray single-crystal diffraction data were collected at 110 K on an Oxford Diffraction SuperNova diffractometer with Cu-Kα radiation (I = 1.54184 Å) using an EOS CCD camera. The crystal was cooled with an Oxford Instruments Cryojet. Diffractometer control, data collection, initial unit cell determination, frame integration and unit-cell refinement were carried out with CrysAlisPro. Face-indexed absorption corrections were applied using spherical harmonics, implemented in SCALE3 ABSPACK scaling algorithm within CrysAlisPro. OLEX2 was used for overall structure solution, refinement and preparation of computer graphics and publication data. Within OLEX2, the algorithm used for the structure solution was ShelXT. Refinement by full-matrix least-squares uses the SHELXL algorithm within OLEX2. Atom-to-atom distances and torsional angles were measured using Mercury version 4.2.0. Crystallographic images of the compounds were produced using Mercury version 4.2.0, where non-essential hydrogens and solvent molecules have been omitted for clarity.

Absorption spectroscopy. Solution-state absorption studies were recorded on an Agilent Technologies Cary 5000 UV–vis–NIR spectrophotometer using standard 10 mm path length quartz cuvettes at 298 K using anhydrous solvent.

Electrochemical measurements. Cyclic voltammetry measurements were carried out at room temperature using a Gamry Reference 3000 potentiostat interfaced to a PC using a standard three-electrode system. All solution-state electrochemical experiments were performed using a glassy carbon working electrode (BASi; 0.071 cm^2). The working electrode surface was polished routinely using a 0.05 μm alumina–water slurry on a clean felt surface immediately before each use. A Pt wire was used as the counter electrode and the reference electrode was an Ag/AgCl aqueous electrode stored routinely in a 3 M KCl aqueous solution. Samples were prepared at 1.0 mM concentrations in dry, degassed CH_2Cl_2 (by freeze-pump-thaw under nitrogen) containing 0.1 M tetrabutylammonium hexafluorophosphate ($TBAPF_6$) as the electrolyte. Samples were further sparged with a fine stream of argon gas for a few seconds (and up to a minute) to expel residual trace oxygen from air prior to each measurement. Cyclic voltammograms were typically acquired at a scan rate of 100 mV s^{-1} unless otherwise noted and electrochemical potentials (V) are reported with respect to the Ag/AgCl reference electrode.

Spectroelectrochemical analysis. Spectroelectrochemistry (SEC) experiments were performed *in situ* at room temperature using an optically transparent thin-layer electrochemical (OTTLE) cell (path length approx. 0.2 mm with two CaF_2 windows separated by PTFE spacers) fitted with a Pt wire mesh working electrode, Pt wire counter electrode and an Ag wire pseudo-reference electrode. The OTTLE cell was operated by the aforementioned Gamry Reference 3000 potentiostat in chronoamperometry mode and the spectra recorded with the Cary UV-vis-NIR photospectrometer. All SEC samples were prepared at 1.0 mM concentrations in dry, degassed CH_2Cl_2 (by freeze-pump-thaw under nitrogen) containing 0.1 M tetrabutylammonium hexafluorophosphate ($TBAPF_6$) as the electrolyte and analysed under a constant applied voltage based on the potentials determined by cyclic voltammetry.

Computational modelling. Density functional theory (DFT) calculations were prepared on GaussView 6.0 and submitted to the University of York Viking High Performance Computing cluster and run on Gaussian 16 using Becke's three-parameter exchange functional with the gradient-corrected correlation formula of Lee, Yang and Parr (B3LYP)[45,46] paired with the split valence double-zeta 6-31G** basis set, PCM solvation model (CH_2Cl_2) and dispersion corrections (D3BJ)[47] applied unless stated otherwise.

5.2 Experimental details

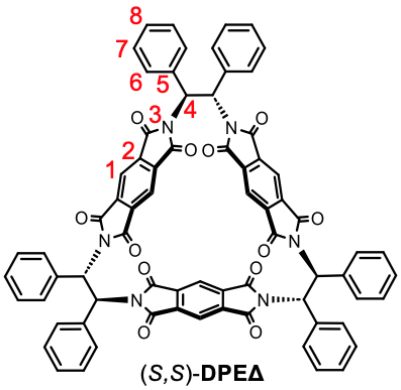

(*S,S*)-**DPEΔ**

(*S,S*)-**DPEΔ**: In a flame-dried round-bottomed flask under N_2, pyromellitic dianhydride (256.9 mg, 1.178 mmol, 1.0 equiv.) was stirred in glacial acetic acid (10 mL) at 80 °C until dissolved. Meanwhile, (*S,S*)-diphenylethylene diamine (250 mg, 1.178 mmol, 1.0 equiv.) is dissolved in additional glacial acetic acid (15 mL) and then added dropwise to the reaction mixture which was then left to stir at 120 °C under N_2 for 24 h. The crude reaction mixture was analysed by TLC (SiO_2: 5% acetone in CH_2Cl_2) to confirm the reaction had completed, before the mixture was concentrated before purification by flash column chromatography (SiO_2: 0–5% acetone in CH_2Cl_2), before a trituration with acetone was conducted to give (*S,S*)-**DPEΔ** (97.2 mg, 82.15 µmol, 21%) as an off-white solid.

^{1}H NMR (400 MHz, $CDCl_3$, 298 K): δ_H 8.06 (s, 6H[1]), 7.63 (d, J = 7.6 Hz, 12H[6]), 7.18 (m, 18H[7,8]), 7.01 (s, 6H[4]). **^{13}C NMR** (101 MHz, $CDCl_3$, 298 K): δ_C 165.9[1], 164.7, 136.6[2], 136.2[3], 135.5, 129.4[ar], 129.1[ar], 129.0[ar], 119.4[5], 54.7[4]. **HRMS** (APCI, +ve) Calculated for $C_{72}H_{43}N_6O_{12}$ = 1183.2933, found $[M+H]^+$ = 1183.2968 (error -3.0 ppm).

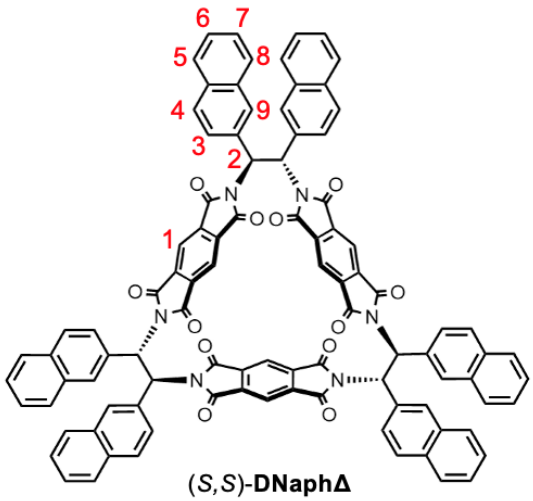

(*S,S*)-**DNaphΔ**

(*S,S*)-**DNaphΔ**: In a flame-dried round-bottomed flask under N_2, PMDA (69.8 mg, 320.1 µmol, 1.0 equiv.) is stirred in glacial acetic acid (5 mL) at 80 °C until dissolved. (*S,S*)-1,2-di(naphthalen-2-yl)ethane-1,2-diamine (100 mg, 320.1 µmol, 1.0 equiv.) is dissolved in additional glacial acetic acid (5 mL) and then added dropwise to the reaction mixture which is then left to stir at 120 °C under N_2

overnight. The crude reaction mixture is analysed by TLC (SiO_2: 5% acetone in CH_2Cl_2) before the mixture is concentrated before purification by flash column chromatography (SiO_2: 0-5% acetone in CH_2Cl_2), to isolate (*S,S*)-**DNaphΔ** (61.4 mg, 41.4 μmol, 38.8%).

^{1}H NMR (400 MHz, CD_2Cl_2, 298 K): δ_H 8.10 (s, 6H[1]), 7.95-7.45 (m, 39H[ar]), 7.28 (s, 8H[9]), 7.22 (s, 10H[2]). **^{13}C NMR** is currently unavailable for this product. **HRMS** (APCI) Calculated for $C_{96}H_{55}N_6O_{12}$ = 1483.3872, found $[M+H]^+$ = 1483.3938 (error -4.4 ppm).

***General Procedure A*: Oxidative cyclodehydrogenation of molecular triangles**

In a flame-dried round-bottomed flask, the (*S,S*)-**DPEΔ** (1.0 equiv) and either DDQ (7.0 equiv) or $FeCl_3$ (30.0 equiv) were cycled three times under N_2 using air-free Schlenk techniques before being dissolved in CH_2Cl_2 along with any required additives. The reaction mixture was stirred at either 0 °C in an ice-water bath or at rt, and reaction progress was monitored by ^{1}H NMR analysis, typically by sampling an aliquot (1.0 mL) from the reaction mixture, evaporating to dryness and redissolving the residue in deuterated solvent.

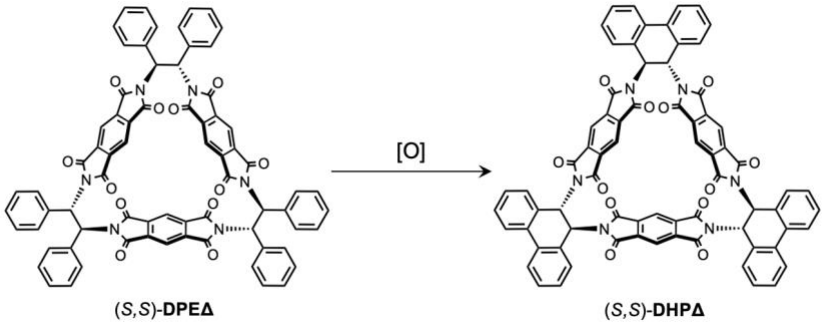

Attempt 1: Applying *General Procedure A* with (*S,S*)-**DPEΔ** (30 mg, 0.0254 mmol, 1.0 equiv.), DDQ (40.3 mg, 0.1775 mmol, 7.0 equiv.), CH_2Cl_2 (15 mL) and methanesulfonic acid (0.19 mL) at 0 °C, no starting material conversion (e.g. to form the desired (*S,S*)-**DHPΔ** product) was observed by ^{1}H NMR analysis after reacting over 2 h.

Attempt 2: Applying *General Procedure A* with (*S,S*)-**DPEΔ** (30 mg, 0.0254 mmol, 1.0 equiv.), DDQ (40.3 mg, 0.1775 mmol, 7.0 equiv.), CH_2Cl_2 (15 mL) and trifluoromethanesulfonic acid (0.32 mL) at 0 °C, no starting material conversion (e.g. to form the desired (*S,S*)-**DHPΔ** product) was observed by ^{1}H NMR analysis after reacting over 2 h.

Attempt 3: Applying *General Procedure A* with (*S,S*)-**DPEΔ** (30 mg, 0.0254 mmol, 1.0 equiv.), $FeCl_3$ (123.4 mg, 0.7607 mmol, 30 equiv.), CH_2Cl_2 (60 mL) and CH_3NO_2 (2 mL) at rt, no starting material conversion (e.g. to form the desired (*S,S*)-**DHPΔ** product) was observed by ^{1}H NMR analysis after reacting over 2 h.

***General Procedure B*: NMR scale oxidative cyclodehydrogenation of molecular triangles**

In an oven-dried NMR tube, (*S,S*)-**DNaphΔ** (1.0 equiv) and an oxidant were cycled three times under N_2 using air-free Schlenk techniques before being dissolved in CD_2Cl_2 along with any required additives and stirred at room temperature for 72 h.

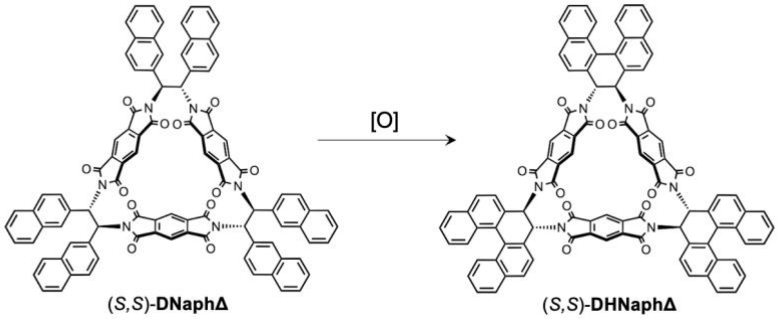

Attempt 1: Applying *General Procedure B* with (*S,S*)-**DNaphΔ** (15.2 mg, 0.0103 mmol, 1.0 equiv.), $FeCl_3$ (49.9 mg, 0.3077 mmol, 30 equiv.), CD_2Cl_2 (0.61 mL) and CD_3NO_2 (0.09 mL), no starting material conversion (e.g. to form the desired (*S,S*)-**DHNaphΔ** product) was observed by ^{1}H NMR analysis after reacting over 72 h.

Attempt 2: Applying *General Procedure B* with (*S,S*)-**DNaphΔ** (15.2 mg, 0.0103 mmol, 1.0 equiv.), $AlCl_3$ (41.0 mg, 0.3077 mmol, 30 equiv.) and CD_2Cl_2 (0.70 mL), no starting material conversion (e.g. to form the desired (*S,S*)-**DHNaphΔ** product) was observed by ^{1}H NMR analysis after reacting over 72 h.

Attempt 3: Applying *General Procedure B* with (*S,S*)-**DNaphΔ** (15.2 mg, 0.0103 mmol, 1.0 equiv.), $MoCl_5$ (16.8 mg, 0.0616 mmol, 6.0 equiv.) and CD_2Cl_2 (0.70 mL), no starting material conversion (e.g. to form the desired (*S,S*)-**DHNaphΔ** product) was observed by ^{1}H NMR analysis after reacting over 72 h.

Attempt 4: Applying *General Procedure B* with (*S,S*)-**DNaphΔ** (15.2 mg, 0.0103 mmol, 1.0 equiv.), DDQ (16.3 mg, 0.0718 mmol, 7.0 equiv.), CD_2Cl_2 (0.62 mL) and trifluoromethanesulfonic acid (0.08 mL), no starting material conversion (e.g. to form the desired (*S,S*)-**DHNaphΔ** product) was observed by ^{1}H NMR analysis after reacting over 72 h.

Compounds **2**, **3**, and **4** were synthesised according to the procedures outlined by Liu, F. *et al.*,[40] with spectroscopic data being consistent with literature.

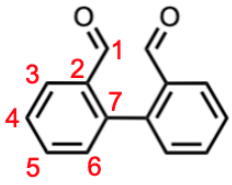

2

Dicarbaldehyde 2: Applying a literature procedure[40] without modification, dicarbaldehyde **2** (2.87 g, 13.7 mmol, 51%) was isolated as a yellow oil.

^{1}H NMR (400 MHz, $CDCl_3$, 298 K): δ_H 9.84 (s, 2H[1]), 8.07 (dd, *J*= 7.7, 1.5 Hz, 2H[3]), 7.67 (td, *J*= 7.7, 1.8 Hz, 2H[5]), 7.60 (t, *J*= 7.7 Hz, 2H[4]), 7.36 (dd, *J*= 7.4, 1.2 Hz, 2H[6]). **^{13}C NMR** (101 MHz, $CDCl_3$, 298 K): δ_C 191.2[1], 141.3[2], 134.7[7], 133.6[3], 131.8[6], 128.9[4], 128.7[5]. **HRMS** (ESI, +ve): Calculated for $C_{14}H_8NaO_2$ = 231.0417, found $[M+Na]^+$ 231.0418 (error -0.6 ppm). Spectroscopic data are consistent with literature.[40]

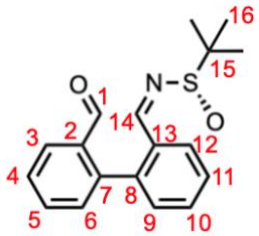

3

Aldehyde-imine 3: Applying a literature procedure[40] without modification, alydehyde-imine **3** (2.01 g, 6.42 mmol, 47% yield) was isolated as a yellow oil.

^{1}H NMR (400 MHz, $CDCl_3$, 298 K): δ_H 9.79 (s, 1H[1]), 8.41 (s, 0.44H[14] minor isomer), 8.38 (s, 0.54H[14] major isomer), 8.16-8.10 (m, 1H[12]), 8.03 (d, *J*= 7.9 Hz, 1H[3]), 7.68-7.62 (m, 1H[6]), 7.59-7.54 (m, 3H[4,9,11]), 7.34-7.27 (m, 2H[5,10]), 1.17 (s, 5.4H[16] minor isomer), 1.11 (s, 5.4H[16] major isomer). **^{13}C NMR** (101 MHz, $CDCl_3$, 298 K): δ_C 191.5[1], 161.3[14], 142.6, 140.0, 134.6, 134.5, 133.8, 133.7, 132.9, 132.8, 131.9, 131.80, 131.7, 131.6, 131.5, 131.4, 129.1, 129.1, 128.8, 128.8, 128.6, 128.5, 57.9[15], 22.7[16]. **HRMS** (ESI, +ve): Calculated for $C_{18}H_{21}NO_2S$ = 314.1209, found $[M+H]^+$ 314.1204 (error 1.5 ppm); calculated for $C_{18}H_{20}NNaO_2S$ = 336.1029, found $[M+Na]^+$ 336.1029 (error -0.1ppm); calculated for $C_{18}H_{20}KNO_2S$ = 352.0768, found $[M+K]^+$ 352.0770 (error -0.4 ppm). Spectroscopic data are consistent with literature.[40]

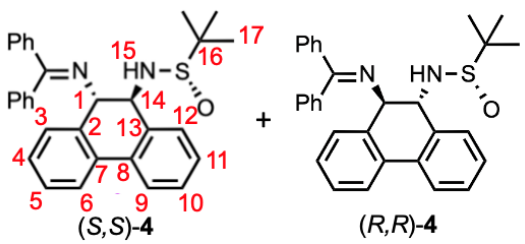

(*S,S*)-**4** + (*R,R*)-**4**

Protected dihydrophenanthrene diamine (*S,S*)-4 and (*R,R*)-4: Applying a literature procedure[40] without modification, protected dihydrophenanthrene diamine (*S,S*)-**4** and (*R,R*)-**4** (2.29 g, 4.79 mmol, 55% yield) was isolated as a white solid.

^{1}H NMR (400 MHz, $CDCl_3$, 298 K): δ_H 7.81 (m, 3H), 7.64 (d, J = 8.2 Hz, 1H), 7.52-7.18 (m, 14H), 7.06 (d, J = 7.8 Hz, 1H), 4.85 (t, J = 8.2 Hz, 0.44H[1/14] minor isomer), 4.77 d, J = 7.1 Hz, 0.56H[1/14] major isomer), 4.73-4.76 (m, 1H[1/14]), 3.33 (d, J = 7.8 Hz, 0.41H[15] minor isomer), 3.05 (d, J = 7.7 Hz, 0.50H[15] major isomer), 1.11 (s, 4H[17]), 1.10 (s, 5H[17]). **^{13}C NMR** (101 MHz, $CDCl_3$, 298 K): δ_C 170.4, 169.5, 139.8, 139.3, 137.7, 136.7, 136.5, 136.5, 135.8, 135.6, 135.4, 133.8, 133.8, 133.4, 133.3, 132.5, 130.4, 130.3, 130.2, 129.1, 129.0, 129.0, 128.9, 128.7, 128.6, 128.5, 128.4, 128.2, 128.1, 128.1, 128.0, 127.9, 127.7, 127.4, 124.2, 124.1, 124.1, 124.0, 66.6, 66.2, 61.5, 59.9, 56.4, 56.2, 22.8, 22.5. **HRMS** (ESI, +ve): Calculated for $C_{31}H_{31}N_2OS$ = 479.2152, found $[M+H]^+$ 479.2149 (error +0.5ppm); calculated for $C_{31}H_{30}N_2NaOS$ = 501.1971, found $[M+Na]^+$ 501.1967 (error +0.8 ppm). Spectroscopic data are consistent with literature.[40]

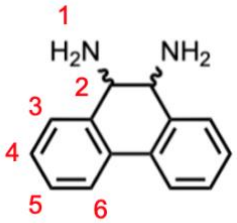

rac-**6**

Racemic *trans*-9,10-dihydrophenanthrene-9,10-diamine *rac*-6: A round-bottomed flask containing **4** (1.30 g, 2.72 mmol, 1.0 equiv.), THF (15 mL) and 6 M HCl (6.5 mL) was stirred at rt for 1 h before being concentrated to remove the majority of THF solvent. Diethyl ether (3 x 15 mL) was then added to wash the aqueous layer containing the chloride salt of the diamine before neutralising it with $NaHCO_3$ to ~pH 7. A polar mixture of CH_2Cl_2-MeOH (2:1 *v/v*, 3 x 30 mL) was then used to extract the free diamine from the aqueous layer before the combined organic layers were dried (Na_2SO_4), filtered and concentrated to obtain the product *rac*-**6** (0.29 g, 1.39 mmol, 51%) as a blue oil.

^{1}H NMR (400 MHz, $CDCl_3$, 298 K): δ_H 7.79 (dd, J = 7.6, 1.4 Hz, 2H[3]), 7.47 (dd, J = 7.3, 1.4 Hz, 2H[6]), 7.35 (m, 4H[4,5]), 3.86 (s, 2H[2]), 1.80 (s (br), 4H[1]). **HRMS** (ESI, +ve): Calculated $C_{14}H_{15}N_2$ = 211.1230, found $[M+H]^+$ 211.1227 (error +1.5 ppm).

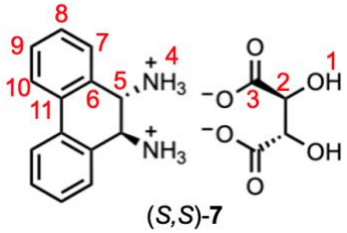

(*S,S*)-**7**

***trans*-9,10-Dihydrophenanthrene-9,10-diammonium tartrate salt (*S,S*)-7**: D-(-)-tartaric acid (214.3 mg, 1.428 mmol, 0.5 equiv.) was dissolved in water (0.75 mL) in a reaction vessel before *rac*-**6** (500 mg, 2.380 mmol, 1.0 equiv.) in a small amount of water and acetone (to assist with transferring) was slowly added to ensure there was no precipitation. Once addition was complete, glacial acetic acid (0.15 mL) was slowly added whilst ensuring the temperature did not exceed 90 °C. The reaction mixture was left to stand in the fridge (4 °C) overnight to encourage crystallisation of the desired tartrate salt, (*S,S*)-**7**. The aqueous mixture was washed with CH_2Cl_2 (3 x 3 mL) to remove any unreacted starting materials or unwanted organic-soluble isomer byproducts, leaving behind predominantly the desired monotartrate salt. The aqueous layer was concentrated to obtain the tartrate salt (561.7 mg, 1.559 mmol, 66%*) as a pale orange solid. *With respect to the corresponding starting enantiomer in the racemic mixture of **6**.

^{1}H NMR (400 MHz, D_2O, 298 K): δ_H 7.98 (d, J = 7.7 Hz, 2H^7), 7.58 (td, J = 7.7, 1.5 Hz, 2H^8), 7.51 (d, J = 7.7, 2H^{10}), 7.42 (td, J = 7.7, 1.3 Hz, 2H^9), 4.79 (s, 2H^5), 4.17 (s, 2H^2), 1.81 (s, 2H^1). **^{13}C NMR** (101 MHz, D_2O, 298 K): δ_C 178.4^3, 132.3^{ar}, 132.2^{ar}, 131.5^{ar}, 129.7^{ar}, 125.3^{ar}, 124.7^{ar}, 73.8^2, 50.3^5.

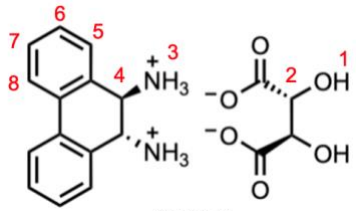

(*R,R*)-**7**

***trans*-9,10-Dihydrophenanthrene-9,10-diammonium tartrate salt (*R,R*)-7**: The diamino-tartrate salt (*R,R*)-**7** (396.9 mg, 1.101 mmol, 71%*) was obtained as a pale orange solid using *L*-(+)-tartaric acid instead of *D*-(-)-tartaric acid using the procedure above. * With respect to the corresponding starting enantiomer in the racemic mixture of **6.**

^{1}H NMR (400 MHz, D_2O, 298 K): δ_H 8.09 (d, J = 7.8 Hz, 2H^5), 7.69 (dd, J = 7.8, 7.4 Hz, 2H^6), 7.62 (d, J = 7.3 Hz, 2H^8), 7.53 (t, J = 7.8, 7.3 Hz, 2H^7), 4.92 (s, 2H^2), 4.38 (s, 2H^4), 2.02 (s, 2H^1).

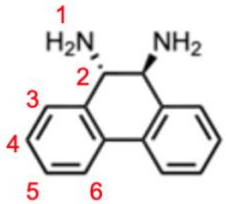

(*S,S*)-**6**

(*S,S*)-9,10-dihydrophenanthrene-9,10-diamine (*S,S*)-6: (*S,S*)-**7** (561.7 mg, 1.559 mmol, 1.0 equiv.) and K_2CO_3 (215.4 mg, 1.559 mmol, 1.0 equiv.) were dissolved in water (2 mL) and left to fully dissolve

for ~10 min. CH_2Cl_2-MeOH (*v/v* 2:1, 6 mL) was added to the reaction mixture and left to react while monitoring the aqueous layer by TLC. The combined organic layers were dried with Na_2SO_4, filtered and concentrated to obtain the free diamine (*S,S*)-**6** (159.3 mg, 0.758 mmol, 49%) as a brown oil.

^{1}H NMR (400 MHz, $CDCl_3$, 298 K): δ_H 7.80 (dd, *J* = 7.6, 1,9 Hz, 2H[3]), 7.48 (dd, *J* = 7.1, 1.3 Hz, 2H[6]), 7.39 (td, *J* = 8.0, 1.8 Hz, 2H[4/5]), 7.34 (td, *J* = 7.6, 1.4 Hz, 2H[4/5]), 3.86 (s, 2H[2]), 1.57 ((br)s, 4H[1]). Spectroscopic data was consistent with literature.[40]

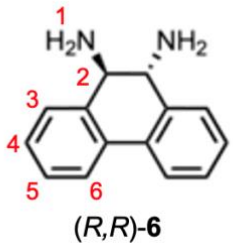

(*R,R*)-**6**

(*R,R*)-9,10-dihydrophenanthrene-9,10-diamine, (*R,R*)-**6** (285.2 mg, 1.357 mmol, quant.) was obtained using (*R,R*)-**7** in a similar procedure as stated above.

^{1}H NMR (400 MHz, $CDCl_3$, 298 K): δ_H 7.79 (d, *J* = 8.0 Hz, 2H[3]), 7.47 (dd, *J* = 7.2 Hz, 1.2 Hz, 2H[6]), 7.41-7.30 (m, 4H[4,5]), 3.85 (s, 2H[2]), 1.74 (s (br), 4H[1]). Spectroscopic data was consistent with literature.[40]

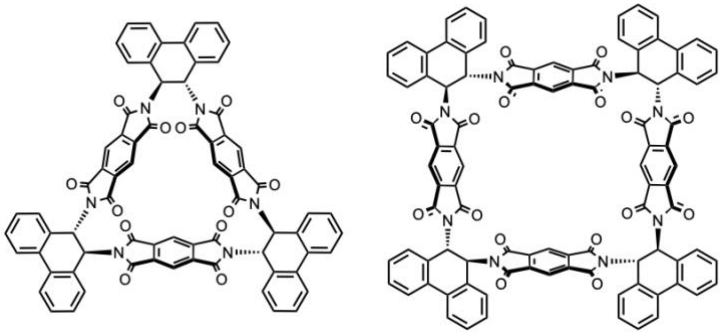

(*S,S*)-DHPΔ and (*S,S*)-DHP□: In a flame-dried round-bottomed flask under N_2, PMDA (165.4 mg, 0.758 mmol, 1.0 equiv.) is stirred in dry DMF (8 mL) at 80 °C until dissolved. (*S,S*)-**6** (159.3 mg, 0.758 mmol, 1.0 equiv.) is dissolved in additional DMF (8 mL) and then added to the reaction mixture which is then left to stir at 120 °C under N_2 overnight. Once cooled to rt, the crude reaction mixture is analysed by TLC (SiO_2: 15% acetone in CH_2Cl_2) to confirm product formation by comparison with known product. The mixture is concentrated before purification by flash column chromatography (SiO_2: 0-15% acetone in CH_2Cl_2) was performed to obtain (*S,S*)-**DHPΔ** and (*S,S*)-**DHP□** as an impure mixture before

purification by an acetone trituration to isolate an inseparable mixture of (*S,S*)-**DHPΔ** and (*S,S*)-**DHP□** (30.5 mg, 7.2%, 31.5:68.5 respectively by ^{1}H NMR analysis).

^{1}H NMR (400 MHz, $CDCl_3$, 298 K): δ_H 8.37 (s, 1H), 8.28 (s, 1H), 8.27 (s, 1H), 8.20 (s, 1H), 7.86 (d, *J* = 7.6 Hz, 5H), 7.47 (t, *J* = 8.0 Hz, 5H), 7.31-7.21 (m, 5H), 6.90-6.83 (m, 5H), 6.80 (s, 1H), 6.78 (d, *J* = 4.8 Hz, 1H), 6.75 (s, 1H). **HRMS** (APCI, +ve): Calculated $C_{72}H_{37}N_6O_{12}$ = 1177.2464, found $[M+H]^+$ 1177.2533 (error +5.8 ppm).

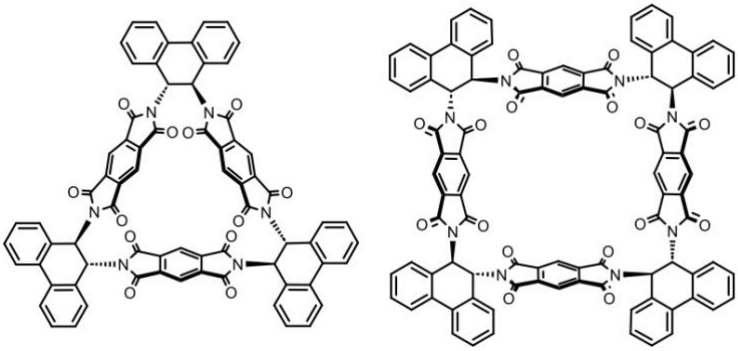

(*R,R*)-DHPΔ and (*R,R*)-DHP□: In a flame-dried round-bottomed flask under N_2, PMDA (296.1 mg, 1.357 mmol, 1.0 equiv.) is stirred in dry DMF (15 mL) at 80 °C until dissolved. (*R,R*)-**6** (285.2 mg, 1.357 mmol, 1.0 equiv.) is dissolved in additional DMF (15 mL) and then added to the reaction mixture which is then left to stir at 120 °C under N_2 overnight. Once cooled to rt, the crude reaction mixture is analysed by TLC (SiO_2: 5% acetone in CH_2Cl_2) to confirm product formation by comparison with known product. The mixture is concentrated before purification by flash column chromatography (SiO_2: 0-15% acetone in CH_2Cl_2) was performed to obtain (*R,R*)-**DHPΔ** and (*R,R*)-**DHP□** as an impure mixture before purification by an acetone trituration to isolate an inseparable mixture of (*R,R*)-**DHPΔ** and (*R,R*)-**DHP□** (25.6 mg, 3.4%, 43:57 respectively ^{1}H NMR analysis).

^{1}H NMR (400 MHz, $CDCl_3$, 298 K): δ_H 8.37 (s, 1H), 8.28 (s, 1H), 8.27 (s, 1H), 8.20 (s, 1H), 7.87 (d, *J* = 7.2 Hz, 5H), 7.46 (t, *J* = 7.2 Hz, 5H), 7.27 (t, *J* = 8.0 Hz, 5H), 6.86 (dd, *J* = 7.6, 3.2 Hz, 5H), 6.81 (s, 1H), 6.78 (d, *J* = 4.8 Hz, 1H), 6.75 (s, 1H). **HRMS** (APCI, +ve): Calculated $C_{72}H_{37}N_6O_{12}$ = 1177.2464, found $[M+H]^+$ 1177.2488 (error -2.0 ppm). Calculated $C_{96}H_{49}N_8O_{16}$ = 1569.3261, found $[M+H]^+$ 1569.3209 (error -2.0 ppm).

6.0 Supplementary data

6.1 NMR spectra

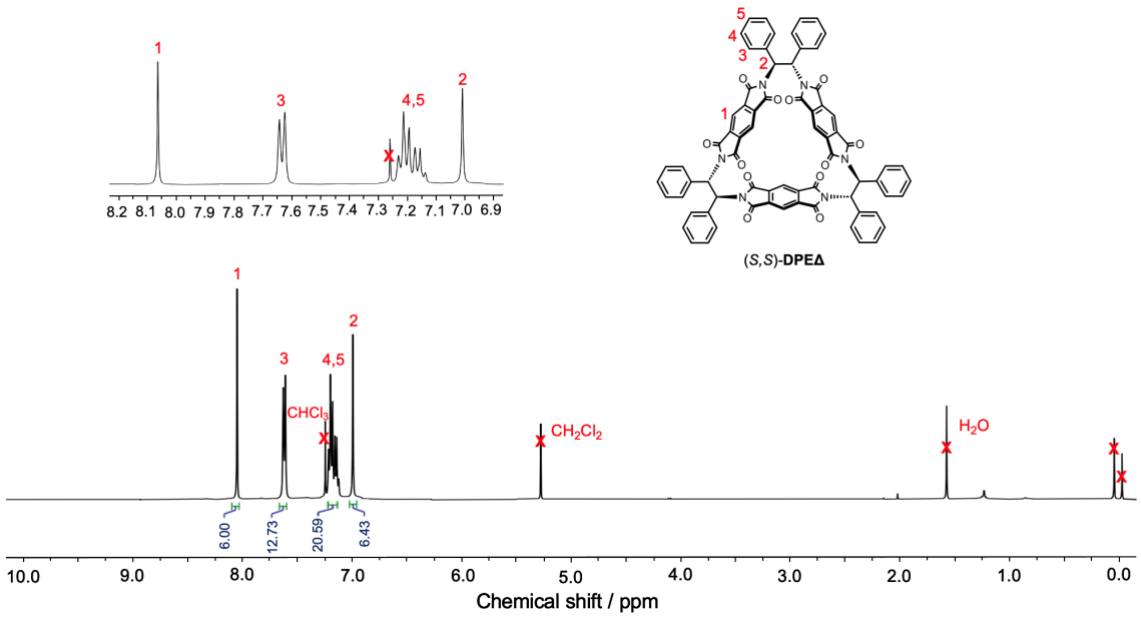

Figure S1.1 ^{1}H NMR (400 MHz, $CDCl_3$, 298 K) spectrum of (*S,S*)-**DPEΔ**.

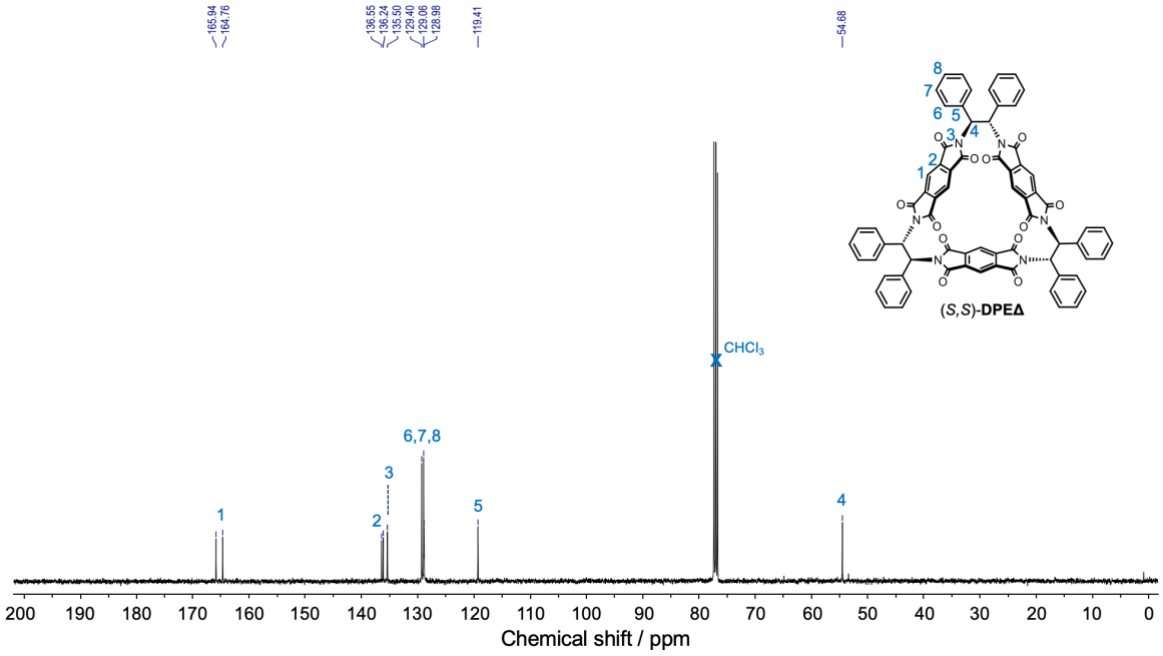

Figure S1.2 ^{13}C NMR (101 MHz, $CDCl_3$, 298 K) spectrum of (*S,S*)-**DPEΔ**.

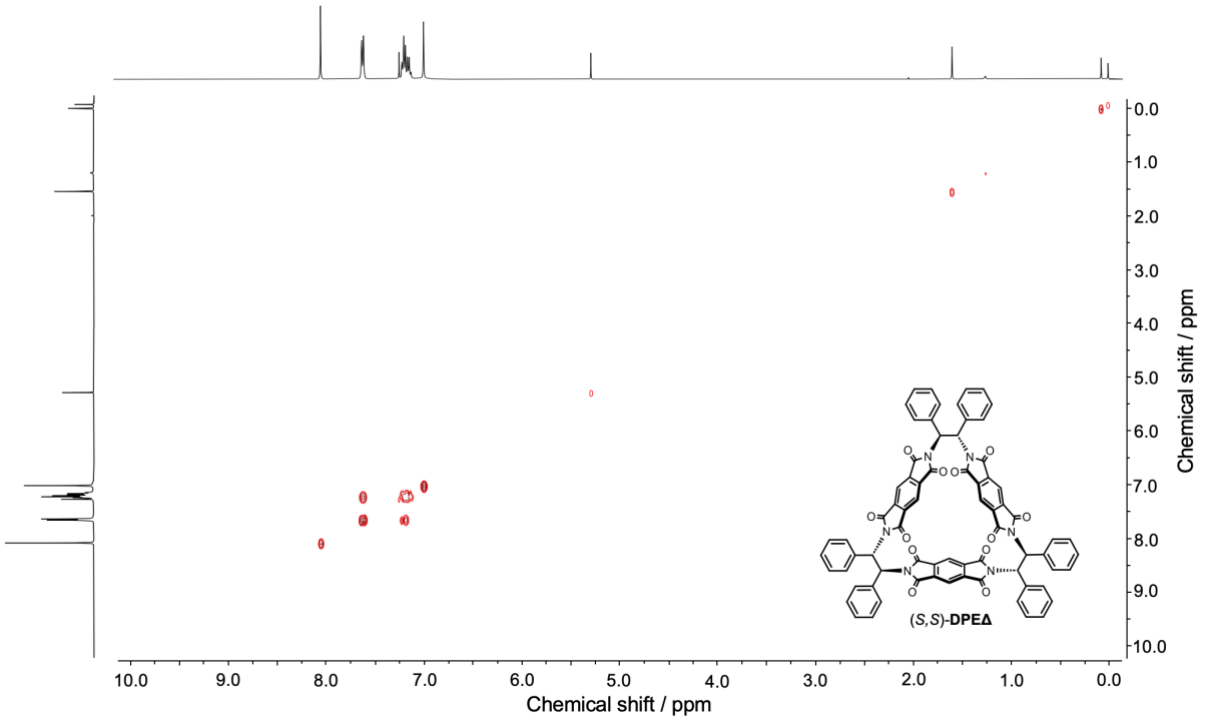

Figure S1.3 ^{1}H-^{1}H COSY NMR (400 MHz, $CDCl_3$, 298 K) spectrum of (*S,S*)-**DPEΔ**.

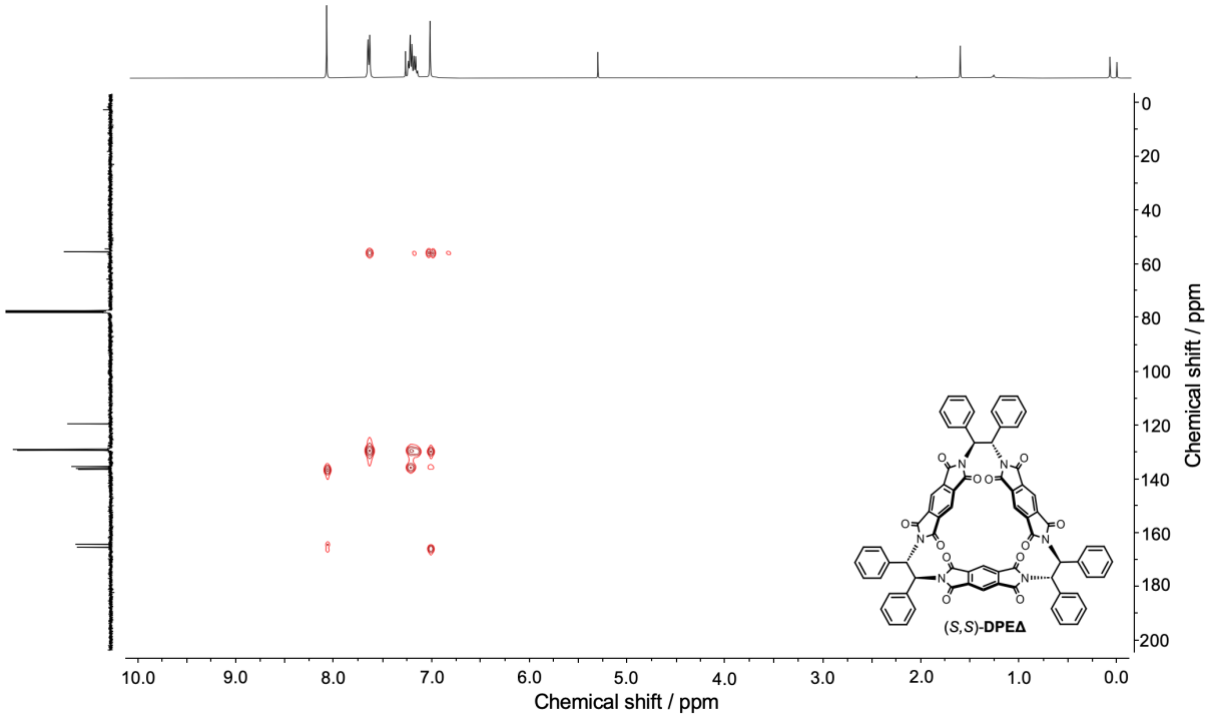

Figure S1.4 ^{1}H-^{13}C HMBC NMR (400 MHz, $CDCl_3$, 298 K) spectrum of (*S,S*)-**DPEΔ**.

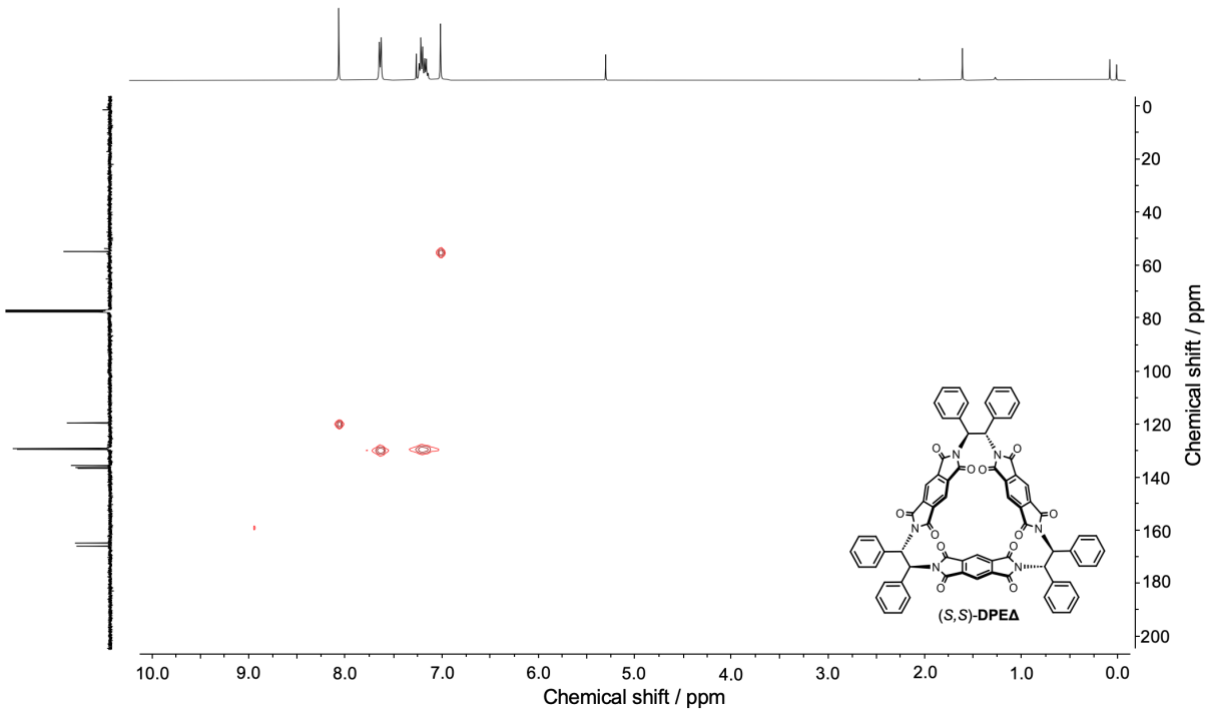

Figure S1.5 ^{1}H-^{13}C HMQC NMR (400 MHz, $CDCl_3$, 298 K) spectrum of (*S,S*)-**DPEΔ**.

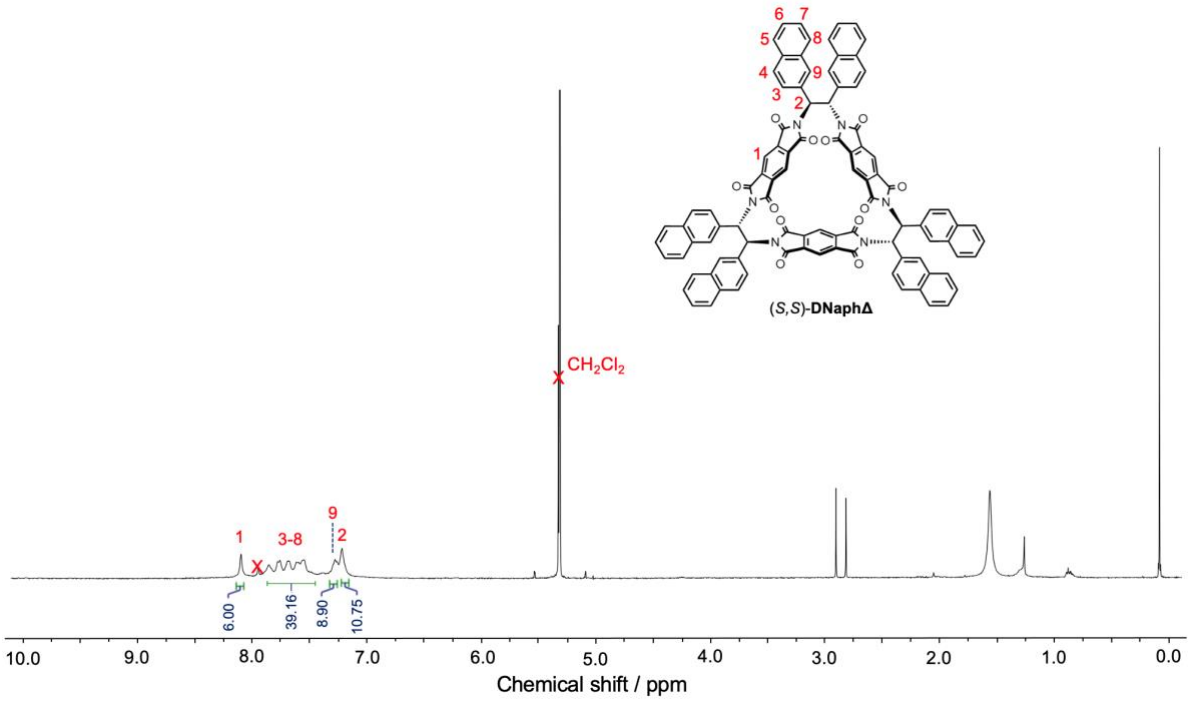

Figure S1.6 ^{1}H NMR (400 MHz, $CDCl_3$, 298 K) spectrum of (*S,S*)-**DNaphΔ**.

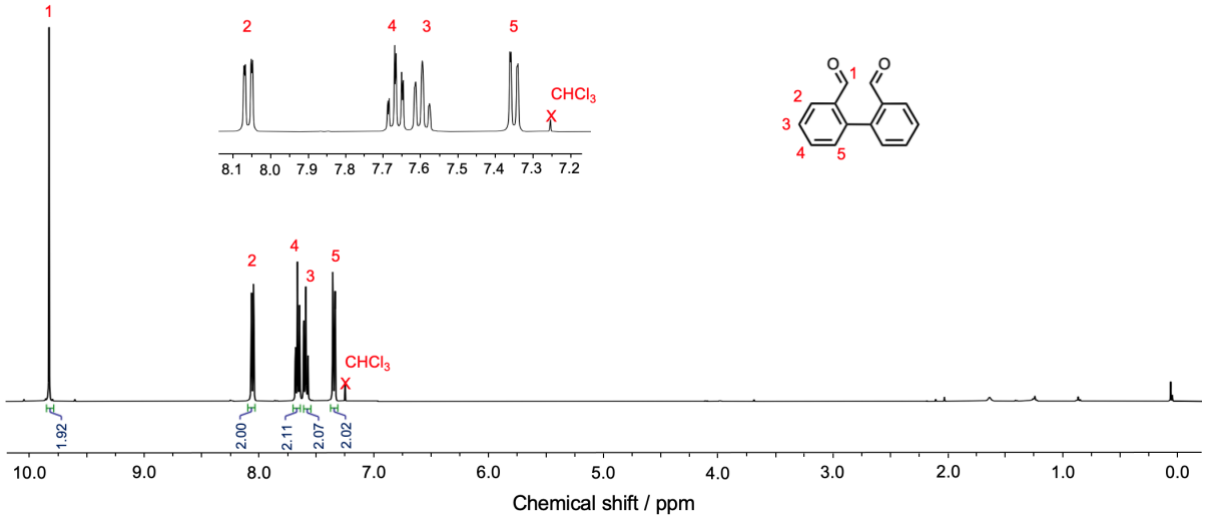

Figure S1.7 ^{1}H NMR (400 MHz, $CDCl_3$, 298 K) spectrum of **2**.

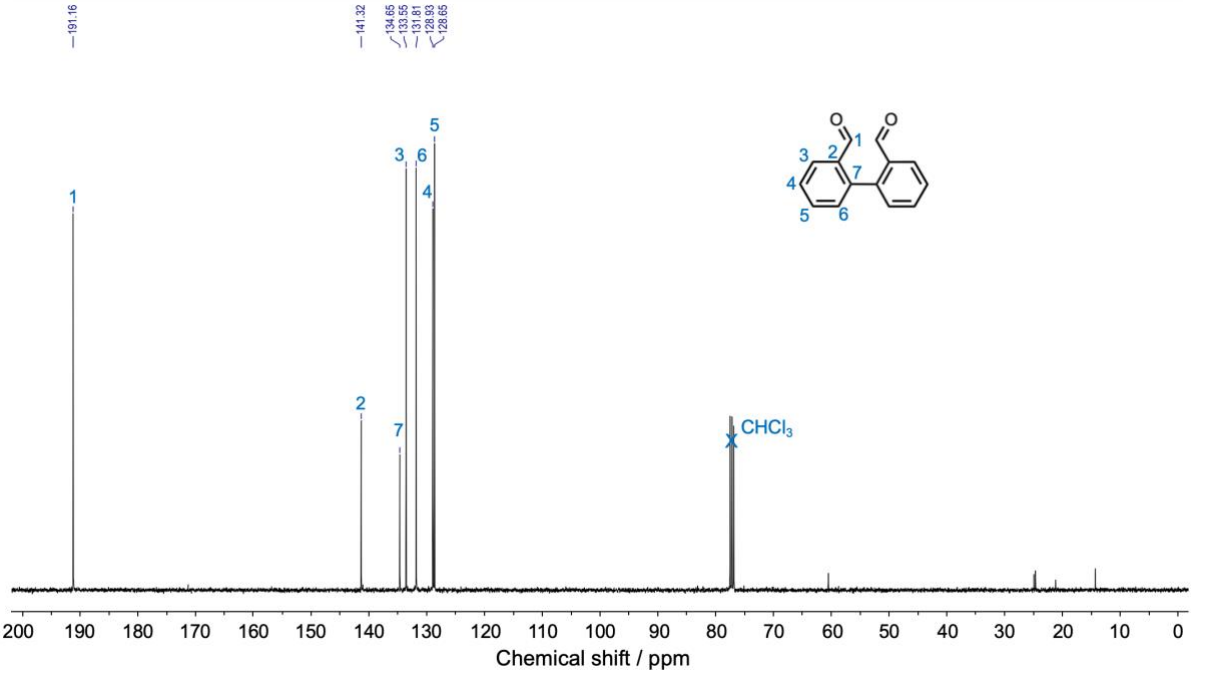

Figure S1.8 ^{13}C NMR (101 MHz, $CDCl_3$, 298 K) spectrum of **2**.

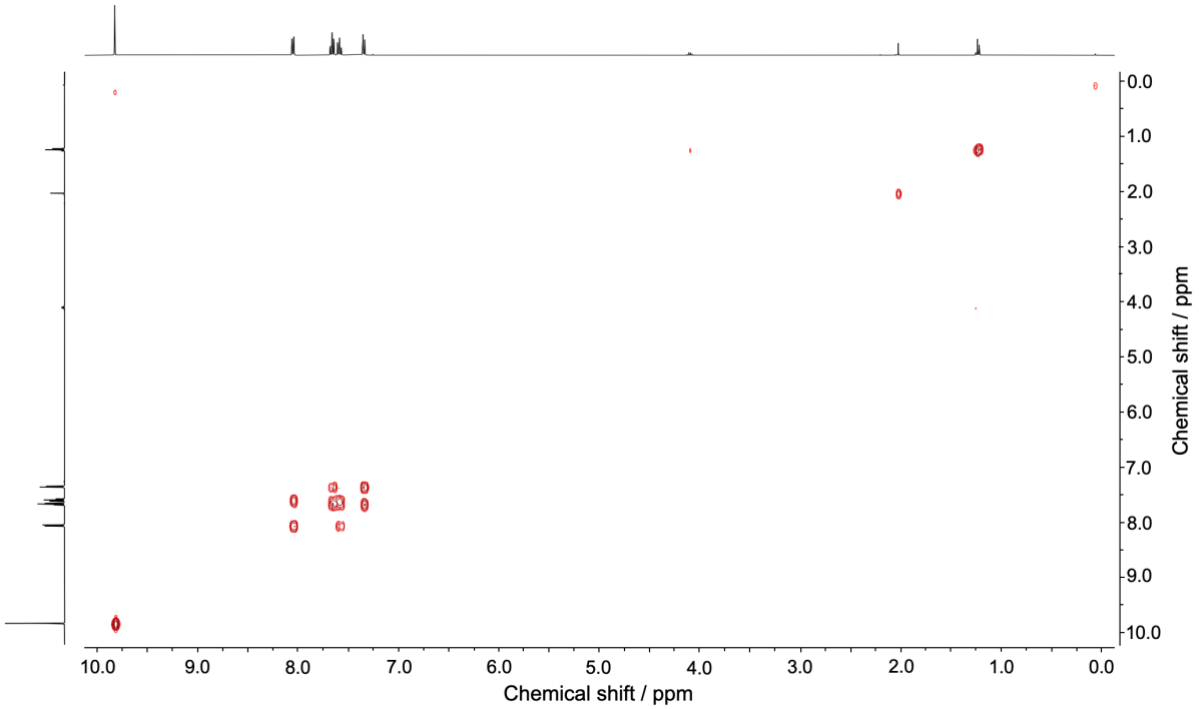

Figure S1.9 ^{1}H-^{1}H COSY NMR (400 MHz, $CDCl_3$, 298 K) spectrum of **2**.

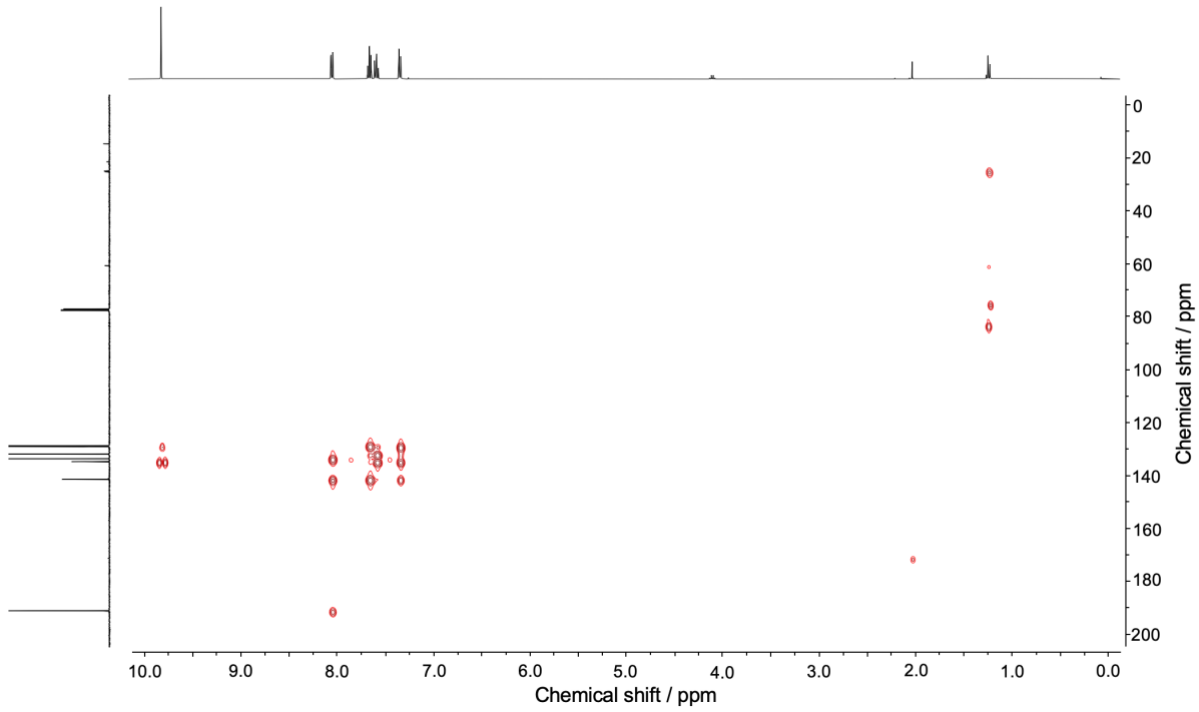

Figure S1.10 ^{1}H-^{13}C HMBC NMR (400 MHz, $CDCl_3$, 298 K) spectrum of **2**.

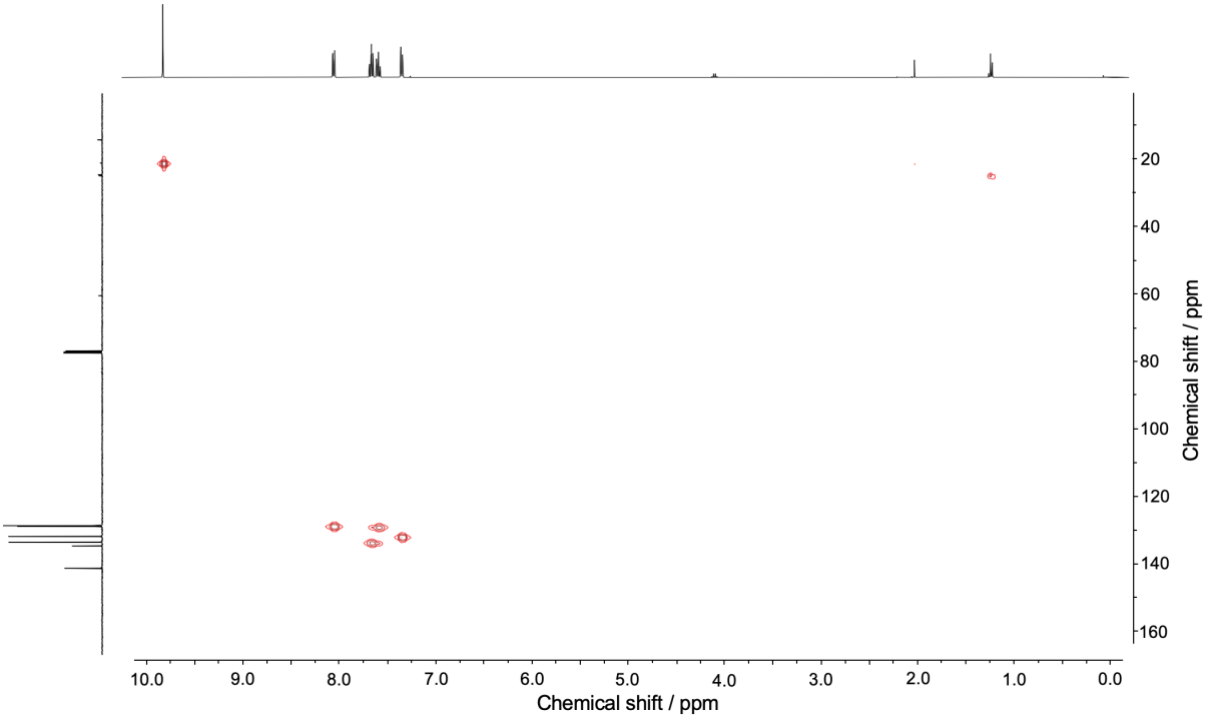

Figure S1.11 ^{1}H-^{13}C HMQC NMR (400 MHz, $CDCl_3$, 298 K) spectrum of **2**.

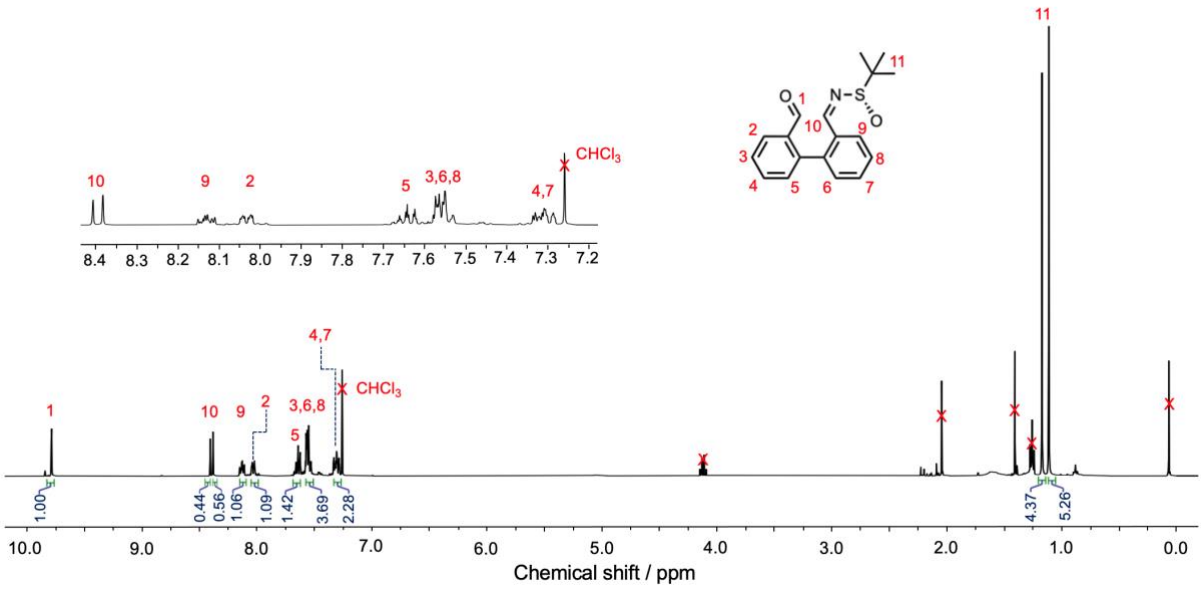

Figure S1.12 ^{1}H NMR (400 MHz, $CDCl_3$, 298 K) spectrum of **3**.

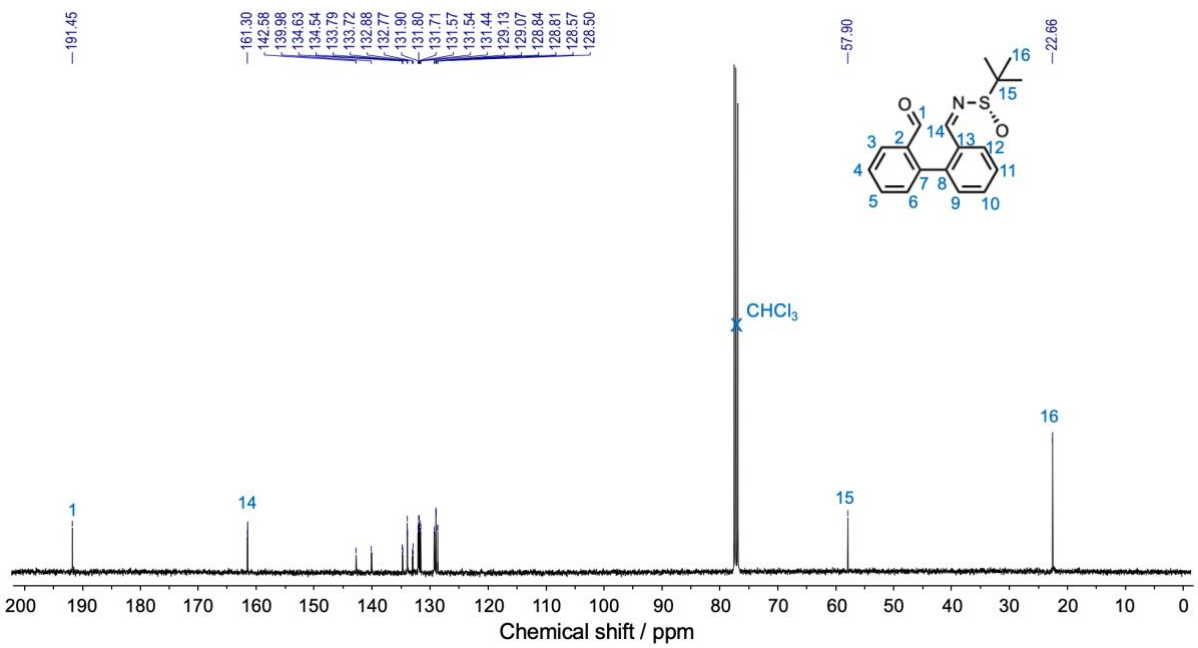

Figure S1.13 ^{13}C NMR (101 MHz, $CDCl_3$, 298 K) spectrum of **3**.

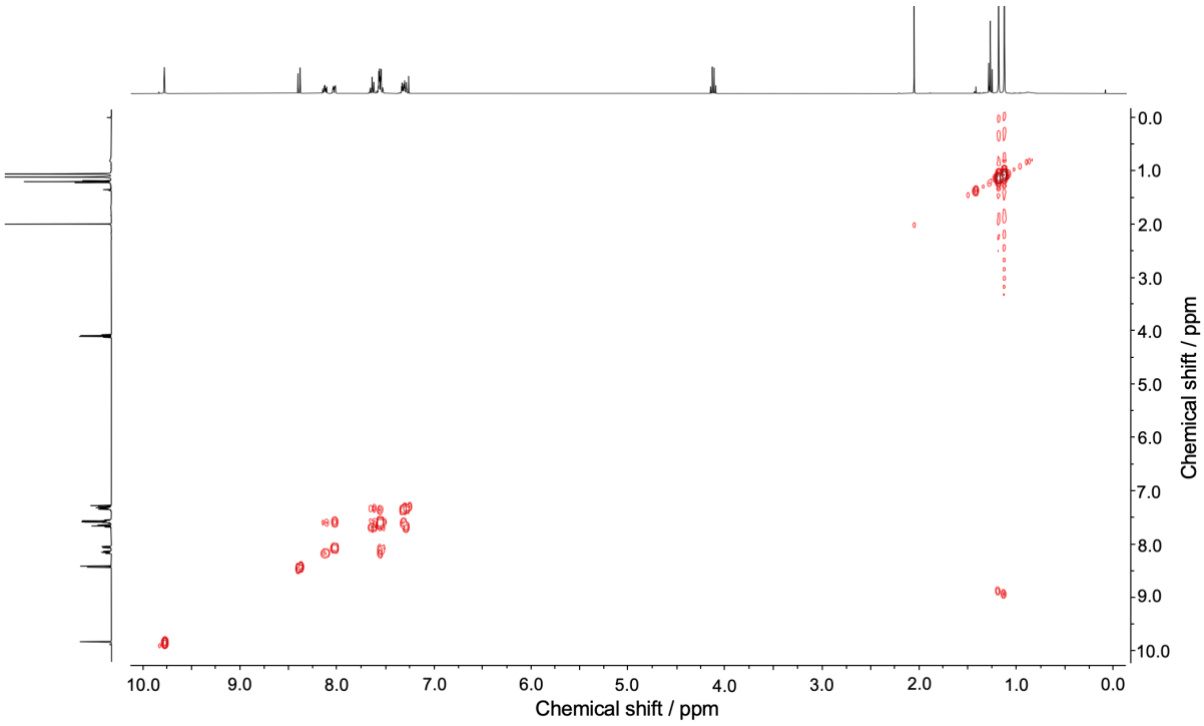

Figure S1.14 ^{1}H-^{1}H COSY NMR (400 MHz, $CDCl_3$, 298 K) spectrum of **3**.

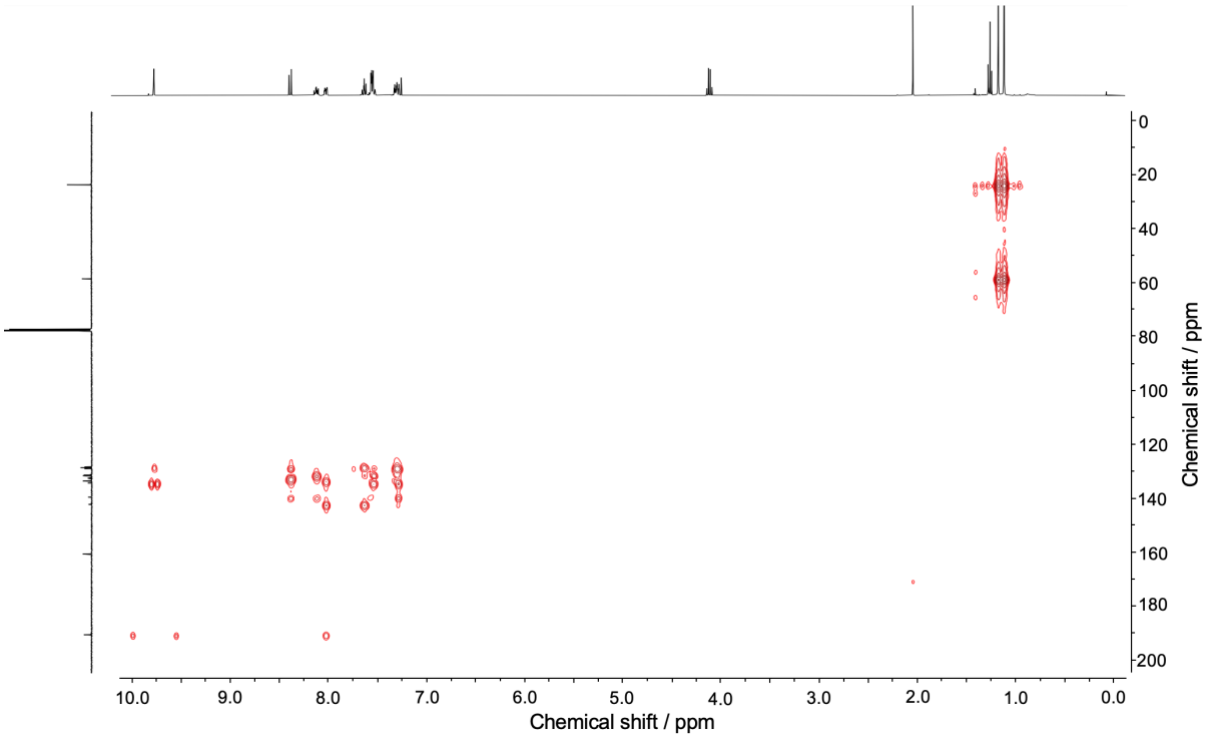

Figure S1.15 ^{1}H-^{13}C HMBC NMR (400 MHz, $CDCl_3$, 298 K) spectrum of **3**.

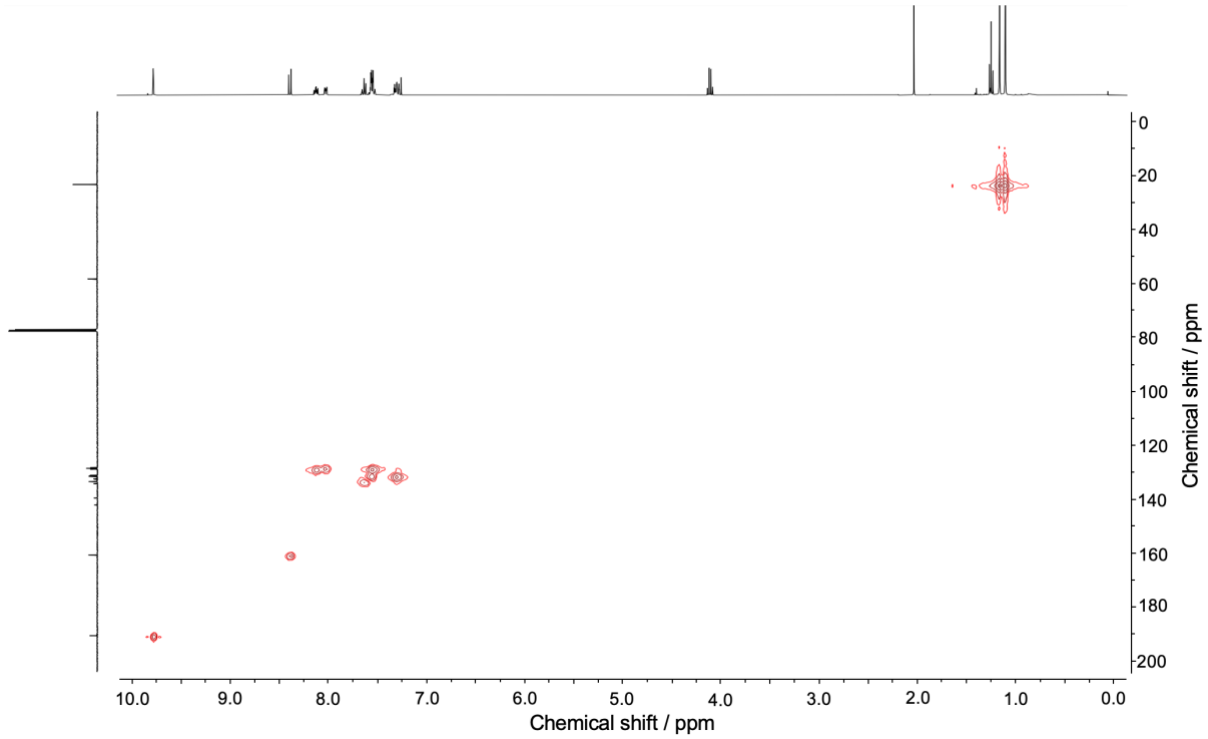

Figure S1.16 ^{1}H-^{13}C HMQC NMR (400 MHz, $CDCl_3$, 298 K) spectrum of **3**.

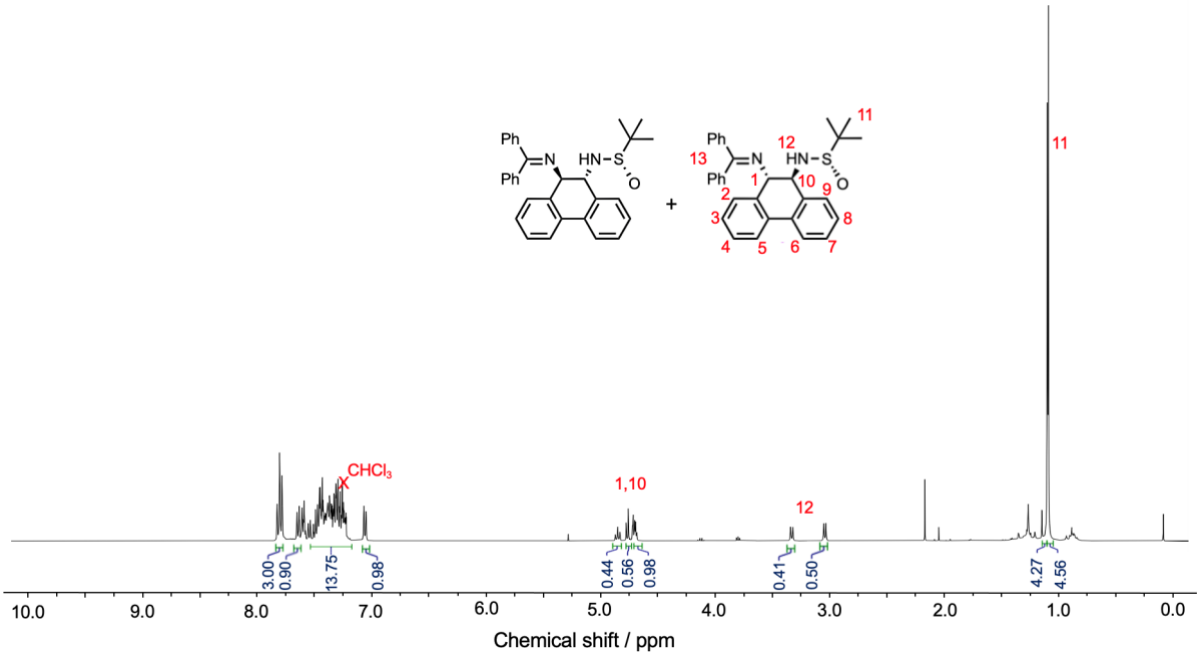

Figure S1.17 ^{1}H NMR (400 MHz, $CDCl_3$, 298 K) spectrum of (*S,S*)-**4** and (*R,R*)-**4** .

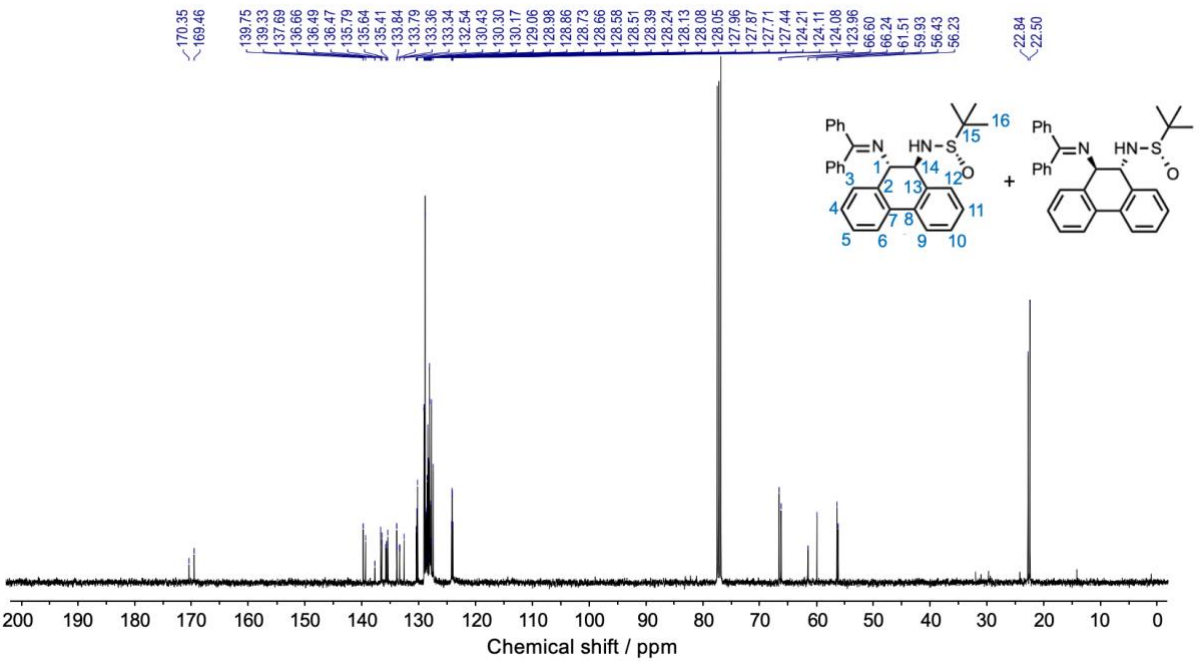

Figure S1.18 ^{13}C NMR (101 MHz, $CDCl_3$, 298 K) spectrum of (*S,S*)-**4** and (*R,R*)-**4**.

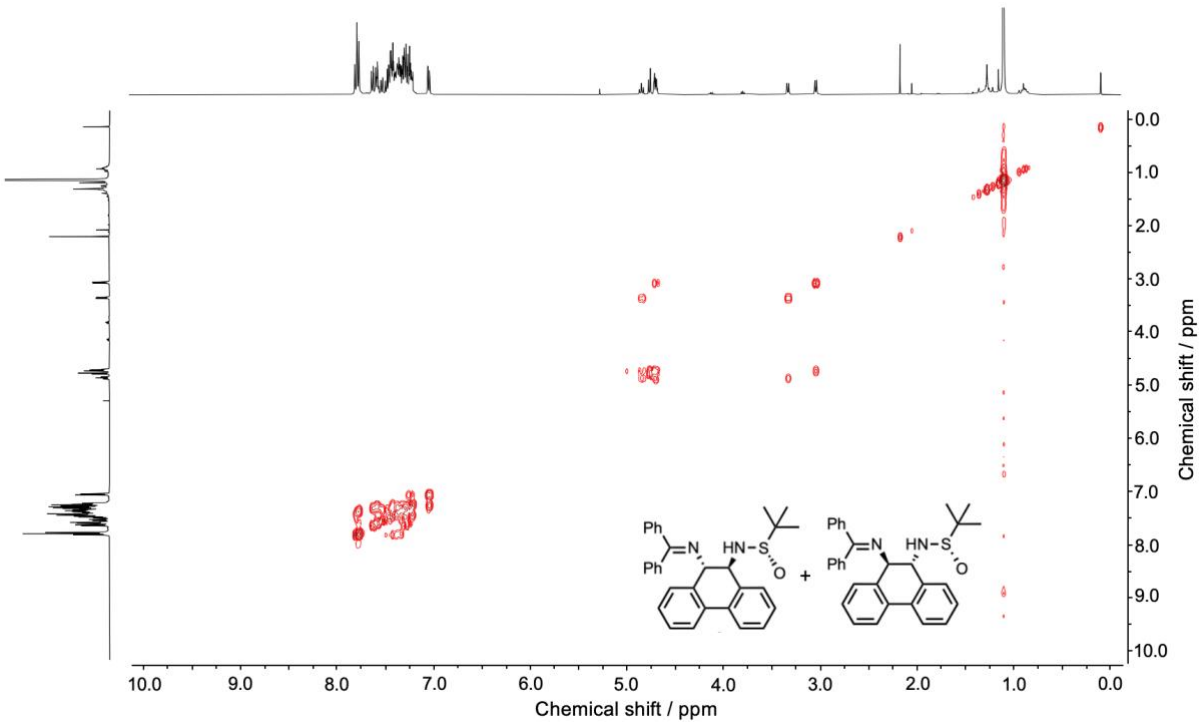

Figure S1.19 ^{1}H-^{1}H COSY NMR (400 MHz, $CDCl_3$, 298 K) spectrum of (*S,S*)-**4** and (*R,R*)-**4**.

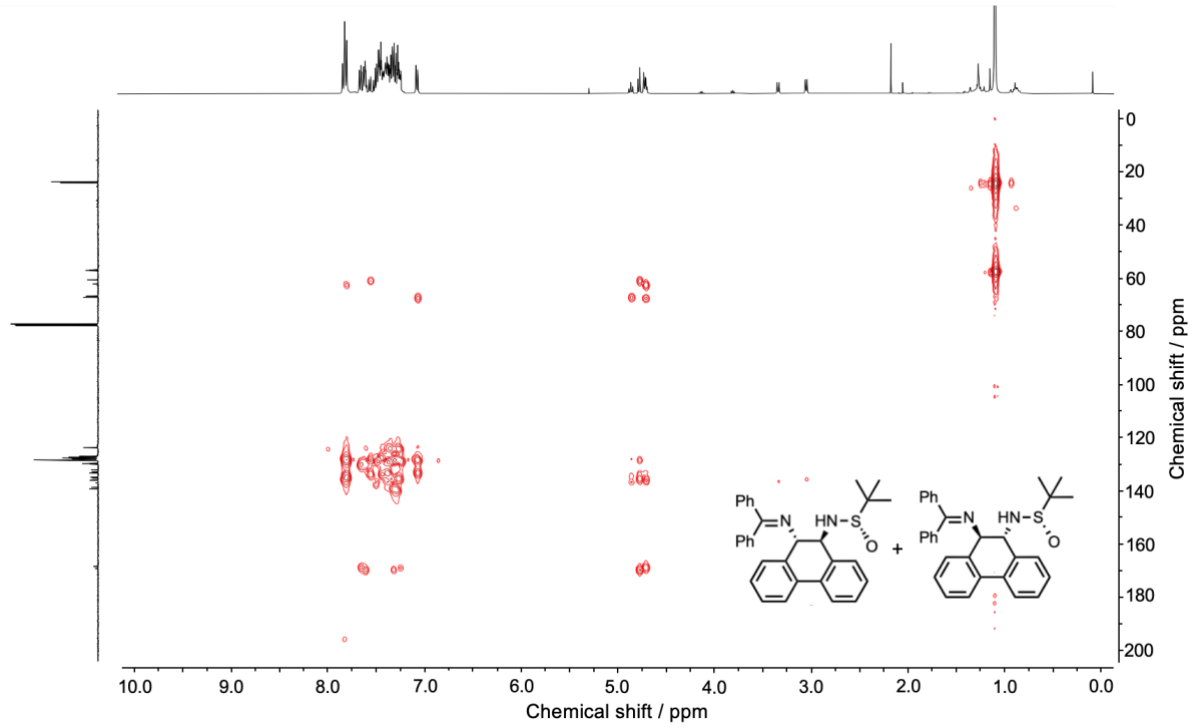

Figure S1.20 ^{1}H-^{13}C HMBC NMR (400 MHz, $CDCl_3$, 298 K) spectrum of (*S,S*)-**4** and (*R,R*)-**4**.

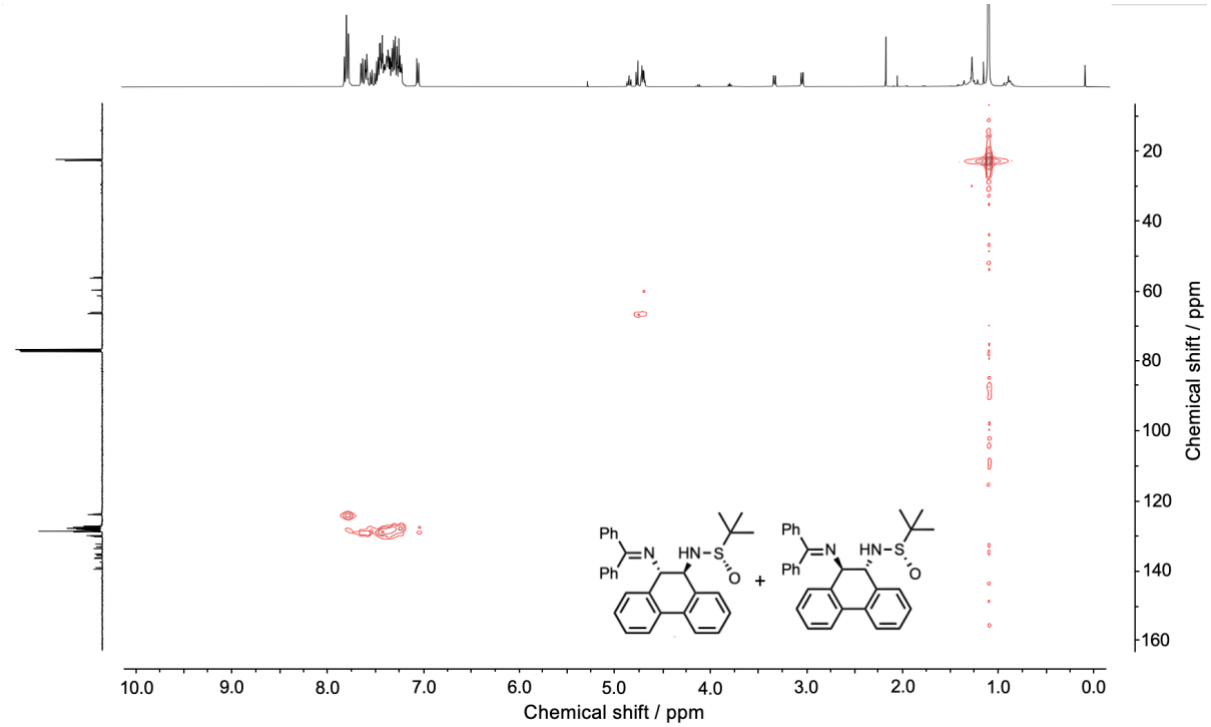

Figure S1.21 ^{1}H-^{13}C HMQC NMR (400 MHz, $CDCl_3$, 298 K) spectrum of (*S,S*)-**4** and (*R,R*)-**4**.

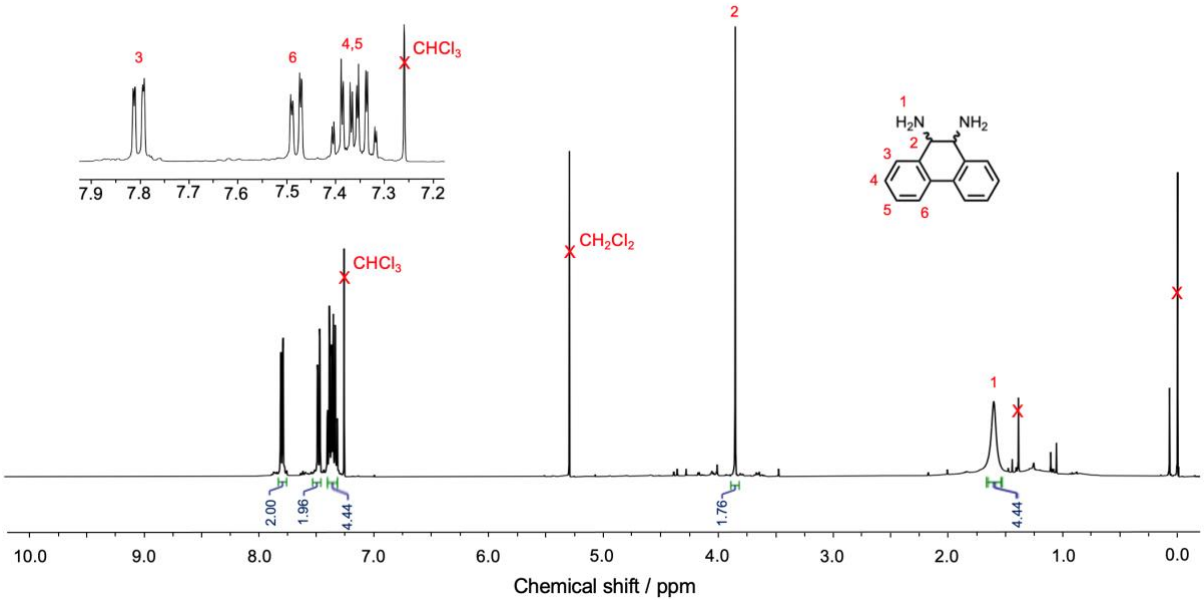

Figure S1.22 ^{1}H NMR (400 MHz, $CDCl_3$, 298 K) spectrum of *rac*-**6**.

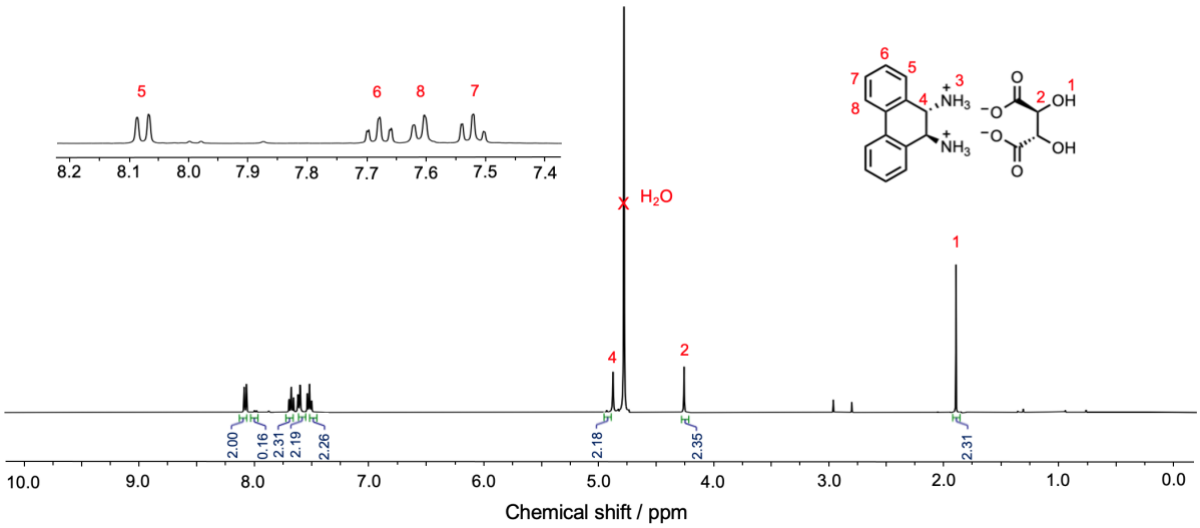

Figure S1.23 ^{1}H NMR (400 MHz, $CDCl_3$, 298 K) spectrum of (*S,S*)-**7**.

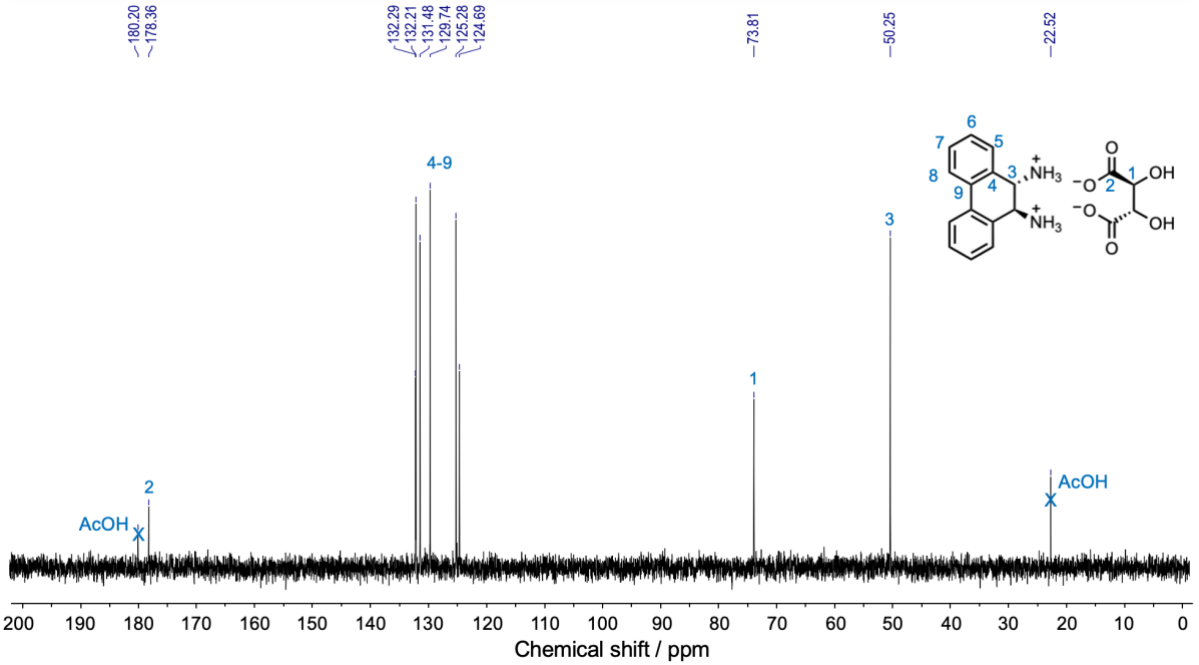

Figure S1.24 ^{13}C NMR (101 MHz, $CDCl_3$, 298 K) spectrum of (*S,S*)-**7**.

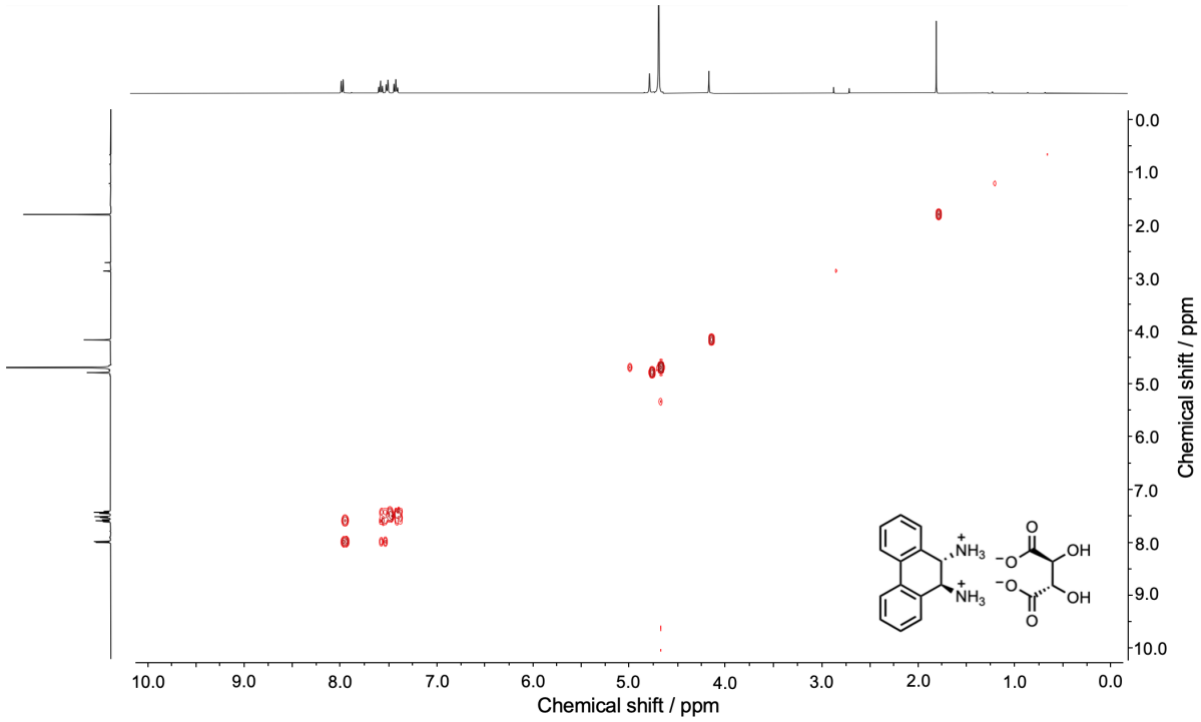

Figure S1.25 ^{1}H-^{1}H COSY NMR (400 MHz, $CDCl_3$, 298 K) spectrum of (*S,S*)-**7**.

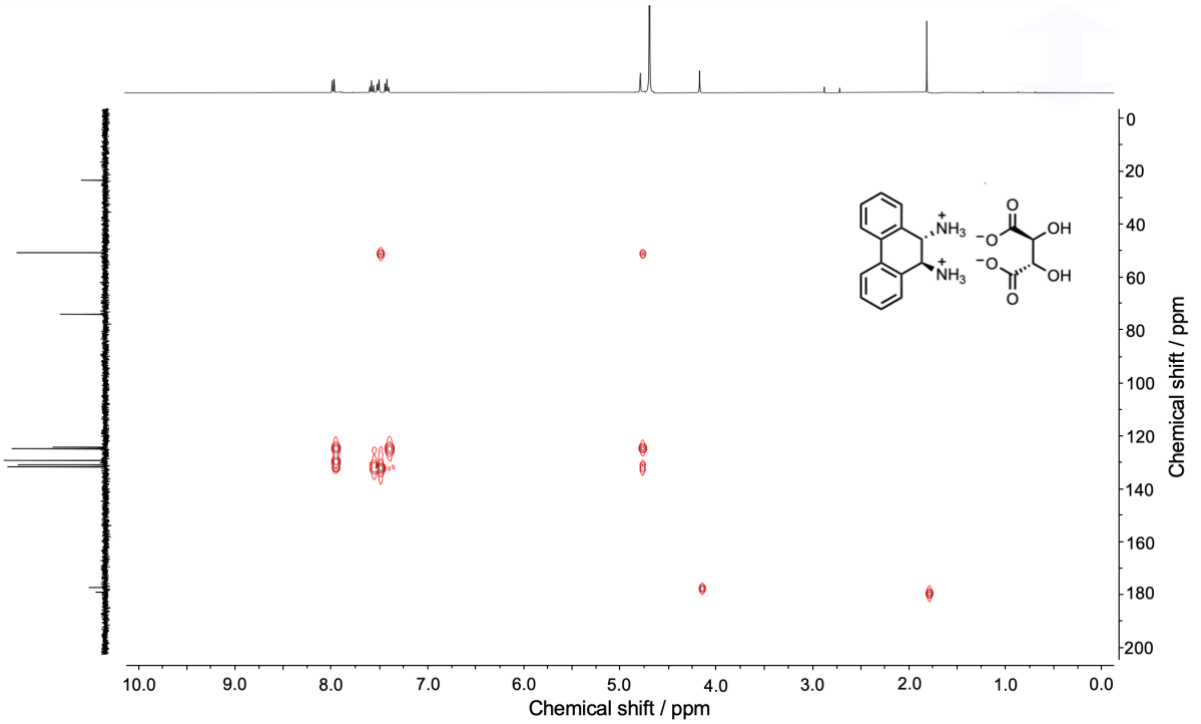

Figure S1.26 ^{1}H-^{13}C HMBC NMR (400 MHz, $CDCl_3$, 298 K) spectrum of (*S,S*)-**7**.

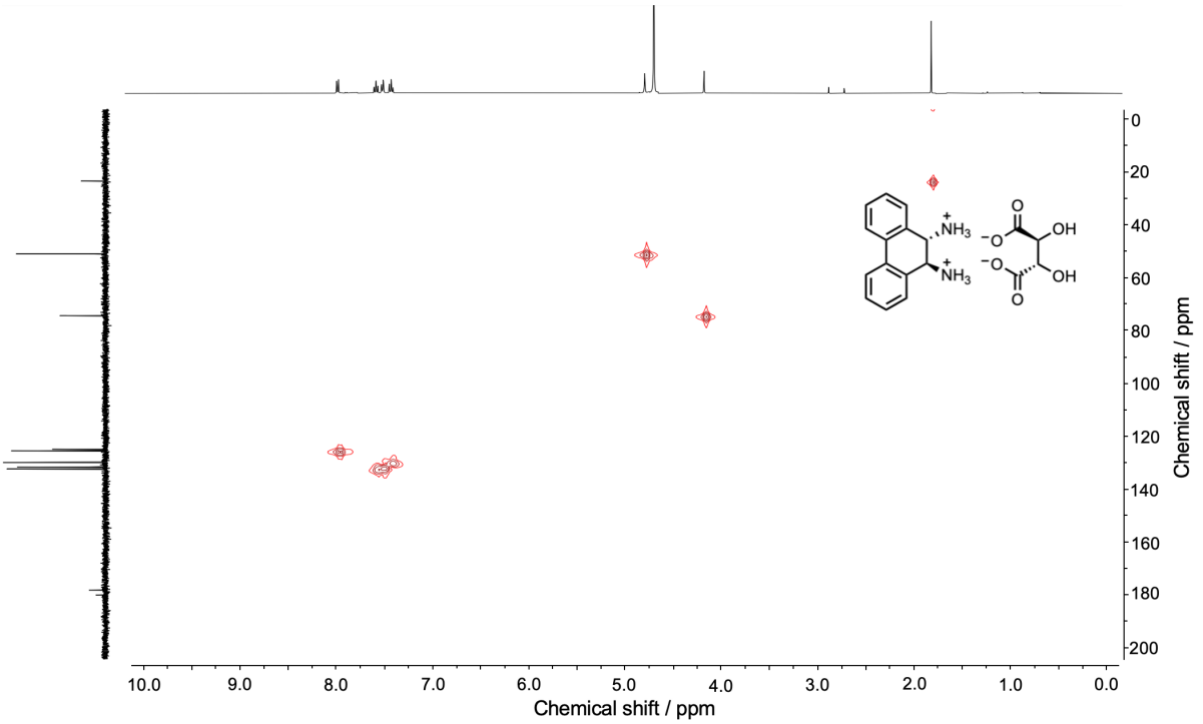

Figure S1.27 ^{1}H-^{13}C HMQC NMR (400 MHz, $CDCl_3$, 298 K) spectrum of (*S,S*)-**7**.

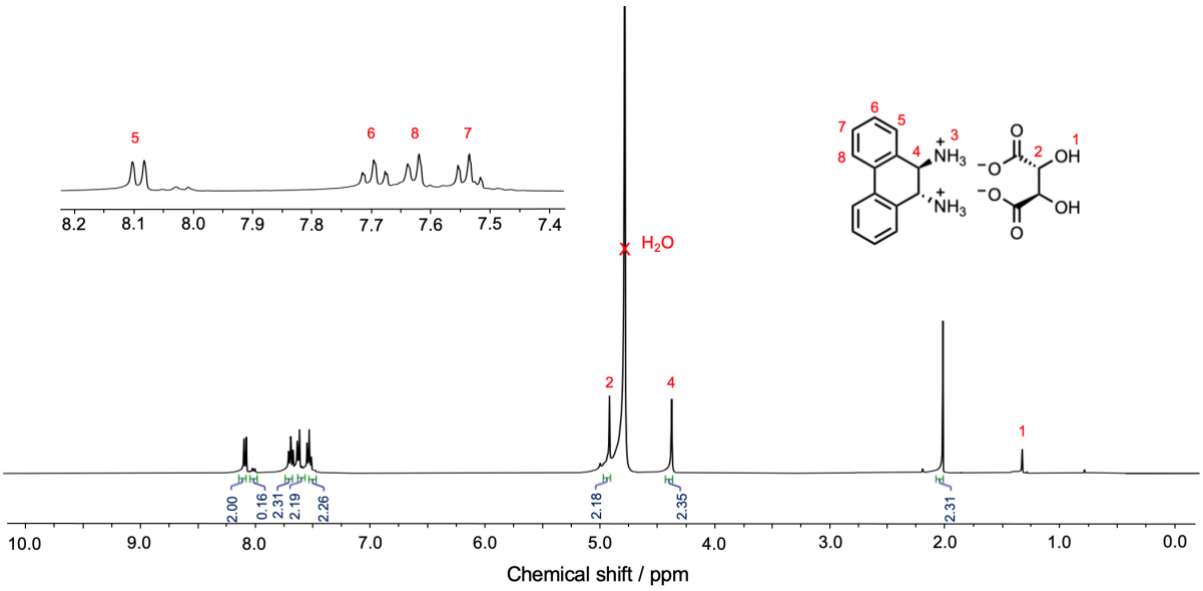

Figure S1.28 ^{1}H NMR (400 MHz, $CDCl_3$, 298 K) spectrum of (*R,R*)-**7**.

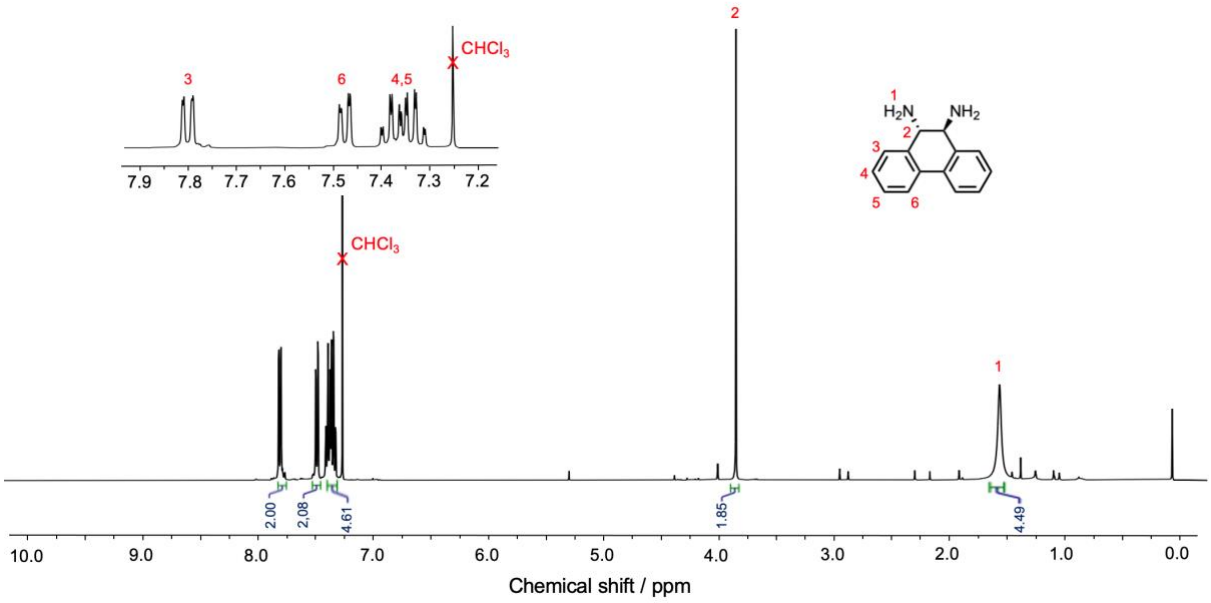

Figure S1.29 ^{1}H NMR (400 MHz, $CDCl_3$, 298 K) spectrum of (*S,S*)-**6**.

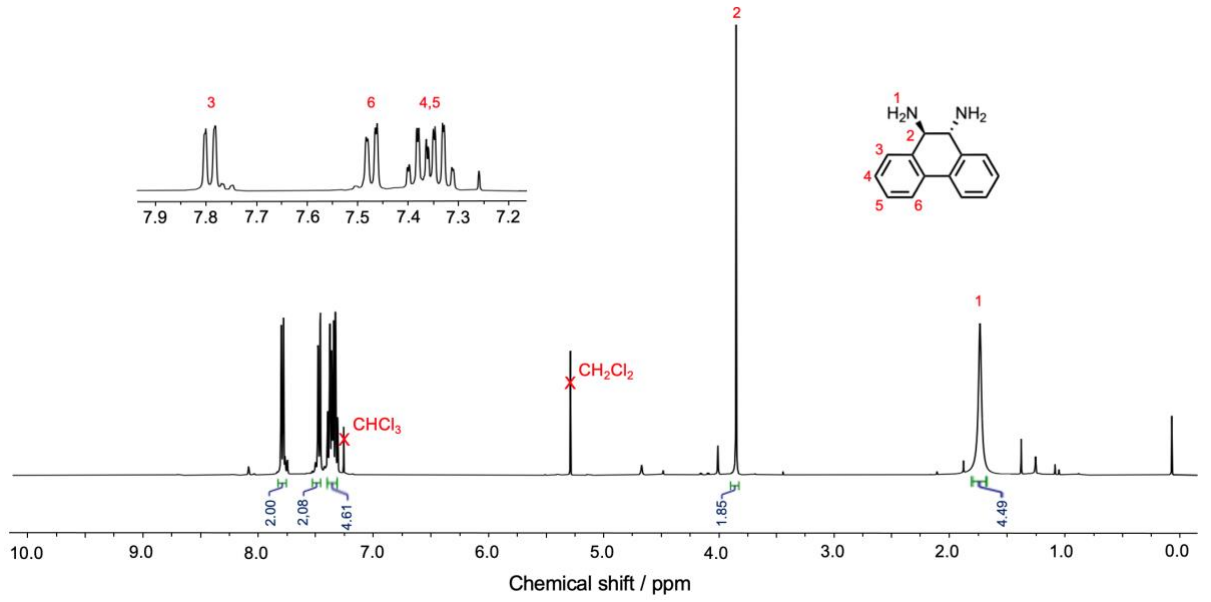

Figure S1.30 ^{1}H NMR (400 MHz, $CDCl_3$, 298 K) spectrum of (*R,R*)-**6**.

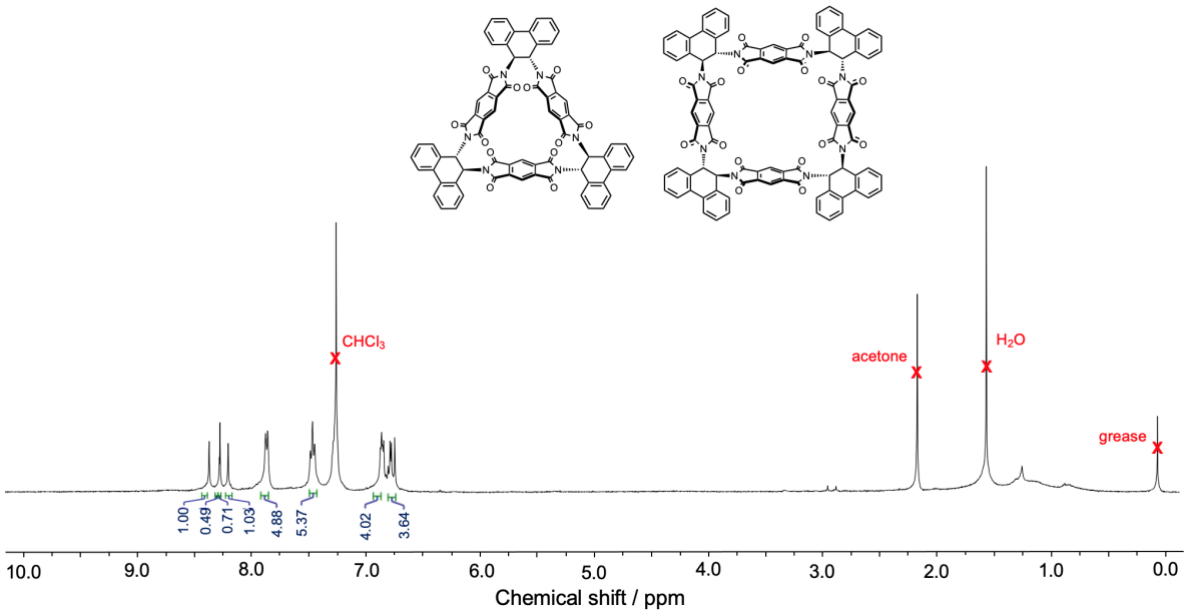

Figure S1.31 ^{1}H NMR (400 MHz, $CDCl_3$, 298 K) spectrum of (*S,S*)-**DHPΔ** and (*S,S*)-**DHP□**.

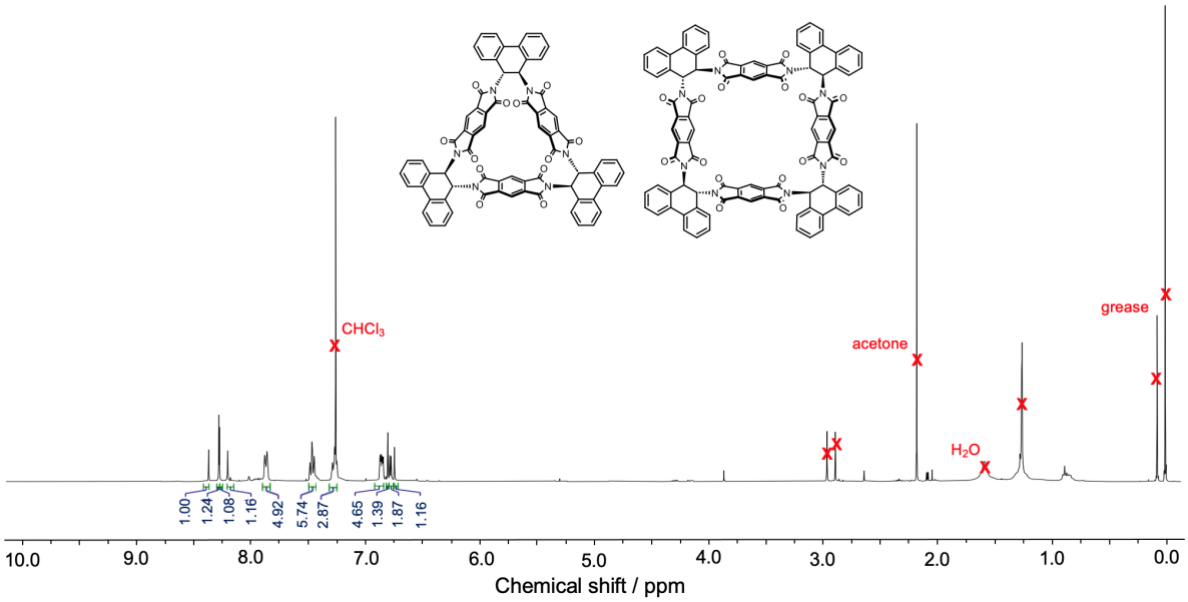

Figure S1.32 ^{1}H NMR (400 MHz, $CDCl_3$, 298 K) spectrum of (*R,R*)-**DHPΔ** and (*R,R*)-**DHP□**.

6.2 X-ray diffraction analysis

Single crystals of **CHΔ**•$(CH_3)_2CO$, suitable for X-ray diffraction, were grown by solvent vapour diffusion of n-hexane into an acetone solution of the sample (~ 0.5 mg mL^{-1}). Crystal data for $C_{51}H_{42}N_6O_{13}$ (M = 946.90 g mol^{-1}): monoclinic, space group $P2_1$, a = 18.4875(6) Å, b = 7.5954(2) Å, c = 32.8636(14) Å, α = 90°, β = 102.305(4)°, γ = 90°, V = 4508.7(3) $Å^3$, Z = 4, T = 110.00(10) K, μ(Cu Kα) = 0.852 mm^{-1}, *Dcalc* = 1.395 g cm^{-3}, 27856 reflections measured (8.11° ≤ 2θ ≤ 134.128°), 12313

independent reflections (R_{int} = 0.0968, R_{sigma} = 0.1103) which were used in all calculations. The final R_1 was 0.0549 (I > 2σ(I)) and wR_2 was 0.1151 (all data).

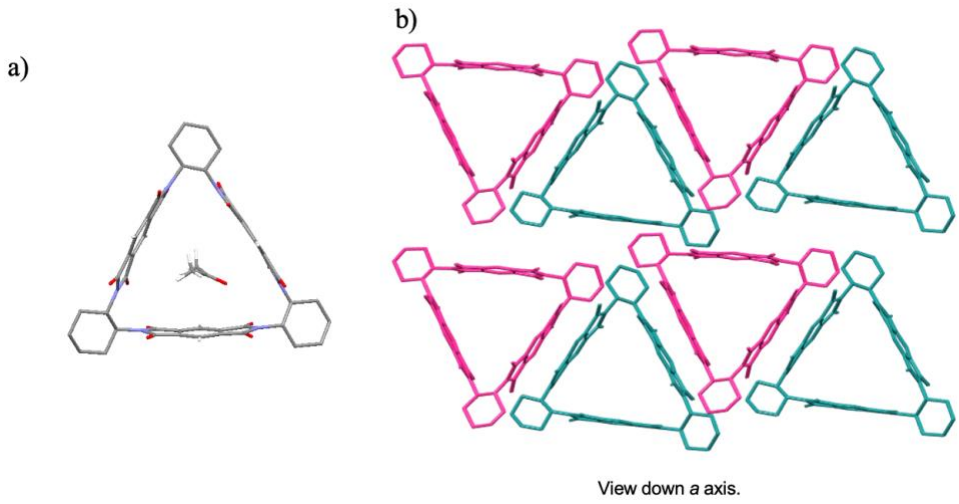

Figure S2.1 X-ray crystal structure of **CHΔ** showing a) single molecule of **CHΔ** and b) the packing arrangement down the *a* axis.

Singles crystals of **DPEΔ**•$(CH_3)_2CO$, suitable for X-ray diffraction, were grown by slow vapour diffusion of acetone into a chloroform solution of the sample (~ 5 mg mL^{-1}). Crystal Data for $C_{81}H_{59}N_6O_{15}$ (M = 1356.34 g mol^{-1}): orthorhombic, space group $P2_12_12_1$, a = 13.7752(3) Å, b = 18.6907(5) Å, c = 29.2788(5) Å, α = 90°, β = 90°, γ = 90°, V = 7538.4(3) $Å^3$, Z = 4, T = 110.2(7) K, μ(Cu Kα) = 0.685 mm^{-1}, *Dcalc* = 1.195 g cm^{-3}, 38867 reflections measured (5.61° ≤ 2Θ ≤ 136.5°), 13733 independent reflections (R_{int} = 0.0963, R_{sigma} = 0.0703) which were used in all calculations. The final R_1 was 0.0995 (I > 2σ(I)) and wR_2 was 0.2831 (all data).

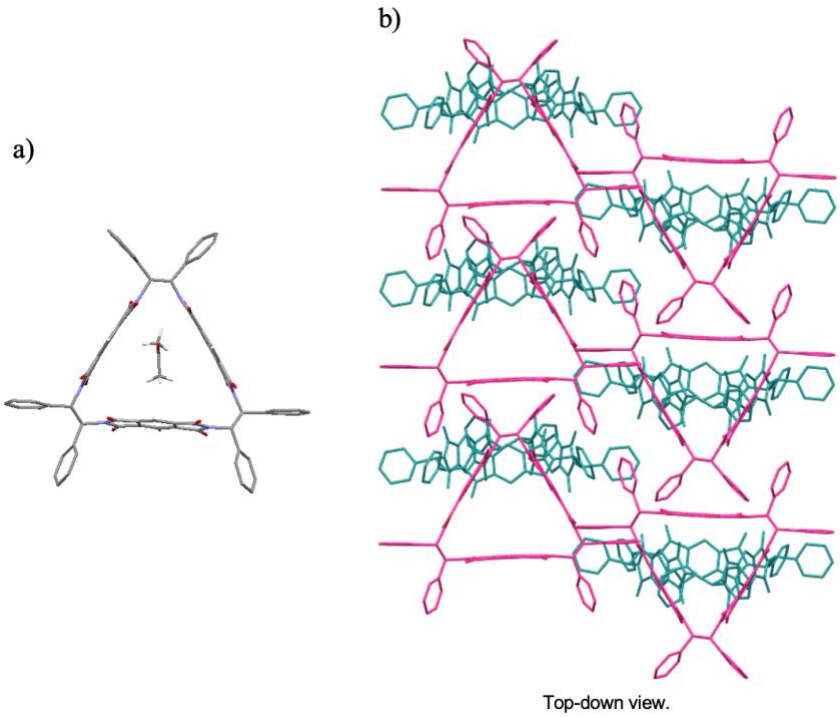

Figure S2.2 X-ray crystal structure of **DPEΔ** showing a) single molecule of **DPEΔ** and b) the packing arrangement from the top-down.

Single crystals of **DHPΔ•**CH_3Cl, suitable for X-ray diffraction, were grown by slow vapour diffusion of methanol into a chloroform solution of the sample. Crystal data for $C_{80}H_{55.3}Cl_{12.62}N_6O_{15.79}$ (M = 1800.70 g mol^{-1}): triclinic, space group P1, a = 16.71353(16) Å, b = 17.0891(2) Å, c = 17.1389(3) Å, α = 116.9106(15)°, β = 98.2938(10)°, γ = 101.1013(10)°, V = 4130.94(11) Å^3, Z = 2, T = 110.00(10) K, μ(Cu Kα) = 4.445 mm^{-1}, *Dcalc* = 1.448 g cm^{-3}, 48129 reflections measured (6.944° ≤ 2Θ ≤ 134.152°), 19599 independent reflections (R_{int} = 0.0361, R_{sigma} = 0.0422) which were used in all calculations. The final R_1 was 0.1032 (I > 2σ(I)) and wR_2 was 0.2925 (all data).

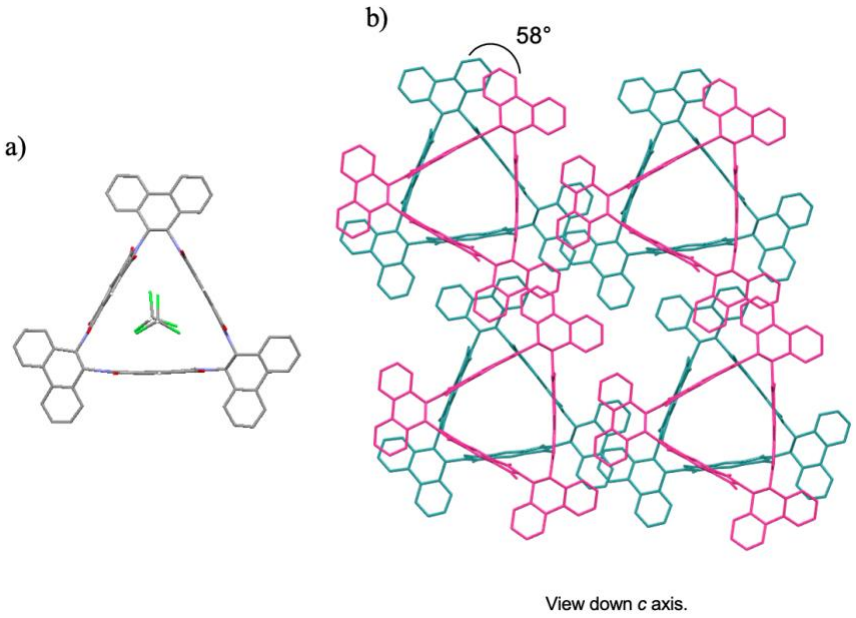

Figure S2.3 X-ray crystal structure of **DHPΔ** showing a) single molecule of **DHPΔ** and b) the packing arrangement down the *c* axis.

	CHΔ•$(CH_3)_2CO$	**DPEΔ**•$(CH_3)_2CO$	**DHPΔ**• CH_3Cl
Empirical formula	$C_{51}H_{42}N_6O_{13}$	$C_{81}H_{59}N_6O_{15}$	$C_{80}H_{55.3}Cl_{12.62}N_6O_{15.79}$
Formula weight	946.90	1356.34	1800.70
Temperature / K	110.00(10)	110.2(7)	110.00(10)
Crystal system	monoclinic	orthorhombic	triclinic
Space group	$P2_1$	$P2_12_12_1$	P1
a / Å	18.4875(6)	13.7752(3)	16.71353(16)
b / Å	7.5954(2)	18.6907(5)	17.0891(2)
c / Å	32.8636(14)	29.2788(5)	17.1389(3)
α / °	90	90	116.9106(15)
β / °	102.305(4)	90	98.2938(10)
γ / °	90	90	101.1013(10)
Volume / $Å^3$	4508.7(3)	7538.4(3)	4130.94(11)
Z	4	4	2
ρ_{calc} / g cm^{-3}	1.395	1.195	1.448
μ / mm^{-1}	0.852	0.685	4.445
F(000)	1976.0	2828.0	1836.0
Crystal size / mm^3	0.208 × 0.029 × 0.023	0.268 × 0.104 × 0.076	0.348 × 0.201 × 0.132
Radiation	Cu Kα (λ = 1.54184)	Cu Kα (λ = 1.54184)	Cu Kα (λ = 1.54184)

2Θ range for data collection / °	8.11 to 134.128	5.61 to 136.5	6.944 to 134.152
Index ranges	-21 ≤ h ≤ 22 -9 ≤ k ≤ 3 -38 ≤ l ≤ 39	-16 ≤ h ≤ 16 -22 ≤ k ≤ 22 -20 ≤ l ≤ 35	-19 ≤ h ≤ 10 -20 ≤ k ≤ 20 -20 ≤ l ≤ 20
Reflections collected	27856	38867	48129
Independent reflections	R_{int} = 0.0968 R_{sigma} = 0.1103	R_{int} = 0.0963 R_{sigma} = 0.0703	R_{int} = 0.0361 R_{sigma} = 0.0422
Data / restraints / parameters	12313 / 44 / 1317	13733 / 0 / 924	19599 / 62 / 2258
Goodness-of-fit on F^2	0.981	1.118	1.392
Final R indexes [I>=2σ (I)]	R_1 = 0.0549 wR_2 = 0.0997	R_1 = 0.0995 wR_2 = 0.2663	R_1 = 0.1032 wR_2 = 0.2867
Final R indexes [all data]	R_1 = 0.0960 wR_2 = 0.1151	R_1 = 0.1161 wR_2 = 0.2831	R_1 = 0.1064 wR_2 = 0.2925
Largest diff. peak/hole / e $Å^{-3}$	0.22 / -0.23	1.27 / -0.49	1.60 / -1.17
Flack parameter	0.0(2)	0.46(19)	0.054(9)

6.3 Absorption spectra

Solution-state absorption studies were recorded on an Agilent Technologies Cary 5000 UV–vis–NIR spectrophotometer using standard 10 mm path length quartz cuvettes at 298 K using anhydrous solvent.

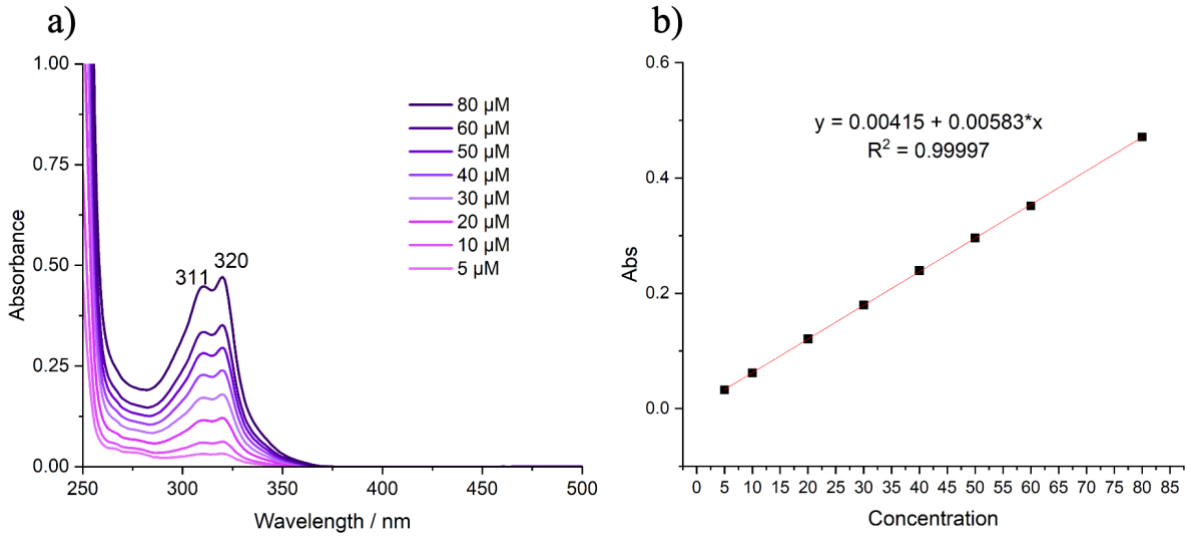

Figure S3.1 a) Concentration-dependent UV-Vis absorption spectrum of **CHΛ** in CH_2Cl_2 (5 µM–80 µM) b) Beer–Lambert plot at 320 nm.

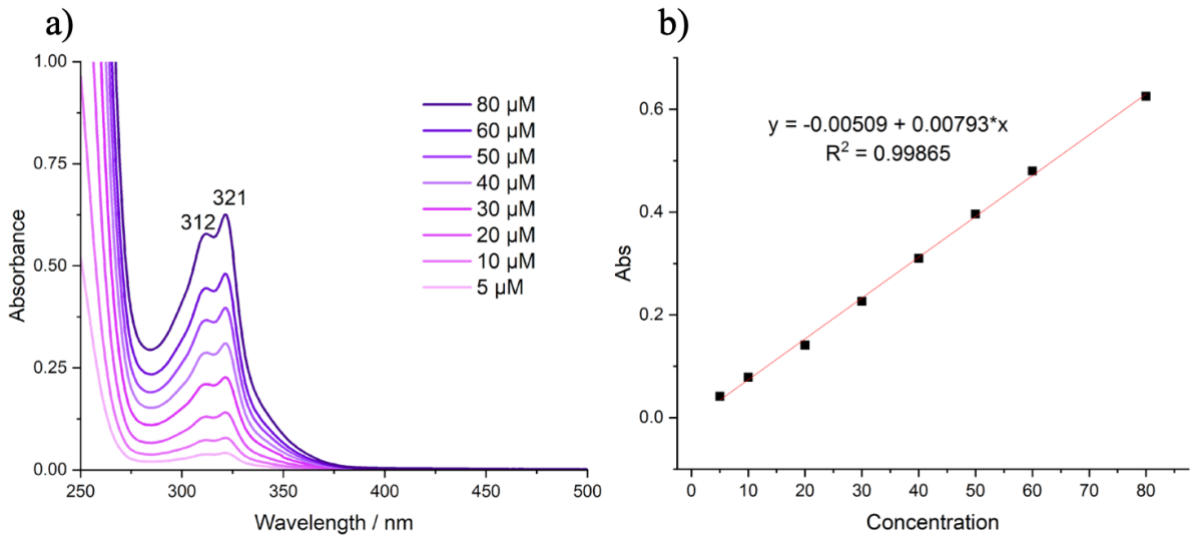

Figure S3.2 a) Concentration-dependent UV-Vis absorption spectrum of **DPEΔ** in CH_2Cl_2 (5 µM–80 µM) b) Beer–Lambert plot at 321 nm.

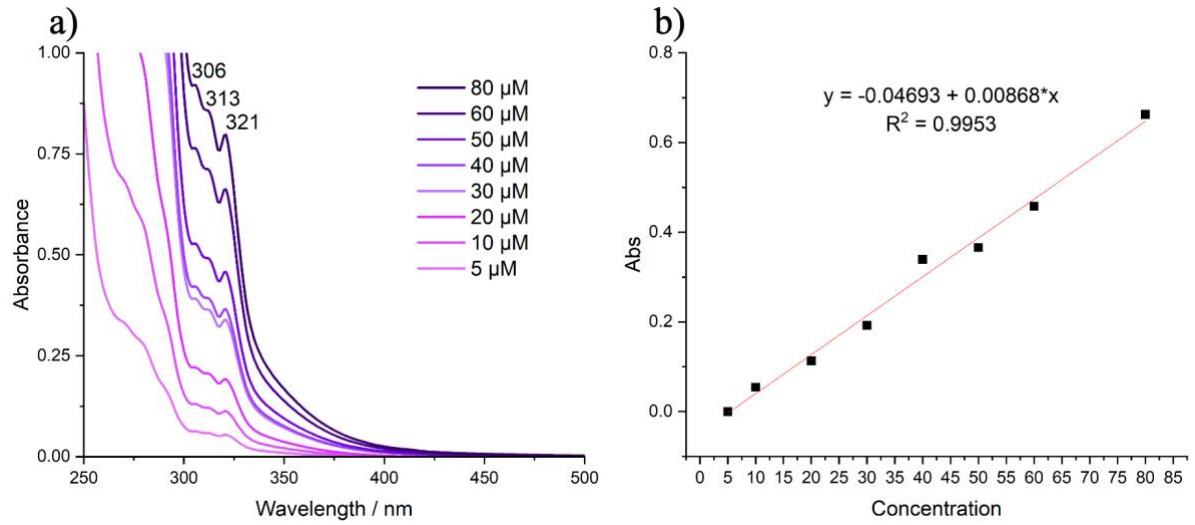

Figure S3.3 a) Concentration-dependent UV-Vis absorption spectrum of **DNaphΔ** in CH_2Cl_2 (5 µM–80 µM) b) Beer–Lambert plot at 321 nm.

6.4 Electrochemical data

Samples were prepared at 1.0 mM concentrations in dry, degassed CH_2Cl_2 (by freeze-pump-thaw under nitrogen) containing 0.1 M tetrabutylammonium hexafluorophosphate ($TBAPF_6$) as the electrolyte. Electrochemical potentials (V) are reported with respect to the Ag/AgCl reference electrode.

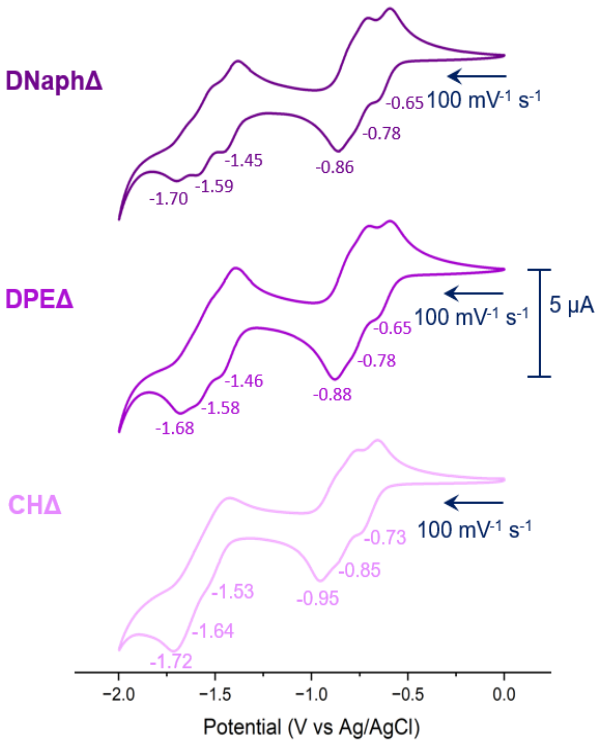

Figure S4.1 Solution-state CV analysis of **CHΔ**, **DPEΔ**, and **DNaphΔ** from -2.0 V to 0.0 V (V vs Ag/AgCl).

Samples were prepared at 1 mM concentrations in dry, degassed CH_2Cl_2 (by freeze-pump-thaw) containing 0.1 M tetrabutylammonium hexafluorophosphate ($TBAPF_6$) as the electrolyte and analysed under a constant applied voltage.

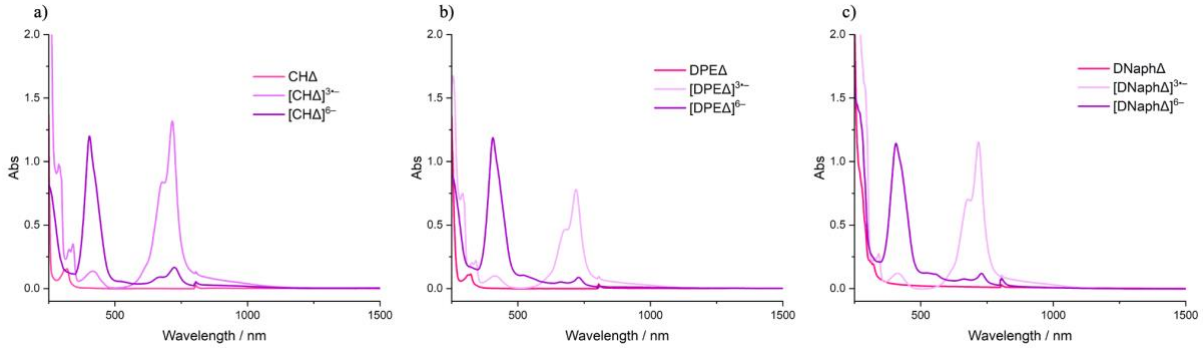

Figure S64.2 Solution-state SEC analysis of **CHΔ**, **DPEΔ**, and **DNaphΔ** based on the CV analysis above in **Figure SX.X**.

6.5 Computational analysis

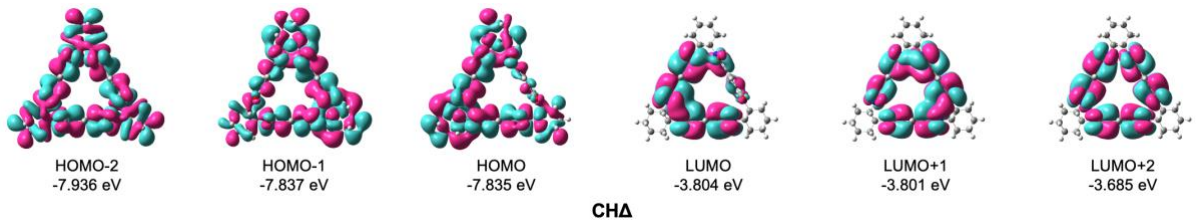

Figure S5.1 Visualised HOMO-2, HOMO-1, HOMO, LUMO, LUMO+1 and LUMO+2 of **CHΔ**.

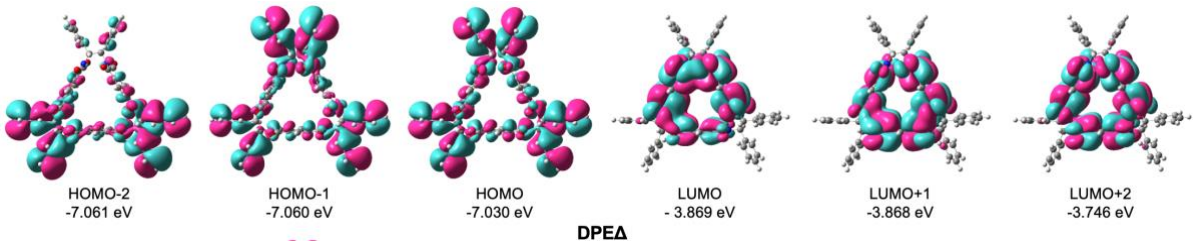

Figure S5.2 Visualised HOMO-2, HOMO-1, HOMO, LUMO, LUMO+1 and LUMO+2 of **DPEΔ**.

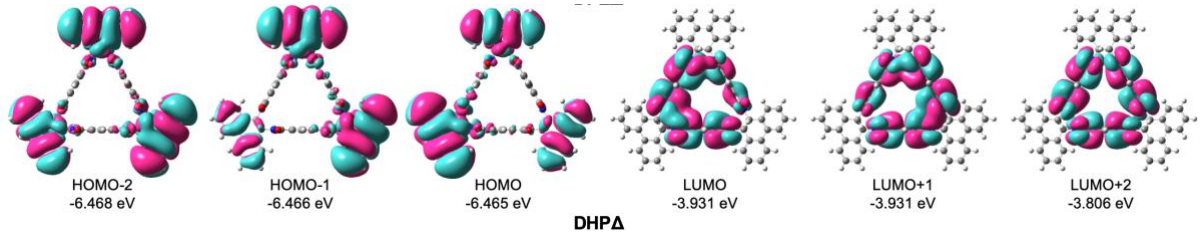

Figure S5.3 Visualised HOMO-2, HOMO-1, HOMO, LUMO, LUMO+1 and LUMO+2 of **DHPΔ**.

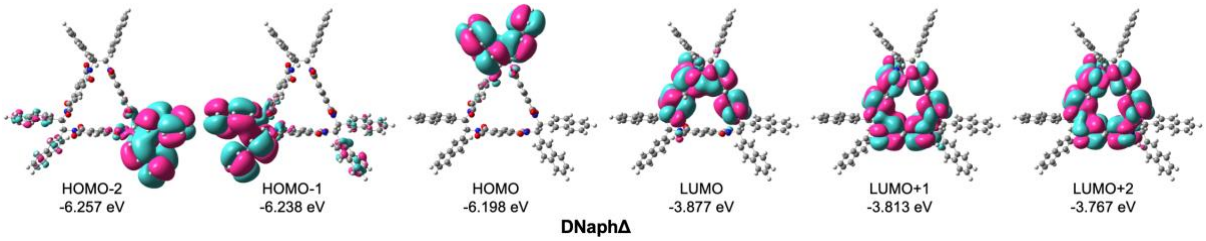

Figure S5.4 Visualised HOMO-2, HOMO-1, HOMO, LUMO, LUMO+1 and LUMO+2 of **DNaphΔ**.

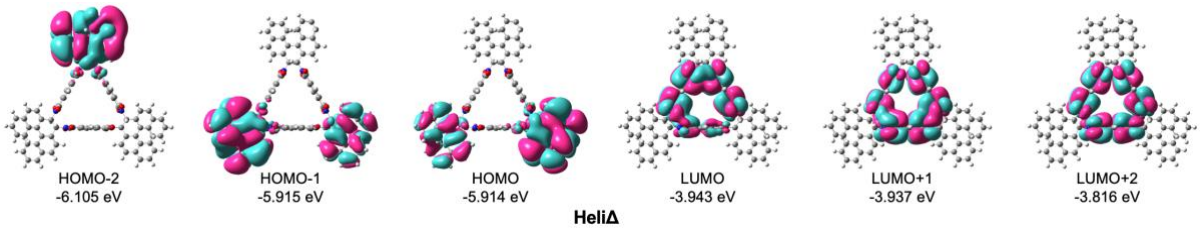

Figure S5.5 Visualised HOMO-2, HOMO-1, HOMO, LUMO, LUMO+1 and LUMO+2 of **DHNaphΔ**.

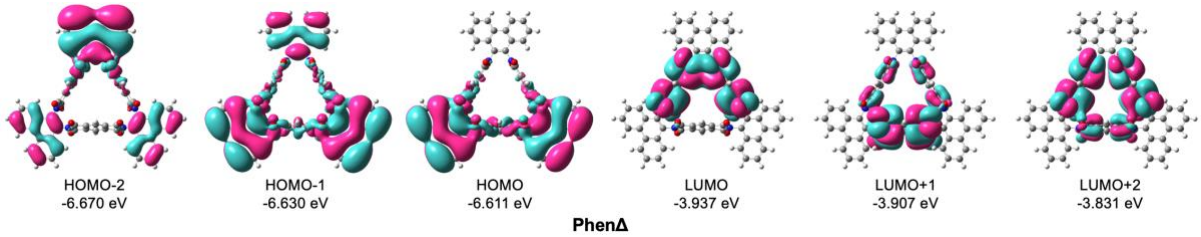

Figure S5.6 Visualised HOMO-2, HOMO-1, HOMO, LUMO, LUMO+1 and LUMO+2 of **PhenΔ**.

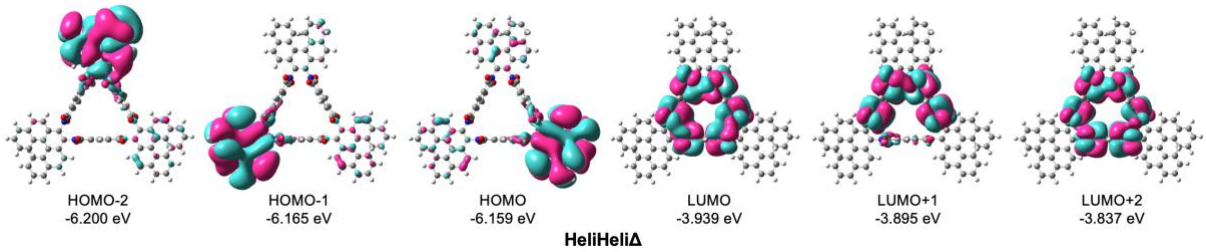

Figure S5.7 Visualised HOMO-2, HOMO-1, HOMO, LUMO, LUMO+1 and LUMO+2 of **HeliΔ**.

6.6 Cartesian coordinates

Table S6.1 Cartesian coordinates of geometry-optimised **CHΔ** at the B3LYP-GD3BJ/6-31G ++ level of theory in CH_2Cl_2, isovalue = 0.004.

C	5.61165950	-8.15586989	17.45116493	**O**	7.31015395	-5.81939830	16.63604384
H	5.40418334	-9.22322284	17.56206805	**C**	15.68473714	-9.09652966	15.07480998
C	4.82995841	-7.62093414	16.22821377	**H**	15.57567323	-10.02972141	15.63324100
H	5.00897929	-6.54660950	16.13794687	**C**	15.20513158	-7.92498203	15.96337775
C	7.92200107	-9.17493065	17.48587007	**H**	15.34710422	-6.98830644	15.41833206
C	9.29775089	-8.71152522	17.15615650	**C**	14.28466591	-10.52061226	13.53105173
C	10.50441880	-9.40833439	17.19689606	**C**	13.46513968	-10.28388667	12.31127943
C	11.62355931	-8.67489678	16.80657529	**C**	12.69471328	-11.17925865	11.57142651
C	13.05239037	-9.09194455	16.72666751	**C**	12.02736182	-10.62363846	10.48144759
C	12.90997660	-6.87661448	16.03871079	**C**	11.12396396	-11.27348834	9.49032553
C	11.53965386	-7.33175057	16.39959581	**C**	11.27187615	-9.01628580	8.95683671
C	10.33511658	-6.63107841	16.37143374	**C**	12.12388290	-9.25988826	10.15335679
C	9.21655637	-7.36385285	16.76384184	**C**	12.90573213	-8.36733145	10.88507579
C	7.79007633	-6.94232676	16.85449208	**C**	13.57362970	-8.92297555	11.97502428
N	7.06638263	-8.07943474	17.25146201	**C**	14.47716297	-8.27412212	12.96743541
N	13.75950389	-7.98576063	16.22509188	**N**	14.83303657	-9.27272436	13.88964969
O	7.56306548	-10.28862550	17.89405491	**N**	10.67762883	-10.25329620	8.63397286
O	13.54763593	-10.18599925	17.03769779	**O**	14.47616928	-11.58605726	14.13418361
O	13.27113923	-5.75459964	15.65611654	**O**	10.81402210	-12.47219557	9.41007347

O	11.10067800	-7.95708959	8.33688508	**H**	7.35295772	-11.79661418	4.69810925
O	14.85983495	-7.09428466	12.99612020	**H**	8.22501833	-12.89572575	5.76807107
C	8.44612557	-11.14010302	7.93245512	**C**	9.39710165	-11.18526873	5.13026631
H	8.68998712	-12.17392307	8.18991795	**H**	9.21255743	-10.16156036	4.77394144
C	9.74330036	-10.41140791	7.51021385	**H**	9.84803813	-11.73705518	4.29731221
H	9.49319225	-9.38931158	7.21501391	**C**	10.38348820	-11.13935429	6.31284883
C	7.48008144	-11.38355319	10.25211476	**H**	11.30112404	-10.61244885	6.02847570
C	6.96105863	-10.45669394	11.29488837	**H**	10.66312033	-12.15728938	6.61198072
C	6.46810647	-10.73794483	12.56800639	**C**	16.03314951	-7.88117383	17.26174609
C	6.06987376	-9.62488001	13.30614938	**H**	15.87245764	-8.80676273	17.82857266
C	5.50827033	-9.55178222	14.68464998	**H**	15.67882486	-7.04749878	17.87824558
C	5.67129016	-7.38553504	13.85879522	**C**	17.52849540	-7.71379131	16.93165369
C	6.16063227	-8.31490036	12.80366283	**H**	18.11222088	-7.71815352	17.85946942
C	6.64187802	-8.03475329	11.52574983	**H**	17.68632236	-6.73407884	16.45801301
C	7.03931998	-9.14793494	10.78723155	**C**	18.02468792	-8.82411747	15.98624181
C	7.59658548	-9.22180576	9.40681496	**H**	17.98410759	-9.79158609	16.50720024
N	7.87111226	-10.57805577	9.16329701	**H**	19.07274283	-8.65030772	15.71607433
N	5.32941414	-8.18706601	14.96678718	**C**	17.16810246	-8.90076561	14.70819466
O	7.55930346	-12.61953651	10.29217380	**H**	17.28092596	-7.98027391	14.12192654
O	5.23899295	-10.48948907	15.45112968	**H**	17.48932110	-9.73787703	14.07842712
O	5.56263631	-6.15224079	13.80713350	**C**	5.15553041	-7.42011629	18.72538596
O	7.78627123	-8.29129731	8.60851107	**H**	5.38719156	-6.35163726	18.63274121
C	7.44342571	-11.13694034	6.76285302	**H**	5.72003659	-7.81021354	19.57964838
H	6.52949596	-11.65176715	7.07946368	**C**	3.64294945	-7.61886765	18.93919125
H	7.17449979	-10.10229018	6.51548980	**H**	3.32157443	-7.06412225	19.82833640
C	8.05979094	-11.83387181	5.53513978	**H**	3.44259144	-8.68221467	19.13486120

C	2.83511734	-7.16470249	17.70869523	**H**	6.40198779	-11.74704504	12.95618875
H	2.93594977	-6.07643239	17.58784596	**H**	12.98523164	-7.31810812	10.62780505
H	1.76922272	-7.37222014	17.85845446	**H**	12.61721495	-12.22900682	11.82713321
C	3.32164961	-7.86395530	16.42507590	**H**	6.70492245	-7.02594544	11.13628030
H	2.78526196	-7.48023803	15.55007164	**H**	10.56726299	-10.44432792	17.50694164
H	3.13032849	-8.94250664	16.48661234	**H**	10.27277828	-5.59394159	16.06515081

Table S6.2 Cartesian coordinates of geometry-optimised **DPEΔ** at the B3LYP-GD3BJ/6-31G ++ level of theory in CH_2Cl_2, isovalue = 0.004.

C	2.13853798	3.64715902	-1.04582220	**H**	9.20667547	-2.60158125	-1.00147006
C	2.59229899	2.33707771	-0.50407450	**C**	9.15519689	-3.21794895	1.06892083
C	2.21680408	2.27603094	0.84915580	**H**	10.23484178	-3.23310069	1.17717533
C	1.49609417	3.53383702	1.18583891	**C**	8.33457776	-3.55563289	2.15285641
C	3.27145200	1.29791278	-1.13758578	**H**	8.77432056	-3.83384044	3.10505984
H	3.55767310	1.33971646	-2.18139732	**C**	6.94170154	-3.53714399	2.00790414
C	3.55637167	0.19981283	-0.32783376	**C**	5.59394101	-6.17813084	-1.27147771
C	3.19943951	0.14776982	1.03081318	**C**	6.07221865	-7.48507756	-1.11463533
C	2.51365612	1.18371352	1.66241541	**H**	6.66178244	-7.94203291	-1.90270474
H	2.23243274	1.14430428	2.70767536	**C**	5.79123337	-8.19675900	0.05877249
C	4.24950308	-1.07127295	-0.67283144	**H**	6.16213037	-9.20879398	0.18447384
C	3.67896972	-1.14993941	1.57998473	**C**	5.03093798	-7.59510135	1.07175862
C	4.84140048	-3.19636771	0.66542651	**H**	4.81135554	-8.14086195	1.98379756
H	4.42843299	-3.54399825	1.61295364	**C**	4.55473858	-6.28826320	0.91537220
C	6.35686622	-3.18342048	0.78240623	**H**	3.96721139	-5.83238748	1.70374385
C	7.18394438	-2.84627325	-0.30267873	**C**	4.83348479	-5.57078987	-0.26051256
H	6.74577472	-2.56950965	-1.25457254	**C**	4.35301024	-4.14328224	-0.46553710
C	8.57599128	-2.86267030	-0.15770160	**H**	4.74866223	-3.78251891	-1.41537967

C	2.29027349	-3.89782274	-1.90214542
C	0.82211062	-3.82257103	-1.66824559
C	0.59606212	-3.97926504	-0.28966410
C	1.91592982	-4.13258651	0.38069522
C	-0.21657769	-3.63395175	-2.57824937
H	-0.04489120	-3.50731565	-3.64018106
C	-1.49401447	-3.62103644	-2.02071472
C	-1.72114876	-3.79924344	-0.64491006
C	-0.68207268	-3.97981678	0.26614627
H	-0.85412497	-4.11129439	1.32742929
C	-2.81219881	-3.43396391	-2.68639033
C	-3.19092307	-3.75345198	-0.41440439
C	-5.24597178	-3.37560281	-1.83206655
H	-5.61057225	-3.23424329	-0.81421796
C	-5.88341424	-4.63506939	-2.39617556
C	-6.70480481	-5.40731342	-1.56059438
H	-6.86318883	-5.09839424	-0.53168997
C	-7.32418546	-6.56622308	-2.04514084
H	-7.95935013	-7.15294253	-1.38957002
C	-7.12497398	-6.96248058	-3.37394234
H	-7.60532034	-7.85853785	-3.75335085
C	-6.30436676	-6.19510166	-4.21291062
H	-6.14734590	-6.49626818	-5.24369466
C	-5.68677193	-5.03618365	-3.72863836
C	-7.90940041	-1.78564783	-1.60265214
C	-9.29115200	-1.59890037	-1.72515976
H	-9.90271707	-1.51538718	-0.83249163
C	-9.88505308	-1.52337515	-2.99314609
H	-10.95706188	-1.38196863	-3.08472245
C	-9.08930644	-1.63396175	-4.14072850
H	-9.54074485	-1.57899358	-5.12593474
C	-7.70658343	-1.81936769	-4.01764442
H	-7.09096101	-1.90957342	-4.90753286
C	-7.10713187	-1.89646391	-2.75120241
C	-5.60525852	-2.11567488	-2.66632201
H	-5.22116388	-2.24703198	-3.67847592
C	-4.19649112	-0.05266812	-3.03083216
C	-3.58362127	0.99484801	-2.16926095
C	-3.96009895	0.73574883	-0.83983017
C	-4.80092832	-0.49261423	-0.82890308
C	-2.76752567	2.06916575	-2.51846947
H	-2.47124103	2.26720836	-3.54131349
C	-2.35826549	2.86928064	-1.45316570
C	-2.75012131	2.62173615	-0.12605857
C	-3.56225826	1.54428197	0.22373995
H	-3.86088817	1.34796965	1.24623868
C	-1.48128889	4.07156950	-1.46006552
C	-2.14515824	3.67627429	0.73325163
C	-0.60461262	5.64751232	0.38445502
H	-0.56863439	5.48711213	1.46240665
C	-1.30260132	6.97257570	0.12316024
C	-1.82936482	7.68307701	1.21263763

H	-1.73619990	7.27379397	2.21411446	**N**	2.88755906	-4.05035836	-0.63208814
C	-2.46673677	8.91490031	1.01814434	**N**	-3.78230028	-3.50022532	-1.67096940
H	-2.86718792	9.45560510	1.86945499	**N**	-4.88272221	-0.92905073	-2.16298989
C	-2.58227219	9.44653575	-0.27273478	**N**	-1.37146218	4.49018330	-0.12236142
H	-3.07328391	10.40191457	-0.42684501	**O**	2.30942932	4.11384319	-2.17977705
C	-2.05844620	8.74042258	-1.36504204	**O**	1.00948268	3.86031286	2.27913575
H	-2.14361025	9.14788070	-2.36733487	**O**	4.72175374	-1.40401440	-1.77052214
C	-1.42051798	7.50994159	-1.17002565	**O**	3.60516136	-1.57026949	2.74220236
C	1.86041138	6.91028878	1.80506090	**O**	2.90316151	-3.85356903	-2.97690623
C	2.63522951	7.96373188	2.30408834	**O**	2.13878899	-4.29590011	1.58996715
H	2.75755245	8.07896959	3.37629121	**O**	-3.03441200	-3.24916899	-3.89265358
C	3.24800192	8.86889126	1.42580886	**O**	-3.81091518	-3.91223795	0.64539237
H	3.84520039	9.68665246	1.81594779	**O**	-4.14724910	-0.16424764	-4.26290857
C	3.08372136	8.71474674	0.04318440	**O**	-5.32961507	-1.04244325	0.14920304
H	3.55229593	9.41194248	-0.64369666	**O**	-0.94010526	4.61085941	-2.43720844
C	2.30958450	7.65964864	-0.45574851	**O**	-2.27620851	3.84749494	1.95243910
H	2.17882404	7.54391340	-1.52751175	**H**	5.81617799	-5.62576430	-2.17956720
C	1.69345477	6.75138945	0.41874740	**H**	6.30634847	-3.80272859	2.84745216
C	0.84763516	5.63254401	-0.16750478	**H**	-7.45993371	-1.84052511	-0.61798805
H	0.80990844	5.76388607	-1.24931889	**H**	-5.05241810	-4.45135471	-4.38442442
N	1.46242308	4.30001656	0.00757953	**H**	-1.02148978	6.97086624	-2.02126625
N	4.26850021	-1.84419419	0.50134716	**H**	1.39238494	6.21500375	2.49213066

Table S6.3 Cartesian coordinates of geometry-optimised **DHPΔ** at the B3LYP-GD3BJ/6-31G ++ level of theory in CH_2Cl_2, isovalue = 0.004.

C	2.36782071	3.67053888	-1.36534473	**C**	2.31604176	3.85299502	0.95677310
C	2.89958824	2.40475236	-0.79258592	**C**	3.37614904	1.26889465	-1.44462911
C	2.86222178	2.51181036	0.60935222	**H**	3.41235983	1.19014146	-2.52430079

C	3.80155178	0.24134273	-0.60485993
C	3.75421610	0.34380502	0.79715991
C	3.28898723	1.48459334	1.44916969
H	3.26045605	1.56656016	2.52883717
C	4.36108704	-1.09366118	-0.95321285
C	4.27333108	-0.92801972	1.36911853
C	5.11183247	-3.10922716	0.42620738
H	4.95683427	-3.34938802	1.48343930
C	6.59034531	-3.23641319	0.09147912
C	7.42656014	-2.12197483	-0.01003949
H	7.02108601	-1.12651551	0.13081819
C	8.78886368	-2.27901806	-0.29364978
H	9.42817515	-1.40663540	-0.37619390
C	9.31476029	-3.56324643	-0.47903601
H	10.36584162	-3.69435986	-0.71339010
C	8.48247381	-4.68180354	-0.37145231
H	8.89791218	-5.66912445	-0.53780669
C	7.11494819	-4.54031912	-0.07353888
C	6.21362736	-5.70917263	0.07004522
C	6.69843452	-6.99624918	0.36548209
H	7.75916884	-7.14731320	0.53004321
C	5.82830139	-8.08567194	0.47264780
H	6.22263422	-9.06926555	0.70491038
C	4.45234232	-7.90316892	0.28939422
H	3.77121450	-8.74334306	0.37158410
C	3.95381010	-6.62508881	0.00831645
H	2.88775216	-6.48590323	-0.13080560
C	4.81897933	-5.53296799	-0.09282516
C	4.31998990	-4.13499741	-0.42560082
H	4.51219217	-3.92295987	-1.48274496
C	1.99696137	-3.87853395	-1.36743137
C	0.63459189	-3.70539475	-0.79498972
C	0.74586674	-3.72555686	0.60696728
C	2.17988218	-3.92425745	0.95474704
C	-0.58767567	-3.55110774	-1.44686314
H	-0.67440613	-3.54480239	-2.52651729
C	-1.69011737	-3.40516849	-0.60684030
C	-1.57716838	-3.41278225	0.79509842
C	-0.35661113	-3.57986677	1.44697201
H	-0.27103544	-3.59493115	2.52663223
C	-3.12669145	-3.22569389	-0.95455114
C	-2.93772114	-3.22590807	1.36745217
C	-5.24746273	-2.86966066	0.42617048
H	-5.37717445	-2.61336658	1.48305281
C	-6.09412469	-4.08941403	0.09555248
C	-5.54411590	-5.36982434	-0.00213819
H	-4.47882336	-5.51355173	0.13853597
C	-6.35898192	-6.47397949	-0.28120969
H	-5.92087190	-7.46307395	-0.36076576
C	-7.73474037	-6.29119485	-0.46578554
H	-8.37210394	-7.13822585	-0.69645654
C	-8.29025319	-5.01210070	-0.36179755

H	-9.35358835	-4.88131127	-0.52701472
C	-7.48629901	-3.89565538	-0.06842275
C	-8.05126071	-2.53173628	0.07207985
C	-9.40858553	-2.31092557	0.36835412
H	-10.06727140	-3.15541056	0.53584590
C	-9.92041900	-1.01377636	0.47257343
H	-10.96954343	-0.86571456	0.70561070
C	-9.07760416	0.08840361	0.28530144
H	-9.46736982	1.09752113	0.36494971
C	-7.72121937	-0.11597965	0.00345971
H	-7.07015349	0.73904810	-0.13918696
C	-7.20449636	-1.41019061	-0.09440704
C	-5.74366245	-1.67364984	-0.42718450
H	-5.65545368	-1.94704292	-1.48405358
C	-4.36416068	0.21278335	-1.36982719
C	-3.53282146	1.30613401	-0.79767542
C	-3.60691697	1.22090567	0.60430677
C	-4.49601281	0.07846496	0.95252505
C	-2.78634107	2.28606467	-1.44979466
H	-2.73655170	2.35699940	-2.52947235
C	-2.10757879	3.16733221	-0.61011288
C	-2.17209309	3.07449455	0.79186585
C	-2.92895258	2.10266759	1.44399713
H	-2.98541015	2.03689989	2.52367622
C	-1.23117081	4.31990233	-0.95793886
C	-1.32870392	4.15818738	1.36426633
C	0.13804597	5.97749169	0.42434262
H	0.42192665	5.96257106	1.48204843
C	-0.49432907	7.32015995	0.09106557
C	-1.87794184	7.48305320	-0.01150200
H	-2.53460880	6.63155805	0.12657471
C	-2.42654796	8.74038369	-0.29286111
H	-3.50197042	8.85489616	-0.37610317
C	-1.58031776	9.84079783	-0.47515195
H	-1.99495412	10.81590682	-0.70782730
C	-0.19505044	9.68312560	-0.36684531
H	0.44995735	10.53874801	-0.53097403
C	0.36957232	8.42915264	-0.07082430
C	1.83288886	8.23680025	0.07394036
C	2.70184700	9.30207507	0.37227258
H	2.29931056	10.29472067	0.53880047
C	4.08091789	9.09696559	0.47983827
H	4.73300427	9.93164396	0.71435670
C	4.61473839	7.81605042	0.29408498
H	5.68337228	7.64925925	0.37640493
C	3.76041634	6.74333098	0.01051511
H	4.17570593	5.75187406	-0.13041979
C	2.38147565	6.94273454	-0.09079473
C	1.42400353	5.80893038	-0.42534106
H	1.14590220	5.86833116	-1.48300088
N	2.01258001	4.48165154	-0.26589443
N	4.59202411	-1.75327943	0.26886591

N	2.87647880	-3.97724377	-0.26746832	**O**	2.33309163	-3.94416004	-2.55660497
N	-3.81291884	-3.09436747	0.26765429	**O**	2.69079727	-4.03254459	2.07803364
N	-4.88825035	-0.50008453	-0.26968976	**O**	-3.64844853	-3.19926219	-2.07773609
N	-0.77380950	4.84766823	0.26458419	**O**	-3.27903304	-3.19903129	2.55663184
O	2.25523820	3.99336419	-2.55463808	**O**	-4.58864442	-0.04610055	-2.55893910
O	2.15247566	4.34933238	2.07992915	**O**	-4.84573414	-0.30925391	2.07588713
O	4.59484929	-1.56012678	-2.07672521	**O**	-0.94703398	4.75846710	-2.08112535
O	4.42406897	-1.23622065	2.55810360	**O**	-1.13564888	4.44110500	2.55338017

Table S6.4 Cartesian coordinates of geometry-optimised **DNaphΔ** at the B3LYP-GD3BJ/6-31G ++ level of theory in CH_2Cl_2, isovalue = 0.004.

C	1.88776317	3.50274124	-0.84627080	**C**	2.36534219	-4.06479418	-1.82168494
C	2.42362719	2.24164888	-0.29286954	**C**	0.89104452	-3.97570607	-1.64062473
C	2.37985021	2.32969793	1.10712833	**C**	0.61405780	-4.15689901	-0.27422864
C	1.86093631	3.68247532	1.47172775	**C**	1.91005635	-4.26130083	0.45103540
C	2.91940712	1.12758938	-0.96478216	**C**	-0.11112167	-3.74561011	-2.58219198
H	2.97388505	1.07410623	-2.04512757	**H**	0.10350016	-3.57290865	-3.62976406
C	3.35235658	0.09405327	-0.14079802	**C**	-1.40931912	-3.74697248	-2.07425633
C	3.27241553	0.15484499	1.26145548	**C**	-1.68895238	-4.01571680	-0.72261635
C	2.79157580	1.28103159	1.93155364	**C**	-0.68585976	-4.21093979	0.22481985
H	2.74764264	1.34095301	3.01213776	**H**	-0.90052033	-4.38459927	1.27219131
C	3.97813116	-1.19765219	-0.52013530	**C**	-2.70048099	-3.47737014	-2.76837239
C	3.79695361	-1.13523240	1.79600130	**C**	-3.16619822	-4.02277086	-0.55505408
C	4.80023988	-3.23908212	0.83335623	**C**	-4.28421852	0.09491258	-3.11768070
H	4.40597562	-3.61432904	1.77837531	**C**	-3.53950681	1.08654274	-2.29053274
C	4.37580169	-4.21207441	-0.30654269	**C**	-3.46695306	0.57559831	-0.98320381
H	4.78889603	-3.84380481	-1.24528522	**C**	-4.22720702	-0.69965021	-0.93483792

C	-2.99541795	2.32426319	-2.63740999
H	-3.07277574	2.73352976	-3.63725287
C	-2.35382545	3.00059252	-1.59813195
C	-2.23341070	2.45325916	-0.30977103
C	-2.79490627	1.23015376	0.04444310
H	-2.72512653	0.82551102	1.04672245
C	-1.71684753	4.34700087	-1.57257066
C	-1.44951630	3.39441938	0.53072129
C	-0.55079593	5.79280143	0.13323607
C	1.01058182	5.67409660	-0.04537697
H	1.12972897	5.70181014	-1.13140081
N	1.56666967	4.33641010	0.25326156
N	4.18224690	-1.90640535	0.67448649
N	2.91702642	-4.18450279	-0.52454141
N	-3.70698365	-3.63658343	-1.80383899
N	-4.65123960	-0.95878873	-2.24736691
N	-1.20479778	4.52687485	-0.26403060
O	1.72220138	3.80565630	-2.03757107
O	1.74276672	4.14685055	2.61140482
O	4.28872531	-1.57664072	-1.66013790
O	3.89965314	-1.50246495	2.97349146
O	3.01335653	-4.06673297	-2.87489626
O	2.08867970	-4.37257434	1.67458237
O	-2.87394621	-3.15259673	-3.95435843
O	-3.82815242	-4.32592473	0.44404322
O	-4.55517265	0.13768271	-4.32443818
O	-4.47069034	-1.39129360	0.06602715
O	-1.63973553	5.18659572	-2.47942279
O	-1.05267033	3.20617704	1.68894738
C	1.76992229	6.87894884	0.47970418
C	2.11898259	7.85000767	-0.44662228
C	2.06836991	7.09588299	1.85659493
C	2.75635627	9.06034716	-0.05759290
H	1.89964019	7.69855433	-1.50065206
C	2.69357809	8.25685956	2.26349655
H	1.80658728	6.34193167	2.58315216
C	3.11165430	10.06648822	-1.00190091
C	3.05120782	9.27200605	1.33153651
H	2.91612324	8.41066615	3.31544413
C	3.72942835	11.23257558	-0.58966406
H	2.88778372	9.90214889	-2.05204283
C	3.68823521	10.48360176	1.72501474
C	4.02006228	11.44300715	0.78616417
H	3.99575036	11.99410943	-1.31542487
H	3.90919801	10.64123948	2.77668567
H	4.50487443	12.36327909	1.09560490
C	-1.11770463	6.42984241	1.39310381
C	-1.89549378	7.56451427	1.21942303
C	-0.86845157	5.96108064	2.71529258
C	-2.45347762	8.26834853	2.32198120
H	-2.08597792	7.94440834	0.21884772
C	-1.39760582	6.62031034	3.80542682

H	-0.25511439	5.08682569	2.86470123
C	-3.24806845	9.43832863	2.14975378
C	-2.20032391	7.78587736	3.64995624
H	-1.19598362	6.25432352	4.80814362
C	-3.77094737	10.10196834	3.24418745
H	-3.43522854	9.80091665	1.14304608
C	-2.75222475	8.49117935	4.75725361
C	-3.52090902	9.62367545	4.55960089
H	-4.37501949	10.99254179	3.10431119
H	-2.55842827	8.12380604	5.76090093
H	-3.93710863	10.15472942	5.40961651
H	-0.82964781	6.47101684	-0.67806922
C	-5.46122806	-2.09406550	-2.73418389
C	-5.15450923	-3.41554559	-1.96763268
H	-5.16580463	-2.21814034	-3.77677047
H	-5.52179393	-3.31337600	-0.94641825
C	-6.94979583	-1.80339822	-2.67670907
C	-7.72356648	-1.97738384	-3.80740260
C	-7.56438610	-1.42417510	-1.44880941
C	-9.13455136	-1.79869849	-3.76849070
H	-7.25970272	-2.27258732	-4.74430860
C	-8.92922276	-1.23523052	-1.38038707
H	-6.95600419	-1.29482140	-0.55998799
C	-9.95206486	-1.99046493	-4.91903532
C	-9.75330435	-1.42016202	-2.52834127
H	-9.39484788	-0.94830746	-0.44215093
C	-11.32179561	-1.81675096	-4.84721628
H	-9.48010405	-2.27904445	-5.85367067
C	-11.16617792	-1.24665053	-2.48724054
C	-11.93423752	-1.44087916	-3.62070778
H	-11.93693035	-1.96734856	-5.72838172
H	-11.63123296	-0.96001658	-1.54842967
H	-13.01039878	-1.30775323	-3.57890794
C	-5.87928418	-4.58015781	-2.61748822
C	-6.92991184	-5.17412278	-1.94398859
C	-5.54520368	-5.01851923	-3.93170328
C	-7.69859513	-6.21128638	-2.54148030
H	-7.19508499	-4.83776457	-0.94555758
C	-6.26680062	-6.02804405	-4.53501713
H	-4.72539176	-4.54722644	-4.46156086
C	-8.79597005	-6.82177193	-1.86902928
C	-7.36179509	-6.64917119	-3.86750727
H	-6.01030148	-6.35753372	-5.53772376
C	-9.52930838	-7.82145051	-2.48079825
H	-9.04828044	-6.48561668	-0.86747185
C	-8.13489654	-7.68252460	-4.46963795
C	-9.19550956	-8.25602542	-3.79254367
H	-10.36500811	-8.27952555	-1.96184646
H	-7.87787367	-8.01181102	-5.47225337
H	-9.77959160	-9.04182845	-4.26051426
C	4.92953633	-5.60390780	-0.06056529
C	5.88071295	-6.10583453	-0.92922664

C	4.53940481	-6.37005385	1.07638206	**C**	6.94748269	-3.70753317	2.03397921
C	6.48876905	-7.37301444	-0.70868315	**C**	7.08652322	-2.60737666	-0.12582348
H	6.18922387	-5.52317969	-1.79282628	**C**	8.36685736	-3.72550977	2.13254153
C	5.10651894	-7.60514211	1.31393721	**H**	6.36273606	-4.14057056	2.84057123
H	3.79808571	-5.97406866	1.76035677	**C**	8.46427186	-2.60439688	-0.05702760
C	7.47995391	-7.89878109	-1.58627175	**H**	6.58794745	-2.19057974	-0.99399647
C	6.09483045	-8.14166466	0.43902587	**C**	9.03905154	-4.28838463	3.25507893
H	4.80764409	-8.18395730	2.18301744	**C**	9.14458154	-3.16299474	1.06375725
C	8.05745155	-9.13055533	-1.33983218	**H**	9.05057892	-2.17876628	-0.86613710
H	7.77602715	-7.31330160	-2.45183451	**C**	10.42023527	-4.29658864	3.31807902
C	6.70677965	-9.40764868	0.66463171	**H**	8.44680567	-4.71356393	4.06013197
C	7.66718217	-9.89191174	-0.20453357	**C**	10.56521746	-3.18511285	1.15888099
H	8.81312540	-9.52246813	-2.01281817	**C**	11.19015192	-3.73981448	2.26080072
H	6.40692115	-9.98658452	1.53338574	**H**	10.92386744	-4.72938852	4.17631742
H	8.12883026	-10.85716724	-0.02343890	**H**	11.15054914	-2.75902228	0.34921392
C	6.31308347	-3.16855532	0.93146532	**H**	12.27343268	-3.75302193	2.32346659

Table S6.5 Cartesian coordinates of geometry-optimised **HeliΔ** at the B3LYP-GD3BJ/6-31G ++ level of theory in CH_2Cl_2, isovalue = 0.004.

C	0.01942317	0.03155425	0.01160231	**C**	1.75158924	0.07500652	3.25989212
C	0.04098391	0.05315385	1.49924563	**H**	2.78635757	0.07777492	3.58004529
C	1.38446612	0.06264173	1.91537180	**C**	-1.51557037	0.07451148	4.95963360
C	2.24538879	0.04760644	0.70120501	**C**	0.71052215	0.09015450	5.64972068
C	-1.02153275	0.05495562	2.40114212	**C**	-1.03560343	0.15655200	7.46622906
H	-2.05623538	0.04271670	2.08100716	**H**	-0.11701271	0.37811101	8.01859026
C	-0.65443016	0.07153439	3.74557273	**C**	-1.66289849	-1.14077520	7.95701773
C	0.68907854	0.08143716	4.16182718	**C**	-1.57056606	-2.33839054	7.21273803

H	-0.96681734	-2.36673295	6.31315369
C	-2.24157363	-3.47073792	7.62668233
H	-2.15384425	-4.39675991	7.06713168
C	-3.10497629	-3.42503295	8.75437333
C	-3.20886012	-2.20854103	9.51651319
C	-2.37703985	-1.08974088	9.15742447
C	-2.29090060	0.16316549	9.95663753
C	-2.18346055	0.18676303	11.39211692
C	-2.24865350	1.45306172	12.07319137
C	-2.34128669	2.65055215	11.31386271
H	-2.40602467	3.60087914	11.83440760
C	-2.28995833	2.61111403	9.93555738
H	-2.29432520	3.53448007	9.36807188
C	-2.23468083	1.37238445	9.25806382
C	-2.06358526	1.29280553	7.74785280
H	-3.00909974	1.02862842	7.26404203
C	-2.53015192	3.32925865	6.33895219
C	-1.74278770	4.51124279	5.89410643
C	-0.45998163	4.41950780	6.46349797
C	-0.40429540	3.17656803	7.28051135
C	-2.12111319	5.56956144	5.07004571
H	-3.11008665	5.64285254	4.63436595
C	-1.13320477	6.52734697	4.84849682
C	0.14960045	6.43613078	5.41811864
C	0.52644326	5.37989537	6.24579403
H	1.51281173	5.31078324	6.68803307
C	-1.19172422	7.77264772	4.03612130
C	0.93350270	7.62353081	4.98113151
C	0.49679287	9.60500359	3.48501808
H	1.58126084	9.65386004	3.62356224
C	-0.18016099	10.84110153	4.05904670
C	-0.87937275	10.80107075	5.28632695
H	-0.86869583	9.89482725	5.88051721
C	-1.56991642	11.90914769	5.73246014
H	-2.08839576	11.88553491	6.68580348
C	-1.66255722	13.07534434	4.92578836
C	-0.96020770	13.12362954	3.67063503
C	-0.12067162	12.01375910	3.30187453
C	0.76590791	12.02244915	2.10720474
C	1.55939942	13.12728557	1.71819411
C	2.28693384	13.05111082	0.46506753
C	2.27118990	11.89307346	-0.29846847
H	2.82874927	11.84858738	-1.22720428
C	1.56574025	10.76841893	0.15926404
H	1.59527221	9.85017421	-0.41558068
C	0.85399600	10.82049129	1.35321597
C	0.19506953	9.58868334	1.95562625
H	-0.89045716	9.62671954	1.82149848
C	-0.22824421	7.57982400	0.49324511
C	0.56043539	6.38631843	0.08192480
C	1.84013797	6.49134402	0.65598503
C	1.89212966	7.75155001	1.44557014

C	0.18964499	5.31253328	-0.72586167	**C**	1.76497870	0.06358434	-1.80647540
H	-0.79439468	5.23244559	-1.17144096	**H**	0.84598214	0.26857177	-2.36460516
C	1.17853528	4.34917698	-0.91828433	**N**	1.36921098	0.05536089	-0.40150670
C	2.45814271	4.45493722	-0.34404474	**N**	-0.63963748	0.11266575	6.06194526
C	2.83057778	5.53077719	0.45963948	**N**	-1.66205142	2.55864001	7.14209726
H	3.81687887	5.61439355	0.89950506	**N**	0.08145766	8.36644222	4.13529443
C	1.12887517	3.08805786	-1.70789723	**N**	0.61879719	8.34178383	1.32746488
C	3.24920339	3.26426059	-0.75763933	**N**	2.38612410	2.47438953	-1.54723051
C	2.79078904	1.19370998	-2.11851099	**O**	-0.95763465	-0.01303249	-0.74635780
H	3.73659538	0.94476831	-1.62726609	**O**	3.48206891	0.02781118	0.63551684
C	2.96166112	1.23316016	-3.63027390	**O**	-2.75209167	0.04635454	5.02566269
C	3.01632617	2.45380803	-4.33978551	**O**	1.68748660	0.06608098	6.40869379
H	3.02041258	3.39124606	-3.79584791	**O**	-3.70967519	3.04893946	6.09170645
C	3.06667679	2.45745792	-5.71866078	**O**	0.53653369	2.74412173	7.96000737
H	3.13081905	3.39395166	-6.26379601	**O**	-2.14753476	8.22840449	3.39373102
C	2.97328574	1.24052677	-6.44641386	**O**	2.08947233	7.94226919	5.28602409
C	2.90875296	-0.00762069	-5.73250353	**O**	-1.38476097	7.88837312	0.17999259
C	3.01770326	0.00614479	-4.29701066	**O**	2.84363233	8.21871996	2.08613697
C	3.10631273	-1.22528749	-3.46533782	**O**	0.19239432	2.63838552	-2.38228313
C	3.93913943	-2.35201021	-3.79619243	**O**	4.42763193	2.99100544	-0.49766109
C	3.83875203	-3.54785314	-3.00158792	**C**	4.63910478	-4.68008962	-3.33446618
C	2.97886075	-3.56426532	-1.87043986	**C**	4.92395170	-2.31717145	-4.82863238
H	2.89463328	-4.47482791	-1.28556130	**C**	2.65882923	-1.19458470	-6.48461792
C	2.30698954	-2.42226037	-1.48534183	**C**	2.89464507	1.23873704	-7.87017567
H	1.70679962	-2.42742652	-0.58283392	**H**	2.53328271	-2.13514193	-5.96499163
C	2.39458641	-1.24532599	-2.26254635	**C**	2.69853961	0.06412644	-8.56802341

C	2.55477922	-1.15973060	-7.86183441	**H**	-5.73064527	-3.16834690	11.62999087
C	5.70789933	-3.42036648	-5.10629604	**H**	-4.34377856	-1.22099225	11.08420074
C	5.54970332	-4.62472032	-4.37029154	**H**	-1.63213795	-1.80994537	14.12290478
H	4.53374044	-5.58177427	-2.73826516	**H**	-1.90972892	0.36995780	15.30733549
H	6.16143117	-5.48807111	-4.61033107	**H**	-2.24576962	2.45051794	13.99512393
H	6.45699915	-3.36479935	-5.88953349	**C**	3.15231344	14.26948064	0.40034800
H	5.06936060	-1.40518846	-5.39219514	**C**	1.76771463	14.31833481	2.61643618
H	2.35407276	-2.07476572	-8.40965854	**C**	-1.19373424	14.24240740	2.81670276
H	2.63053532	0.07356148	-9.65083092	**C**	-2.47361677	14.18060251	5.31780833
H	2.96849310	2.18743579	-8.39372089	**H**	4.07344347	14.13661799	0.98069285
C	-2.17152019	1.48842539	13.49662070	**H**	1.44263263	14.21802349	3.64649237
C	-1.93447931	-0.98019811	12.17522537	**H**	-2.97818559	14.13775937	6.27854185
C	-4.19612400	-2.14746242	10.54536278	**H**	-0.73845596	14.26488584	1.83528419
C	-3.90502855	-4.54888463	9.11514495	**C**	-2.63931518	15.26863147	4.48469543
H	-1.80836898	-1.93395624	11.68042464	**C**	-2.01098084	15.28402746	3.21118708
H	-3.79723358	-5.46592848	8.54330289	**C**	2.43047179	15.40081264	0.68681748
C	-4.81837072	-4.46703063	10.14679521	**C**	2.29311002	15.50368624	2.17729771
C	-4.97957981	-3.24379977	10.85030350	**H**	1.48919337	15.54886718	0.14616502
C	-1.83210325	-0.90949761	13.55116279	**H**	2.40289992	16.37574193	2.81383704
C	-1.97647749	0.33236753	14.22506113	**H**	-2.18117840	16.11884548	2.53911151
H	-5.42988548	-5.32436505	10.40801964	**H**	-3.26541695	16.10141782	4.78727417

Table S6.6 Cartesian coordinates of geometry-optimised **PhenΔ** at the B3LYP-GD3BJ/6-31G ++ level of theory in CH_2Cl_2, isovalue = 0.004.

C	2.25562274	3.71241423	-1.13312433	**C**	2.41933688	3.79792810	1.19959157
C	2.80653671	2.41745577	-0.65634645	**C**	3.16737556	1.29181212	-1.39338032
C	2.94223763	2.48104693	0.74226239	**H**	3.04871718	1.23804721	-2.46865814

C	3.69672329	0.24213693	-0.64607641
C	3.88360809	0.32306616	0.74594442
C	3.50066776	1.44149538	1.48568661
H	3.62975657	1.49947793	2.55954909
C	4.15995549	-1.09288521	-1.10301984
C	4.53319118	-0.93695586	1.20333055
C	5.16432943	-3.08416302	0.03297013
C	6.58848181	-3.27263145	0.07674464
C	7.47229846	-2.16600641	0.12616209
H	7.06687233	-1.16184005	0.13561017
C	8.84347689	-2.35676925	0.15498550
H	9.51110897	-1.50301296	0.19153496
C	9.36877976	-3.66685440	0.13554674
H	10.44244309	-3.81914276	0.15962959
C	8.51940244	-4.76234608	0.08124459
H	8.95191890	-5.75408968	0.06099592
C	7.11102471	-4.60264148	0.04760760
C	6.19527660	-5.73406974	-0.01831523
C	6.64685212	-7.07802082	-0.02464297
H	7.70704789	-7.29196412	0.01056383
C	5.75486894	-8.13930517	-0.06908538
H	6.12908605	-9.15736996	-0.07201181
C	4.36425954	-7.90043429	-0.10346428
H	3.66940040	-8.73260504	-0.12888556
C	3.88984963	-6.59950960	-0.10331183
H	2.82229775	-6.41886108	-0.12271130
C	4.78529976	-5.50136166	-0.06837276
C	4.30412779	-4.14577131	-0.05950417
C	2.07807358	-4.08887663	-1.25140117
C	0.69198126	-3.75043405	-0.81922809
C	0.73350665	-3.38958264	0.53940623
C	2.13682362	-3.48578813	1.00903120
C	-0.50028790	-3.78798972	-1.54353976
H	-0.53599407	-4.07225445	-2.58811587
C	-1.64518166	-3.44963801	-0.82090940
C	-1.59551552	-3.09168628	0.53831051
C	-0.40636913	-3.04527077	1.26054584
H	-0.37260060	-2.77703397	2.30938044
C	-3.07108053	-3.42156989	-1.25618150
C	-2.97786950	-2.82863248	1.00602633
C	-5.23774298	-2.89594085	-0.06648812
C	-6.06288963	-4.07380837	-0.08399635
C	-5.49280777	-5.37074278	-0.12886522
H	-4.41574116	-5.48102580	-0.14803925
C	-6.29734865	-6.49771796	-0.13896716
H	-5.84997506	-7.48499660	-0.17217071
C	-7.70132299	-6.35690808	-0.10465612
H	-8.33363440	-7.23813901	-0.11556300
C	-8.27770613	-5.09645040	-0.04973463
H	-9.35654831	-5.01987710	-0.01413393
C	-7.48365815	-3.92195848	-0.03287420
C	-8.06384740	-2.58769673	0.04586933

C	-9.46380015	-2.36688365	0.08442345
H	-10.14468088	-3.20755868	0.05752019
C	-9.99068030	-1.08542590	0.15224368
H	-11.06606451	-0.94648639	0.17993795
C	-9.13525771	0.03701004	0.18109674
H	-9.55136713	1.03727629	0.22885125
C	-7.76279000	-0.14373754	0.14737661
H	-7.10582898	0.71705712	0.16467787
C	-7.20545935	-1.44524911	0.08356428
C	-5.78263233	-1.64353927	0.03519371
C	-4.28442730	0.01200539	-1.09620707
C	-3.49014905	1.17991565	-0.63846835
C	-3.64222298	1.30058145	0.75473732
C	-4.59902998	0.25376269	1.21136280
C	-2.71553299	2.06246324	-1.38761210
H	-2.62313707	1.98548815	-2.46404135
C	-2.07413177	3.05528729	-0.65082221
C	-2.17615619	3.14320008	0.74941000
C	-2.97794380	2.27858006	1.49458151
H	-3.08028812	2.36277067	2.56960095
C	-1.21750010	4.17078582	-1.12963319
C	-1.32727201	4.27843340	1.20542786
C	0.09984099	5.97666962	0.02203777
C	-0.48608636	7.28952085	0.00850590
C	-1.89272462	7.46176926	-0.00482605
H	-2.53648261	6.59033779	-0.01156227
C	-2.44934851	8.72968737	-0.01123519
H	-3.52688363	8.85114921	-0.02139859
C	-1.60865005	9.86362796	-0.00520402
H	-2.04234030	10.85779368	-0.00901374
C	-0.22942110	9.71461202	0.00355735
H	0.38887385	10.60273358	0.00505919
C	0.37342274	8.43147498	0.00858783
C	1.81834709	8.24407427	0.00726716
C	2.72799562	9.33145509	0.00109274
H	2.35600401	10.34767105	0.00406948
C	4.09968323	9.12453737	-0.01060276
H	4.77211689	9.97558991	-0.01512800
C	4.62380467	7.81389883	-0.01886520
H	5.69670813	7.65691486	-0.03162977
C	3.76275815	6.72944092	-0.01122477
H	4.16397266	5.72312878	-0.01996799
C	2.35861798	6.92062250	0.00555094
C	1.45745594	5.80021123	0.02072329
N	1.99937666	4.47689625	0.03066005
N	4.63530795	-1.75710682	0.05029476
N	2.89656300	-3.90386559	-0.10777390
N	-3.81687058	-3.03645903	-0.11279584
N	-4.91750381	-0.50633902	0.05644419
N	-0.76244491	4.83659773	0.03368697
O	2.07562428	4.09324186	-2.29401991
O	2.35125774	4.24832492	2.34842850

O	4.14200840	-1.56986491	-2.24367843	**O**	-3.36154176	-2.50065521	2.13432222
O	4.94371782	-1.22923571	2.32981500	**O**	-4.39123209	-0.45172046	-2.23755417
O	2.47035701	-4.47753695	-2.35577286	**O**	-5.07022221	0.07728579	2.33809612
O	2.58979622	-3.26305379	2.13734859	**O**	-0.96073281	4.50193914	-2.29135379
O	-3.54755807	-3.69314089	-2.36244025	**O**	-1.13101787	4.68775959	2.35494628

Table S6.7 Cartesian coordinates of geometry-optimised **HeliΔ** at the B3LYP-GD3BJ/6-31G ++ level of theory in CH_2Cl_2, isovalue = 0.004.

C	0.27977488	0.08781497	-0.00905397	**C**	-3.17324554	-2.24936268	9.64545824
C	0.16422070	0.05976127	1.47312090	**C**	-2.42951648	-1.07325320	9.20661879
C	1.46178435	0.01131164	2.01473617	**C**	-2.28032526	0.13621370	9.98423195
C	2.43426777	-0.08042332	0.89196174	**C**	-2.29263481	0.18548984	11.44218756
C	-0.97933062	0.05748955	2.27030013	**C**	-2.43944682	1.45031603	12.09742817
H	-1.97868727	0.05873946	1.85249685	**C**	-2.45547333	2.65256923	11.31805380
C	-0.74309073	0.04687160	3.64392322	**H**	-2.60418078	3.60126588	11.82358455
C	0.55532274	0.07238035	4.18502711	**C**	-2.19393269	2.61271699	9.97805111
C	1.69841097	0.03378214	3.38814153	**H**	-2.11328654	3.53273298	9.41259971
H	2.69758805	0.01754361	3.80605006	**C**	-2.03856620	1.36120004	9.29578680
C	-1.71715455	-0.00867859	4.76776925	**C**	-1.62866626	1.31897640	7.93033370
C	0.44067415	0.12193123	5.66664763	**C**	-2.17267708	3.10166601	6.25550708
C	-1.47557013	0.11530852	7.27804226	**C**	-1.50083048	4.34606344	5.80768734
C	-1.87938767	-1.10602663	7.89200370	**C**	-0.32267255	4.51052948	6.55748372
C	-1.74633413	-2.35172855	7.19504038	**C**	-0.19362888	3.34656924	7.47952930
H	-1.24084456	-2.36549196	6.23732455	**C**	-1.91173154	5.26219202	4.84295546
C	-2.23665818	-3.50885616	7.72986205	**H**	-2.81803969	5.13066627	4.26465190
H	-2.10529864	-4.45450381	7.21389830	**C**	-1.07843208	6.36658186	4.68741939
C	-3.01839764	-3.48072164	8.93034096	**C**	0.08568540	6.55223227	5.45529953

C	0.50481191	5.62424551	6.40905521
H	1.40303800	5.76306981	6.99823137
C	-1.22522687	7.52285452	3.76923529
C	0.69213904	7.85801089	5.07081125
C	0.09170090	9.61202662	3.35909397
C	-0.26687276	10.84269128	4.00017724
C	-0.84295882	10.84076936	5.30996243
H	-0.90132197	9.91035511	5.86000567
C	-1.31715955	11.99680554	5.86720174
H	-1.72369805	11.99653015	6.87341624
C	-1.37030430	13.20442744	5.10330881
C	-0.82302640	13.22631014	3.77725817
C	-0.10725992	12.06098166	3.28847955
C	0.69387041	12.05765219	2.07436095
C	1.36376485	13.21437126	1.55579726
C	1.93839800	13.15135006	0.23813991
C	1.99918444	11.93486719	-0.46288031
H	2.46514452	11.90663791	-1.44133169
C	1.51285150	10.77701885	0.11725327
H	1.62781350	9.82989344	-0.39409674
C	0.89087265	10.81024547	1.38906589
C	0.54624997	9.59380371	2.06466356
C	-0.03033424	7.79929836	0.38832212
C	0.58240802	6.48594234	0.04079856
C	1.73116075	6.31464417	0.83458093
C	1.86624044	7.49228284	1.72658838
C	0.18117171	5.53971166	-0.90274174
H	-0.70400150	5.66844535	-1.51355489
C	1.00941728	4.42197029	-1.01188736
C	2.16947018	4.26875017	-0.23213676
C	2.56308838	5.20409846	0.72126080
H	3.45663319	5.08238890	1.32114961
C	0.90001393	3.24282728	-1.91704867
C	2.84562980	3.01229593	-0.63768122
C	2.34212480	1.20527638	-2.29788093
C	2.76118426	1.22045918	-3.66104462
C	2.91625623	2.45747753	-4.36944197
H	2.82744789	3.38933504	-3.82500441
C	3.18874536	2.46930659	-5.70776952
H	3.33746977	3.40749567	-6.23253232
C	3.18471374	1.25020412	-6.46076504
C	3.03963558	-0.00064698	-5.77893090
C	3.01646164	-0.01792245	-4.32028521
C	3.16830548	-1.20894241	-3.51540942
C	3.92223488	-2.38971055	-3.92361984
C	3.76987243	-3.60627448	-3.18311760
C	2.97951161	-3.61342109	-1.98791904
H	2.84946771	-4.54866595	-1.45300685
C	2.47915896	-2.44798055	-1.48128252
H	1.96641468	-2.44411686	-0.52725420
C	2.61051043	-1.21655088	-2.20360401
C	2.19599170	0.01542226	-1.61912640

N	1.66321054	0.02170161	-0.29406134
N	-0.94434337	0.09373964	5.95221179
N	-1.33335030	2.53632423	7.24427138
N	-0.13046082	8.37571140	4.03800929
N	0.77757172	8.34087592	1.42085231
N	2.03199953	2.43419809	-1.64000741
O	-0.61884265	0.15481775	-0.85566658
O	3.65477714	-0.25508089	0.94208509
O	-2.94134729	-0.15737254	4.71982821
O	1.34024994	0.17695271	6.51296292
O	-3.25488036	2.63483052	5.88503580
O	0.69704479	3.10607735	8.30065025
O	-2.10311157	7.73372393	2.92458852
O	1.67831036	8.42537040	5.54981625
O	-1.01248741	8.35329899	-0.11400621
O	2.73281718	7.72270239	2.57777623
O	0.03039898	2.99150807	-2.75697301
O	3.91207217	2.54423255	-0.22491436
C	4.47409326	-4.77124559	-3.58883189
C	4.90695940	-2.36132842	-4.94847359
C	2.79367357	-1.15742835	-6.56748929
C	3.23680752	1.27714783	-7.87990068
H	2.57625721	-2.09792128	-6.08003799
C	3.06457613	0.11906517	-8.61867668
C	2.80525797	-1.10140222	-7.95177602
C	5.61453330	-3.49937437	-5.30014037
C	5.37281741	-4.72749725	-4.64084204
H	4.32029789	-5.69100646	-3.03242518
H	5.91595526	-5.61891278	-4.93635027
H	6.36673363	-3.44388988	-6.08014086
H	5.12256203	-1.43056889	-5.45476194
H	2.60354938	-1.99896213	-8.52705127
H	3.09248602	0.15039375	-9.70273114
H	3.37813112	2.23251379	-8.37636625
C	-2.48091280	1.50834624	13.51599859
C	-2.03422176	-0.95222543	12.25419142
C	-4.15088016	-2.20485993	10.67653571
C	-3.71246647	-4.64093839	9.36611345
H	-1.81514038	-1.90203880	11.78596894
H	-3.55682444	-5.57157411	8.82863389
C	-4.60400778	-4.57993540	10.42332852
C	-4.84876334	-3.33933840	11.05772394
C	-2.03574613	-0.86568524	13.63693396
C	-2.29676710	0.36781414	14.27877145
H	-5.13942432	-5.46806053	10.74191434
H	-5.59577101	-3.27165426	11.84173268
H	-4.36862142	-1.26473702	11.16426293
H	-1.82471666	-1.74922311	14.23028008
H	-2.31670530	0.42286780	15.36205396
H	-2.62362127	2.47375973	13.99223123
C	2.68975334	14.41239072	-0.00955594
C	1.70017166	14.38394681	2.44923358

C	-1.11071895	14.35722256	2.96289811
C	-2.03277499	14.35424980	5.60997587
H	3.74580377	14.34869106	0.27669974
H	1.59056239	14.23364380	3.51797253
H	-2.41280279	14.32858762	6.62677599
H	-0.81842657	14.35262560	1.92179357
C	-2.23016096	15.46860258	4.81295349
C	-1.79567759	15.45044450	3.46638119
C	1.96762720	15.48011049	0.46538997
C	2.15641499	15.57227629	1.95271670
H	0.91273204	15.51264849	0.17044125
H	2.46684843	16.41134185	2.56489312
H	-2.01051053	16.29392657	2.81870470
H	-2.74774314	16.33805112	5.20413256